University of Neuchâtel
Faculty of Science
Institute of Microtechnology

Master of Science in macro and nano technology
Master Thesis

Effect of oscillator instability on GNSS signal integration time

by

Pascal Olivier Gaggero

Supervisors
Prof. Gérard Lachapelle, University of Calgary
Prof. Pierre-André Farine, University of Neuchâtel

January 27, 2008

pascal.gaggero@unine.ch

Contents

Acknowledgements

Special thanks to:

- Prof. Gerard Lachapelle (UofC) who gave me the opportunity to join the PLAN Group at the University of Calgary for my masters thesis.
- Aiden Morisson (UofC) for assistance with electronics/PCB development
- Daniele Borio (UofC) for assistance with theoretical component
- the PLAN Group for general support and their cordial welcome
- Yves Schwab (Oscilloquartz), for crucial help and support.
- Prof. Pierre-André Farine (UniNE) and Cyril Botteron (UniNe) for general support
- To my family who supported me during my studies

Project industrial sponsors:

- Oscilloquartz SA, Neuchâtel, Switzerland
- Fordahl SA, Biel/Bienne, Switzerland
- Micro Crystal SA, Grenchen, Switzerland

***Thesis reviewers*:**

- Aiden Morisson (UofC)
- Daniele Borio (UofC)
- Gerarad Lachapelle (UofC)
- Sid Kwakkel (UofC)

“C’est avec la logique que nous prouvons
et avec l’intuition que nous trouvons.”
[*Henri Poincaré*]

Chapter 1

Preface

1.1 Abstract

Oscillators are indispensable hardware components of many RF circuits and wireless systems. In the last few decades the growing demand of precise oscillators has motivated the development of new techniques allowing more stable and more accurate devices requiring less and less power and with reduced size. Moreover, as the oscillator precision increases the need of reliable techniques for assessing their performance has become more and more stringent.
On the other hand Global Navigation Satellite Systems (GNSSs) provide an extremely accurate frequency reference, indispensable for precise positioning. This reference is freely available to the user and can be used for assessing the oscillator performance.
In this work a wide set of oscillators manufactured by the Swiss companies Oscilloquartz, Fordahl and Micro Crystal has been analyzed by using the GPS signal as frequency reference. The basic idea is to compare the precision of the oscillator under test with the one of the oscillator on board GPS satellites.
GPS L1 samples have been collected using a front-end driven by the oscillator under test, post-processed and analyzed by custom developed software. Coherent power accumulations up to 99.9 seconds have been considered. Several frequency errors, such as Doppler frequency and bit transitions have been removed possibly leaving only the errors induced by the local oscillator. A perfect frequency reference would have led to an accumulated power linearly growing with the integration time. The appearance of artifacts and the saturation of the accumulated power reveal the limits of the local oscillator and thus can be used as a metric for assessing its performance. The analysis developed in this thesis shows that coherent integrations up to 60 seconds are possible.
The proposed method can also be used to quantify the precision of the satellite oscillators. This result is possible if the local oscillator is extremely precise (i.e. Allan deviation $\sigma(\tau) < 1 \cdot 10^{-12}$ with $0.2 < \tau < 10s$) such as the Oscilloquartz 8607: in this case the

satellite clock short term behavior dominates the other frequency error sources.
The developed methodology is general and can be also applied to new GNSSs such as the European Galileo, the Russian Glonass and the Chinese Compass.
A further contribution of this thesis is the analysis of indoor position that is possible only if long coherent integrations are employed. Indoor positioning has been successfully performed even with extremely attenuated signals (attenuations between 40 and 45 dB). The user position has been determined within a precision of less than 20 meters in the horizontal plane and of 100 meters in height using 5 satellites.

1.2 Thesis organization

- Chapter 1 is an introduction chapter.
- Chapter 2 discusses the fundamentals of GPS.
- Chapter 3 is an introduction to the world of oscillators.
- Chapter 4 describes the hardware and software used during the project.
- Chapter 5 presents the obtained results.
- Chapter 6 contains the conclusions and future work ideas.
- Several appendixes containing additional material.

1.3 Project organization and schedule

The goal of this section is to give an overview of the project organization. The master thesis project will be conducted by Pascal Olivier Gaggero as a visiting student at the University of Calgary. The supervising professor in Calgary is Prof. Lachapelle, who is the Positioning, Location and Navigation (PLAN) Group leader[1].

September 07 tasks:

- Arrive in Calgary of Pascal Oliver Gaggero September 4th 2007.
- Familiarization with the GPS and wireless location domains
- Attend the Institute of Navigation(ION) conference in Houston, Texas
- Attend the course Engo 625 given by Prof Lachapelle
- Execute data collection with Rob Watson[2], with intent to try to reproduce his previous results, and to become familiar with the software and data collection

[1] http://plan.geomatics.ucalgary.ca/
[2] PLAN group research engineer.

hardware. After that, Pascal decided to develop a Graphic User Interface(GUI) to facilitate the software use and avoid manual operations that often introduce errors. The GUI also provides new interesting features.

- Oscillator Printed Circuit Board(PCB) design

October 07 tasks:

- Oscillator PCB finalization.
- Oscillator PCB parts soldering.
- GUI development.
- Negotiation of the loan for the 8607 with Oscilloquartz.
- Preparation of a tutorial session on the importance of oscillators within wireless location and GPS.

November 07 tasks:

- Pascal present a tutorial on oscillators to the PLAN Group.
- Reception of the 8607 oscillator.
- Completion of the GUI, and beta testing of the oscillators boards.
- Test of the different data collection methodologies.

December 07 tasks:

- Finalize data collection methodology.
- Final measurements under 3 different signal conditions: open-sky, in the lab and in the corridor.
- Data processing and Analysis.
- Initial thesis drafting.

January 07 tasks:

- Data processing and analysis.
- Thesis writing.
- Thesis presentation to the PLAN Group.

February tasks:

- Hard copy of the thesis will be transmitted to Prof. Farine.
- Thesis presentation to ESP Lab in Neuchâtel.

Chapter 2

GNSS systems are precise clock networks!

2.1 Introduction

The American Global Positioning System (GPS) has strongly impacted our every day life during the last 5 years, essentially due to the drop of the receiver prices and size, and the increase of their capabilities. Anybody will now be able to get his position within a few meters anywhere in the world, 24 hours per day, under any weather condition. This system is so common that most of the users don't know that in fact GPS, or more generally speaking a Global Navigation Satellite System system (GNSS), is in essence a large distributed timing system. The first basic function of these systems are to provide accurate time (about 1 nano second) everywhere in the world. The resulting ability to obtain a user position is based on the very simple formula that relies the length s, speed of light c and time t.

$$s = c \cdot t \tag{2.1}$$

So if one is able to calculate the wave travel time between a user (on the earth) and some satellites with known positions, one can calculate the user-satellite distance. Then by processing these known distance with respect to known satellite coordinates, one can extract the user position by trilateration. To summarize in a simplistic manner, the GPS system can be seen as a large, distributed and precise clock that provides accurate timing globally with a precision of a few nano seconds. This timing information is broadcast by a 31[1] satellite constellation.
In this chapter the reader will receive an overview of the history of the GNSS. This explanation will focus on the well know GPS system for the reason that this is the only fully operational GNSS currently available.

[1] On October 16th 2007, http://www.navcen.uscg.gov/archives/GPS/2007/OPSADVISORIES/289.OA1

2.2 Description of GPS system

2.2.1 Historical development

GPS, the currently most widely known GNSS, is not the first satellite localization system to orbit the earth[2]. Before modern GPS was created, the so called TRANSIT system[3], constituted of 6 satellites constellation, was used by the US Navy in order to localize surface vessels on the sea and fire ballistic missiles from submarines. TRANSIT service began in November 1964 and was in use for nearly 30 years, until replaced by the current GPS system in 1991. The working principle of this system was to measure the Doppler shift of the satellite from its own orbit, and from this information calculate the user position. The measured Doppler shift pattern is closely related to the user position on the earth relative to the satellite so it follows that if one knows the precise satellite position and timing it's possible to extrapolate the user position. In the best case this system was able to localize slowly moving ships with known altitude to within 100 metre range.

Navigation System for Timing and Ranging (NAVSTAR) system, also known as GPS, was originally developed by the department of defense of the United State of America for military purposes, including vessels location and weapon delivery. At that time, in the 1980's the GPS receiver was far away from the performance of a modern, small handled unit. For example, with the 1980's technology, only one channel (satellite signal) could be tracked at a time, the receiver weighed more than 500kg and cost approximately 150000$ [11, ch1.1 p.5].
GPS signals are provided free of charge to users all around the world, and since 2001 have been available without any intentional signal degradation via the Coarse Acquisition (C/A) or access unencrypted code, while military[4] users may also access the armed force reserved signal called P-code. The latter is an encrypted signal providing a much better accuracy than the civilian one (C/A-code), which is especially designed to be more resistant to jamming[5] and spoofing[6][11, ch2.6 p.91-97]. However easily used by civilians, saying GPS is freely available doesn't mean that it costs nothing! In fact the USA spends a large amount annually for the maintenance of the system (ground control, research, satellite replacement, ...), totaling about 750 million of US dollars each year. A rough estimation of the money spent so far in the project could be estimated as eight to ten billions of US Dollars, not accounting for inflation since the inception of the system!

[2]There was/is also ground base navigation system like: LORAN-C.
[3]The soviet also launched in 1974 the TSIKADA system which is comparable to the US TRANSIT.
[4]USA and allies.
[5]Voluntary perturbation of the GPS signal.
[6]Broadcasting wrong GPS signal, without the user is able to know it.

time	event
1973	Project start
1974-1979	Proof of concept and testing
1978-1985	11 Block I satellites are lunched
1983	The USA decided to allow civilian use of GPS
1989	First Block II satellite is launched
17th July 1995	Fully operational capabilities with a 24 satellites constellation is announced
1 may 2000	Selective Availability is turned OFF by President Clinton[16].
25 September 2005	The first Block IIR-M GPS satellite as been launch(L2C + M-code, see[2.4])
October 2007	4 L2c and M-code capable satellite are in orbit

Table 2.1: Brief review of the GPS satellite development.

2.2.2 The space segment

The space segment consists of the satellites that provide the GPS service to earth, which since program inception has included many different satellites types with each new generation bringing substantial improvements to the capabilities of the system.

- 4 TIMATION satellites (launched: 1967-77), test purposes and proof of concept.
- 11 GPS BlockI satellites (launched: 1978-85), first GPS satellite generation.
- 9 GPS Block II satellites (launched: 1989-90), second GPS satellite generation, including a civilian signal on L1.
- 18 GPS BlockII-A satellites (launched: 1990-96), to achieve a fully operational system.
- 11 GPS BlockII-R satellites (launched: 1997-04), which are replenishment satellites; 12 have been launched so far, with the 8 remaining ones destined to be modified to transmit new L2C and M-code signals (see BlockII-RM).
- 4 GPS BlockII-RM satellites (launched: 2005-07), this new generation includes 2 new signals L2C(for the civilians) and a new military code M-code.
- BlockII-F satellites (planned launch: 2008±?), a third civilian frequency L5 with a new modulation type dedicated to high accuracy, and safety of life aviation purposes.
- BlockIII satellites (planned launch: 2013±?), better security level of the system, and better self monitoring capabilities (integrity monitoring).

A fully operational satellite constellation is constituted of 24 Satellite Vehicles (SV) allocated to 6 different orbital planes (4 SV per orbital plane), with active spare satellites also on orbit, bringing the total number of flying satellites as high as 31. One can note

that the more satellites are available, the better the positioning capabilities of the system, so the ideal is to have more and more satellites in the future. However one must not forget that the lifetime of one satellite is limited (slightly over 10 years for GPS historically) and that many currently flying SVs have already passed this design limit! Therefore the risk to see the number of SV decreasing is not negligible.

Figure 2.1: The last generation of flying GPS satellite BlockII-RM, first launch September 25th 2005.

2.2.3 The control segment

The GPS control segment includes the stations on the earth used to:

- Communicate with the satellites.
- Observe satellite motion and position in order to monitor exactly their orbital behavior, which in turn is used to build the orbital model of the satellite which is broadcast in the navigation message and posted on the Internet.
- Monitor and correct the satellite clocks.

The US military personnel that are responsible for monitoring and operating the GPS system are the 50th Space Wing's 2nd Space Operations Squadron, based on the Schriever Air Force Base in Colorado[7]. They also operate the master control station of the system,

[7]Their are spare master control station in Rockville (Maryland) and Sunnyvale (California).

which centralizes the information from the monitoring stations around the world and re-broadcasts the control information destined to the satellites through the ground antenna (uploading station).
The monitoring precision and reliability of the network depends on the capability of the ground control network to continuously monitor the satellites, even if one or more control stations are out of service. The monitoring network was originally composed of 4 stations (Hawaii, Ascension Islands, Diego Garcia and Kawajalein), but in 2005 6 more ground stations were added. With these new stations, the control segment can potentially always cover each satellite with at least 2 monitoring stations[8]. Five more stations are planed for the next several years, which will extend the monitoring capabilities to 3 stations per satellite globally.

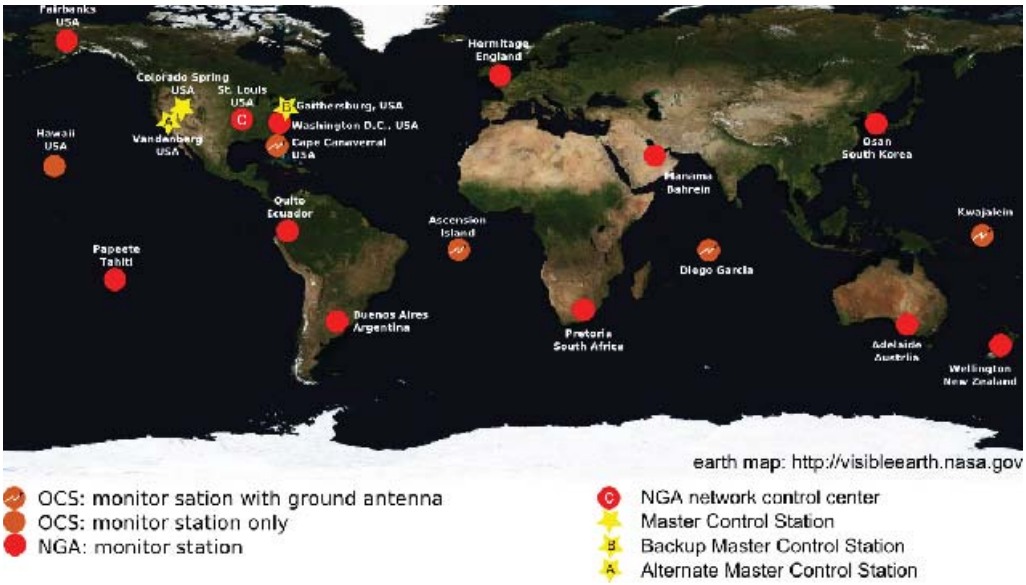

Figure 2.2: Geo-localization of the different ground segment stations. (Source:[19],[23])

[8]One must keep in mind not to forgot that some of the station can be out of order.

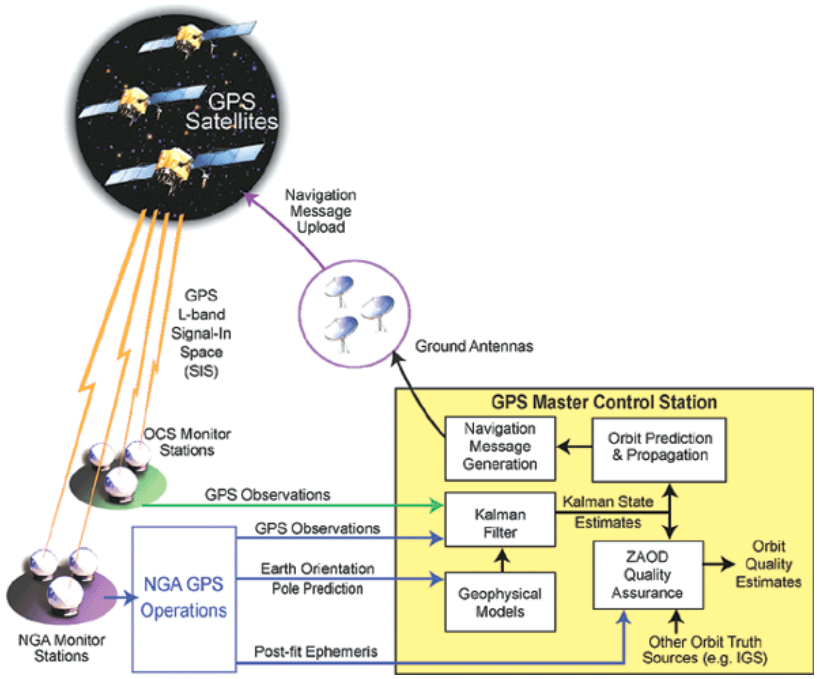

Figure 2.3: Space-ground control concept. (Source:GPS World[19])

2.2.4 The user segment

The GPS user segment includes all people or machines using the GPS service. Some of the common user application are:

- Getting a position with a precision of about 3 metres, with a probability of 50%, referred to as Circular Error Probable (CEP)[9]. CEP is generally used by the GPS handheld manufacturers in their data sheets, in order to exaggerate the accuracy of their product, and attract consumers, but other, less generous estimators can also be used [11, ch6.3 p.15-21].

- Getting time by resolving the least mean square equation, for both position and time, it is possible to obtain precise timing from the GPS signals. Basically it is possible to 'read' the satellite clocks, which are regularly corrected by the most precise atomic clocks on the earth. In principle the time that is available through a GPS based time reference is very accurate, because the time provided does not come from only one atomic clock, but from a network of atomic clocks.

- Atmospheric measurement uses the fact that the electromagnetic (EM) Waves have to travel from the satellite through the atmosphere to the user before measurement. The ionosphere contains a variable density of free electrons, which attenuates and

[9] 50% probability to be in circle of i meter around the true value.

bends the GPS signals, allowing to measure this electron density[10] using a pair of GPS signals from the some satellite. Measuring the troposphere is also possible by removing the ionospheric error (ionosphere-free linear combination), and has application to the Water Vapour Density measuring which is useful to weather forecaster. However water vapor measurements are more difficult to perform than those intended to measure the ionosphere.[11, ch 5.6, p.18-67].

The US-military and allies users have specialized GPS receivers that are able to read the encrypted P-Code, which in turn offers them better spoofing and jamming protection than is available to civilian users.

2.3 Receiver basic principles

Firstly, it has to be clear that GPS user units are only receivers, meaning that they can only listen to the satellites, and are not required to transmit information to operate normally. Nevertheless some users with specialized equipment can also get or transmit information over mobile telephone networks or in some cases even between multiple receivers them self, both known as Assisted GPS(AGPS). Getting almanac and rough position using ground based networks can significantly enhance the satellite acquisition speed and capabilities.

2.3.1 GPS signal structure

The signal energy arriving on the earth from a given GPS satellite is so low that the noise energy signal seen on the receiver antenna is higher, yet it will be shown that despite the weakness of the signal, it is still possible to acquire and track the information transmitted. In normal operation, GPS satellites simultaneously broadcast several signals on different frequencies, with some dedicated to authorized (usually military) users, including the so called Precise P(Y) signal, and in the future the Military/M code signal. Civilian users however have until recently only had access to the coarse or clear code (CA code), broadcast on only one of the available carrier frequencies. The available and planned carriers are L1 (1575.42MHz), L2 (1227.6MHz) and L5 (1176.45 MHz) with L1 and L2 currently transmitted by all satellites. Due to the progressive modernization of the constellation, each signal is not presently broadcast by all satellites, with these limitations especially concerning L5[11] which is not yet broadcast by any satellites. Since the inception of the system several improvements in the signal structure have been realized, through the addition of new signals, in order to enable new features and application for the network. For example, there will be a data-less pilot channel added with the L2C, L5 and L1C signals, to facilitate satellite tracking in degraded signal power conditions.

[10] The free electrons density varies with the sun activities.
[11] L5 Civilian

Due to the longevity and wide utilization of the classic L1 CA transmission, the restricted nature of the P(Y) and M code signals, as well as the limited current deployment of the modernized civilian signals, the rest of the document will restrict discussion to only consider the L1 CA code.

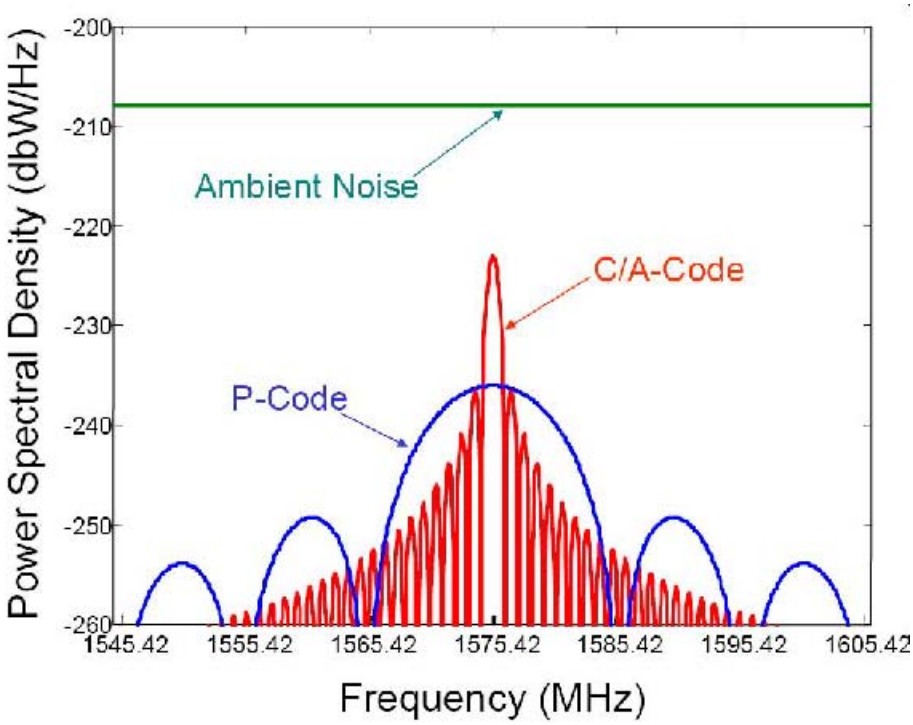

Figure 2.4: Spectrum representation of the L1 signal, compared to the noise floor, (image from:[18])

GPS satellites use the Code Division Multiple Access(CDMA) technique to broadcast their message, which means they multiply their fundamental carrier frequency by the navigation message and subsequently perform an additional multiplication with a Pseudo Random Noise (PRN) code sequence, which is unique for each satellite.

2.3.2 Getting a position

Getting a position using the GPS satellite signals will use the following process flow, in case of a cold start[12]:

- First the receiver must to search the whole Search Space (SS)[13], on each PRN (or channel) in order to find the satellites. This operation could be potentially quite time consuming, but with modern electronic capabilities it is quite easy to parallelize the processing by multiplying the number of hardware correlators. The

[12]No prior information available.
[13]Code and Doppler space.

modern receiver also has several channels, so many satellites can be search for, and finally tracked at the same time[14]. During the receiver design process one has to find a tradeoff between hardware cost (money, size and power consumption) and the speed of acquisition searches.

- Once one is tracking satellites one has to download from the satellites the ephemeris, which contains the orbital model parameters used to calculate satellite position and trajectory. The ephemeris is part of the GPS almanac, and is situated in every 3 first sub-frames of each frame of data broadcasted. Ideally the time required to get the complete ephemeris is at least $3 \cdot 6 = 18$ seconds, and in the worst case could be up to 30 seconds[15]. These orbital model parameters are updated every 2 hours using past uploads from the ground segment, which once an updated model is available through the ground observation, notifies the constellation via ground satellite link antenna to upload it to the satellite constellation[16]. Without updates the model is still useful for several hours, but beyond normal update latency, users may experience severe position accuracy degradation, which is one of the motivations behind the IIF GPS satellites having the ability to communicate with each other and inter correct their model, without human (or ground) interaction for about 180 days when operating in autonomous navigation mode (14 day otherwise). This autonomy is planned to be extended and perfected in the coming block III satellite.

- Once one receives the above information one is ready to get a position. The average time of the whole process is between 30 seconds to 1 minute, as once one knows the position for at least 4 satellites and the user to satellite distance[17] it is possible to solve the pseudo range equation for time and position.

2.3.3 First stage of a GNSS receiver acquisition block

A GNSS receiver is made of several functional blocks. The first stage of a GNSS receiver is the acquisition block that is aimed to provide a first raw estimation of the delay and the Doppler frequency of the received signals.
This section presents a simplified architecture of a GPS acquisition block (see figure 2.5) in order to understand the basic principles of its operations. The first stage of the receiver is used to remove the carrier and the satellite Doppler shift. The user must then remove the spreading PRN code and to integrate over some milliseconds(usually 1 or 2) to increase the SNR above the noise floor. It is necessary to square and sum the integrated signal components, and if the code delay (τ) and Doppler shift frequency (F_D) used in

[14]Typically 12.

[15]Almanac duration=750s ↪ 25 frames of 30s ↪ 5 subframes of 6s ↪ 10 words of 0.6 s ↪ 30 bits per word.

[16]This process occur in average twice a day.

[17]Determined by the time of fly the signal, using the z-count information of the given at the beginning of every sub frame.

the carrier and code wipeoff stage are correct, one will detect the signal with power distributed between the in-phase (I) and quadra-phase (Q) branches of the receiver. The next step is to synchronize the phase of the carrier generator to concentrate the power in one branch (typically I) only. Once this synchronization is successful, one can begin to track the code correlation peak, by observing 3 code delays Early ($\tau - d$) Prompt τ and Late ($\tau + d$) and trying to keep the difference $S(\tau - d, F_D) - S(\tau + d, F_D)$ as close as possible to 0. Once the code and carrier phase or frequency lock are stable, the receiver will conduct a bit-synchronization in order to be able to increase the integration time.
The bit synchronization is necessary because otherwise if one integrates over two navigation bits of different sign (+1 and -1) the resulting apparent power of the signal will be reduced. To avoid this loss, one has to be sure to begin and end the signal integration at the right time (i.e. at the beginning of a navigation bit). The time duration of a NavBit is 20 ms, which under normal circumstances limits the integration time to 20 ms, but by using data prediction techniques or AGPS, one can increase it through use of known data bit signs. In other words to go to several seconds of coherent integration time one has to use data aiding techniques, i.e. to know in advance the transmitted data bits and compensate for them.
In weak signal conditions one is not tracking the satellite because the signal is so attenuated that it's impossible to do so and in order to later analyze the signal with data bit aiding, one will record the I and Q data with a front-end (see [2.3.4]) and post-process them to get the peak. The receiver considered is then called a software receiver because once the I and Q samples are recorded for later analysis, the rest of the receiver may be composed entirely of software.

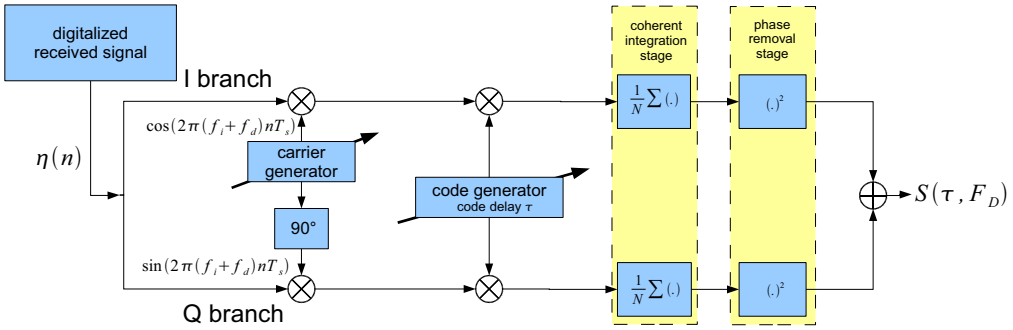

Figure 2.5: Simplified acquisition block of a GPS receiver. The digitalized signal created using a front-end is stored on hard-drives.

2.3.4 Front-end

In the front-end (see figure 2.6) one first down converts the incoming GPS Radio Frequency (RF) signal to an intermediate frequency (f_{IF}) as opposed to direct conversion from RF to baseband. The reason we choose to do so is that if one directly goes to base-

band one is no longer able to recognize the correct Doppler frequency sign. To avoid this problem one has to choose $f_{IF} > |f_{D_{max}}|$, and following this down-conversion, the signal is filtered before analog to digital conversion, to remove mixing artifacts. The conversion is done at a certain rate ($f_s = \frac{1}{T_s}$) and with a given number of bits[18], to yield the required quantization fidelity. By using an intermediate frequency $f_{IF} = \frac{f_s}{4}$ it is possible to use the signal representation discussed in the following. This representation is the one adopted by the front-end used for this project.

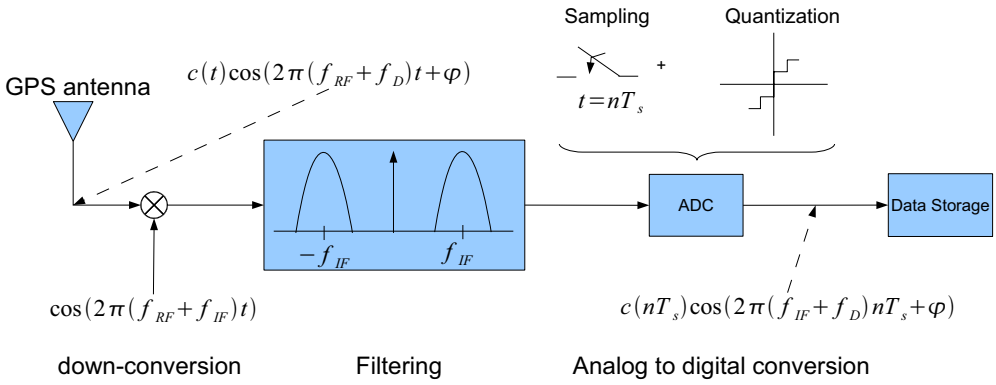

Figure 2.6: Front-end architecture.

The signal stored has the following form:

$$c(nT_s)\cos(2\pi(f_{IF} + f_D)nT_s + \varphi) \tag{2.2}$$

By assuming that $f_{IF} \gg |f_D|$, one gets:

$$c(nT_s)\cos(2\pi f_{IF} nT_s + \varphi) \tag{2.3}$$

If one writes $n = 2m$ one receives the even samples:

$$c(2mT_s)\cos(2\pi f_{IF} 2mT_s + \varphi) \tag{2.4}$$

For the odd sample one gets $n = 2m + 1$:

$$c((2m+1)T_s)\cos(2\pi f_{IF}(2m+1)T_s + \varphi) = c(2mT_s + T_s)\cos(2\pi f_{IF} 2mT_s + 2\pi f_{IF} T_s + \varphi) \tag{2.5}$$

Using the relation between the sampling frequency and the intermediate frequency $\left(f_{IF} = \frac{f_s}{4}\right)$, one gets:

$$c(2mT_s + T_s)\cos\left(2\pi f_{IF} 2mT_s + 2\pi\frac{f_s}{4}\frac{1}{f_s} + \varphi\right) \tag{2.6}$$

$$= c(2mT_s + T_s)\cos\left(2\pi f_{IF} 2mT_s + \frac{\pi}{2} + \varphi\right) \tag{2.7}$$

$$= c(2mT_s + T_s)\sin(2\pi f_{IF} 2mT_s + \varphi) \tag{2.8}$$

[18]Choosing $n_{bit} = 1$ will gives a signal loss of about 3 dB at the output, with $n_{bit} = 3$ the quantization loss became negligible.

From the above equations, one sees that by taking the even and odd samples one gets the real (in-phase) and imaginary (quadrature) components of the equivalent complex representation for the input signal.
Then one must store this data flow in real time on hard drives that have to be fast and large enough in order to be able to store this large amount of data.

2.3.5 Signal strength and statistics

As represented in figure [2.4], one can see that the signal strength of the GPS signal received on the earth surface is about -220dBW/Hz whereas the signal strength of the thermal noise on the receiver antenna is about -208dBW/Hz. An analogy to this level of signal to background noise is likened to observing a small light bulb from a distance of 2500km[6, p. 69]. The fundamental difference between the noise signal and the GPS signal is that the noise is a Gaussian random variable, while on the contrary the GPS signal is not random. So by observing coherently a random signal one can expect it to self cancel, and the non-random component to appear. Considering only the I branch for example one sees:

$$\sum_{y=0}^{N}(I_{s_x} + I_{n_x}) = NI_s + \sqrt{N}I_n \tag{2.9}$$

I_s signal I sample
I_n noise I sample
N number of coherently integrated(summed) samples

Considering this relation one sees that the signal component will grow faster than the noise component when samples of the composite noise plus signal are summated over time. One can note that summing is equivalent to integration since it works with time quantized values after analog to digital conversion stage of the receiver.
Knowing the probability density function (pdf) of the noise (see appendix[A.1]) in the receiver architecture is a useful piece of information, and can be used to decide if one has acquired the peak out of the noise or not. Because the GPS signal does not follow the pdf of the noise alone any out of prediction peak would be the indication of the presence of the GPS signal, as shown in figure [2.7].

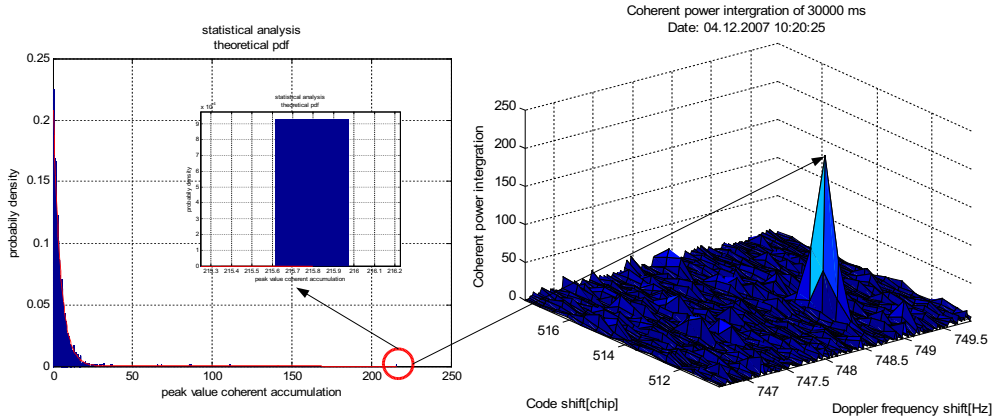

Figure 2.7: Left: pdf repartition of a real GPS signal, red line is the theoretical pdf; Right: peak obtained after 30s of coherent integration time.

2.3.6 Integration time

Herein the reader will be introduced to the theoretical aspects of Signal-to-Noise Ratio (SNR) increase through longer integration time. In this section we will assume that one uses a software receiver which is able to get the correlation peak in the search space in post-mission mode, and that one uses the transmitted data bits, collected for example with a second independent receiver. In doing so, we are able to compensate for the data bit sign of the incoming GPS signal, in order to increase the integration time of the post mission receiver to several seconds and beyond.

Coherent integration

If one accumulates I and Q separately for a fixed duration, and then squares and sums the result, one is said to be doing a coherent accumulation over the duration of the summation. This approach is the way to get the largest processing gain[19] for a given duration of signal samples. If one assumes C/No value of 47dB-Hz[20], the SNR minimum to get the peak is given by:

$$SNR = C/No + 10log_{10}(T_c) = 47 - 27 = 20dB \tag{2.10}$$

Assuming $T_c = 2ms$, is purely arbitrary and depends of the quality of the receiver.
Assuming now a given attenuation a, one may wish to determine what would be the time T_c needed to get a given peak quality(given SNR):

$$SNR = C/No - a + 10log_{10}(T_c) \tag{2.11}$$

[19]Only true if the oscillator introduced error are not too big, otherwise non-coherent accumulation could be better.

[20]Typical open-sky conditions.

To determine this, one must solve for T_c:

$$T_c = 10^{\frac{SNR-C/No+a}{10}} \tag{2.12}$$

For example, assuming $a = 30$dB, one would determine a coherent integration time $T_c = 2s$ to obtain the desired SNR. One should note that an $SNR_{min} = 20$ is a quite high value, with modern receivers able to work with values of SNR down to 14dB, which results in the determination of the formula:

$$T_c = 10^{\frac{14-47+a}{10}} = 10^{\frac{-43+a}{10}} \tag{2.13}$$

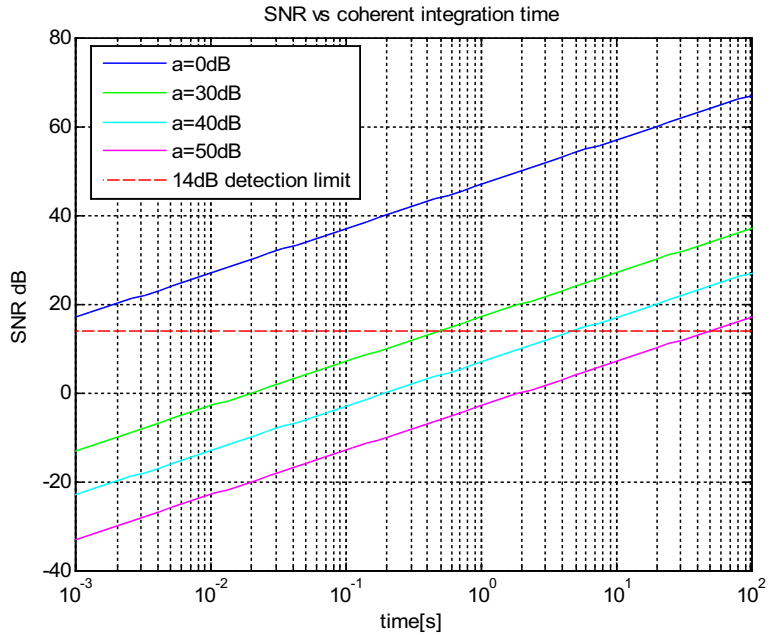

Figure 2.8: SNR versus coherent integration time for various C/No conditions.

Non-coherent integration

Doing a non-coherent integration consists of taking the sum several subsequent coherent integration results. For example, one non-coherent sum may consist of 20 adjacent 1 second coherent integrations. The gain obtained with this method is smaller than with coherent integration techniques, due to squaring losses incurred from increasing both the noise and the signal components, as discussed in [11, sec 3.9]

2.4 Future of GNSS

In the coming years, several new GNSS systems will certainly be launched or completed to reach global coverage, such as GLONASS (Russia), COMPASS (China) and GALILEO (Europe).

2.4.1 GLONASS

GLONASS is the Russian GNSS system, and shares the status of "operational" with GPS, as their satellites are already flying, and in the past comprised a complete constellation of over 20 space vehicles. Unfortunately, for the moment they are not able to propose a global coverage due to the existence of only 13 actively transmitting satellites. Despite the fact the network reached a complete constellation in 1991, financial problems after the collapse of the Soviet Union put the project in doubt, and reduced founding to a level not sufficient to maintain the satellite constellation at operational levels. President Vladimir Putin wants Russia to regain is political and technical power relative to the US, Europe and China, which has resulted in a plan to extend the GLONASS system to reach global coverage before 2011. Historically the Russian GLONASS satellites did not use the previously discussed CDMA technique, but instead utilized FDMA, whereby each satellite was broadcasting on a different frequency, which increases the technical difficulties and the cost of Glonass receivers relative to GPS. Russia will eventually consider also broadcasting CDMA signals with their new GLONASS-K satellites to allow further interoperability with the other GNSS systems.
Politically, it should be noted that India is a partner in the GLONASS project since 2007, as the government of India found negotiation to join the Galileo program was not satisfying enough from the military standpoint, and as a result, India is expected to assist in the replenishment of the GLONASS constellation in the near future. [21]
Figure [2.9] shows a rocket start three new GLONASS satellites.

[21] http://timesofindia.indiatimes.com/India_joins_Russian_GPS_system/articleshow/1502481.cms

Figure 2.9: Proton-M rocket carrying three new GLONASS satellites, blasts off from Baikonur cosmodrome, Kazakhstan, October 26th 2007.

2.4.2 COMPASS

COMPASS is the Chinese GNSS system, whose first medium earth orbit satellite, called M-1 was launched on the 14th of April 2007. The current system design calls for 30 Medium Earth Orbit, and 5 geostationary satellites. The International Telecommunication Union has reserved 4 frequency bands for the COMPASS system centered around: 1589.74MHz (E1), 1561.1MHz (E2), 1268.52MHz (E6) and 1207.14MHz (E5b). They will also divide their service between a civilian one, and an authorized military user component similar to GPS and GLONASS. Figure [2.10] shows the launch of the first Compass satellite M-1. For more information see [7].

Figure 2.10: First Compass satellite M-1, launched on April 14th 2007.

2.4.3 Galileo

Galileo is the European GNSS system, which for the moment has only one satellite called Giove-A in orbit[22]. The Galileo program has experienced delays due to funding issues between the various interested parties in the system, both at the political and business level. The root problem of course was the determination of exactly who will pay what component of the system. Recently these issues were resolved, with the decision that the whole program will finally be financed with public money, again similar to the GPS and GLONASS systems. Barring further delays, the constellation deployment is planed for 2011, leading to the interesting debate of whether it will be the Chinese Compass or the European Galileo that will next reach the status of a "complete" constellation. Figure [2.11] shows engineers at work during satellite preparation Giove A.

Figure 2.11: Giove A during satellite preparation.(Source: ESA / Surrey Satellite Technology Ltd)

[22]Giove-B has experienced some rocket problem and is still on the earth.

Chapter 3

Oscillators: Theory and Practice

3.1 Introduction

This chapter is essentially a literature review, designed to give the reader the basic oscillator[1] knowledge needed to understand the remainder of the thesis. Today, oscillators are of great importance, especially in the defense, positioning, communication, time keeping and general electronics fields. Being able to choose the right time reference for the right application considering the technical and economics characteristic of the system, is very important for any design engineer. With this in mind, some of the tools to understand the basic principles that rule the oscillator world will be provided.
The precision, accuracy and stability words are qualifiers that are necessarily used to characterize time references; herein we will examine their meaning in order to make sure of their correct interpretation in this thesis.
When qualifying frequency reference three properties have to be considered for determining their quality:

- **Precise:** refers to the target nominal frequency obtained compared to the desired one.
- **Accurate:** refers to frequency fluctuation around the obtained nominal frequency.
- **Stable:** refers to the same characteristics as the accuracy but over the time.

[1] More generally: frequency reference or frequency generator.

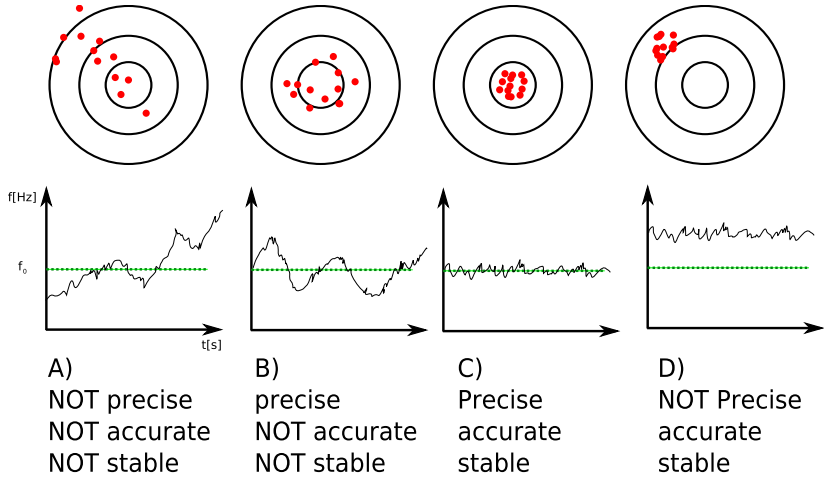

Figure 3.1: Precision, accuracy and stability comparison, inspired from [26].

Figure [3.1], case c) is of course the ideal situation, but one will never observe perfection in reality. One unavoidably arrives at a frequency offset like in case d). This can be corrected by doing a calibration procedure on the oscillator, while it is also possible to buy already calibrated devices within a certain range given in the data sheet. Case b) represents the performance of an oscillator that is correctly calibrated but experiencing poor frequency stability, while case a) is a model of what happens to all oscillators, as they drift over time. Of course the way they drift, will depend on the oscillator quality, and what is important to keep in mind is that every frequency reference is imperfect, the question is only how bad are the remaining instabilities.

3.1.1 Introductive example

One of the applications of precise oscillators are Frequency Hopping Systems, where the idea is to change the frequency of transmission several times per second, with the goal of avoiding jammers, which attempt to perturb the communication in a military application[2]. In the following example, one will assume that two users want to communicate with each other using frequency hopping, and that a 'perfect follower'[3] jammer try is trying to perturb the communication channel.

[2] A civilian application of this principle is the well known Bluetooth.
[3] As soon as the jammer receives a transmission, he is able to jam it at the correct frequency

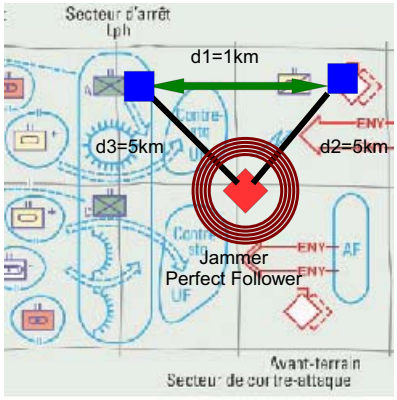

Figure 3.2: Fictional tactical situation, blue squares are allies that intend to communicate with each other, while the red square represents the Jammer(perfect follower), example inspired from[26], map from [24].

The RF propagation time is $3.3\frac{\mu s}{km}$. The time duration of a message per frequency (before jamming) is given by $t_{hop} = (t_2 + t_3) - t_1 = 30\mu s$, where the t_i represents the RF wave travel time for the distance d_i. This leads to a hopping rate of $\frac{1}{30\mu s} = 33.3kHz$. One will assume that the allowed clock error is equal to $0.2 \cdot t_{hop} = 6\mu s$, where the 0.2 is a rule of thumb factor.
The question now is how good must the oscillator be in each RF unit be to stay synchronized within $6\mu s$ for a given network re-synchronization rate. Note that one should keep re-synchronization rates as low as possible in order to avoid the network to being detected too easily by enemy electronic warfare troops. For the sake of argument it is assumed that one re-synchronize the network every 4 hours:

$$\frac{6 \cdot 10^{-6} s}{4 \cdot 60 \cdot 60 s} = 4 \cdot 10^{-10} \tag{3.1}$$

The number $4 \cdot 10^{-10}$ is unitless, and defines the oscillator precision is needed to realize this frequency hopping system.

3.2 Time keeping evolution

Being able to measure the passage of time has always been of great importance for human civilizations. Thus, even several thousand years before Christ the Mesopotamian and other civilizations including the Chinese developed the first calendars based on precise astronomical observations. Even prior to this, suggestions of time keeping can be found in remains of prehistoric societies.

But it is only with the beginning of the colonization process by the world powers[4]

[4]England, France, Spain and Portugal.

at the beginning of 17th century that the time keeping technology became joined to the science of geolocalization. At that time it was already possible to estimate his own Latitude (N-S) position using sun angle measurements and a calendar,[5] but the problem of determining the Longitude was almost unsolved.

Let's assume one defines 0° Longitude at Greenwich in England, to agree with modern maps, one also knows that the earth rotates on itself in exactly 24 hours, so one can directly relate the time with the distance (angle of Longitude) the planet will rotate through. If one knows the solar local time of the 0° Longitude point and the locale in which one is interested to get the Longitude, one simply calculates the time difference and transforms it to an angular value. Getting the user local time is relatively easy, as it is alway possible to measure the sun highest point to get the local midday time. To then get Greenwich local time, the simplest solution was to take a clock on board the boats. The time requirement set during a clock design competition in Britain was to be precise within 2 minutes after 2 months of use at sea (vibration, shocks, humidity, temperature variations,...). John Harrison (1693-1776)[6] was the first to accomplish and surpass this level of stability, with his last product the mechanical chronometer H4 able to keep time within 5 second after 82 days at sea[7].

Figure 3.3: John Harrison (1693-1776) was the winner of the Longitude Prize.

Figure [3.4] displays the time keeping evolution history. Interesting to note are the capabilities of the NIST-F1 cesium fountain[8], which according to its web site[9] can reach a frequency uncertainty of $5 \cdot 10^{-16}$, which means assuming the time uncertainty to be

[5] One can note that a calendar is just a (passive) clock with a one day accuracy.
[6] He also won the longitudinal price of 20000 Pounds Sterling, several millions of today Euros.
[7] More information can be found here: http://www.solarnavigator.net/history/john_harrison.htm.
[8] NIST: National Institute of Standards and Technology, United state governmental agency
[9] http://tf.nist.gov/timefreq/cesium/fountain.htm

linear in time, this clock can potentially keep the time within 1 second for 60 millions of years:

$$5 \cdot 10^{-16} \cdot 60 \cdot 10^{6} \cdot 365 \cdot 24 \cdot 60 \cdot 60s \cong 1s \tag{3.2}$$

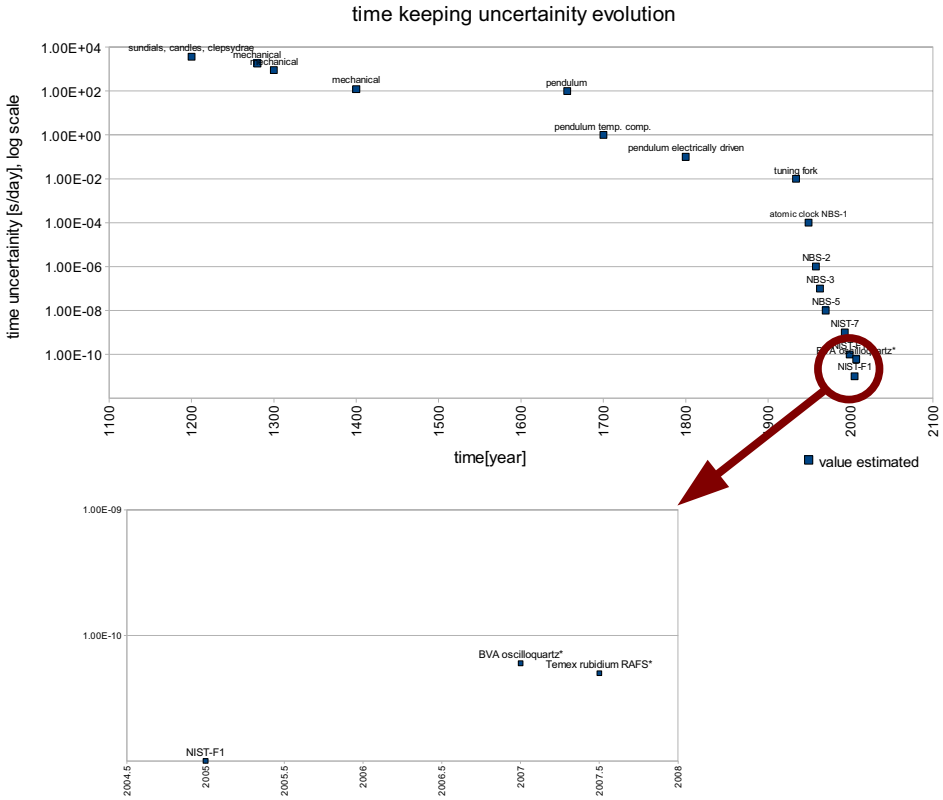

Figure 3.4: time keeping evolution representation

3.3 Quartz

The quartz crystal is the essential material of today's most common oscillators. Quartz basic molecule is SiO_2, meaning one silicon atom and two oxygen atoms. These two elements compose the majority of the earth's crust, meaning that quartz is not rare in nature. Quartz is solid at room temperature and appears usually in a crystalline form. The crystal properties of quartz are the key to understanding quartz based oscillators. The goal here is not to give the reader a full text book description of crystals, but to provide the basic tools necessary to understand crystal oscillator behavior. Nevertheless people interested to go deeper inside crystals and solid state theory should direct attention to references [13] and [10].

3.3.1 Physical basics principles

The basic oscillator principle is to be able to build a circuit that has a specific resonance frequency, that will be excited by an external force. Basically it is possible to build an oscillator using Resistors, Inductors and Capacitors(RLC) parts only, if done in a well designed circuit, but the resulting oscillator will for various reasons have poor performance. Using quartz crystals as the resonating component is a more desirable and more common approach. This very well known effect of the resonance frequency of mechanical structures does not only apply to quartz, but also to physical structure, such as bridges. Anyone can demonstrate this by standing at the center of a small wood, or light metallic bridge, and jumping at the right frequency (i.e. the resonance frequency of the bridge), one can cause the structure to resonate. On a large scale, this effect could lead to dramatic incidents like the wind induced excitation of the Tacoma Narrows Bridge in November 1940. Since this famous resonance induced collapse, design engineers have tried to adapt structures to avoid resonance with wind, or other natural influences.

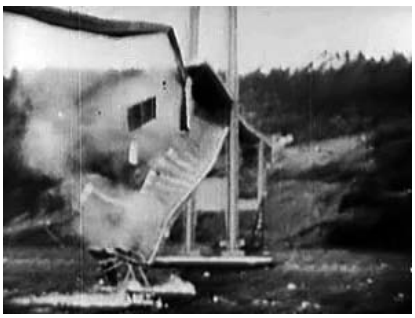

Figure 3.5: November 7^{th} 1940 Tacoma bridge collapse, because of the wind excitation at the resonance frequency of the structure.

In the case of an oscillator the mechanical structure of the quartz is electrically exited using the piezoelectric effect, which is a property exhibited by certain materials, including quartz, whereby if an electric tension is applied at the edges of the crystal, one will cause a mechanical deformation of the crystal. The inverse is also true, where an appropriate mechanical deformation is applied on the crystal, one will produce a voltage on the electrodes. This effect is due the geometrical repartition of the atoms in the crystal and to the fact that the oxygen (χ = 3.44) atoms have a stronger electro negativity than their Silicon (χ = 1.9) counterpart[10]. The consequence is that plus (Si atoms) and minus (O atoms) “poles” appear in the crystal.

[10]The electro negativity is a measure of how strongly the electrons are attracted by the owner atoms.

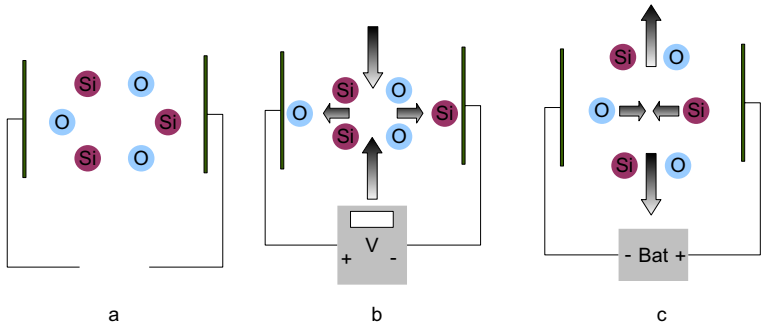

Figure 3.6: Simplified representation of the piezoelectric effect in a quartz crystal. a) system when neither electrical nor mechanical force are applied b) External mechanical force applied on the crystal resulting in a voltage c) Application of an electrical force resulting in a mechanical force displacement.

Let's now assume one applies a tension momentarily and then stops. In this case, once the crystal is mechanically deformed and the electrical field removed, it tends to recover its original shape. During this recovery process the crystal will produce a tension at the electrodes, consequently if one amplifies this signal and feeds it back to the crystal, one would soon get to the resonance frequency where the vibrations are self sustaining. It should be noted that for quartz crystals, there is a fundamental resonance mode as well as multiples of this frequency known as overtones. To get the crystal to resonate in an overtone mode, some special start techniques are necessary.

3.3.2 Vibration modes

The vibration modes are the way the crystal is vibrating and in which overtone. The choice of the vibration mode will strongly influence the performance of the oscillator.

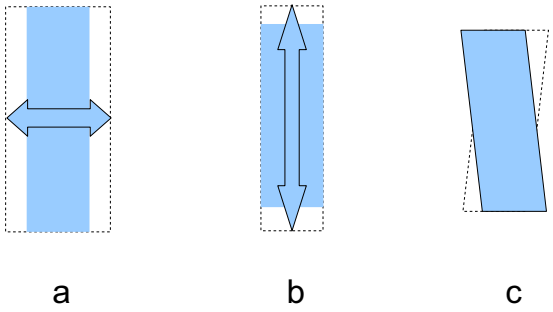

Figure 3.7: Schematic representation of the vibration modes. a) Longitudinal mode, b) Transversal mode, c) Shear mode.

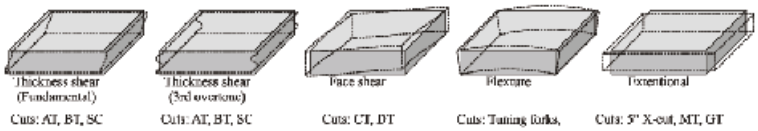

Figure 3.8: Schematic representation of the vibration modes. Here the shear 3rd overtone mode of the SC-cut crystal is of interest, because the best close-in phase noise behaviors are obtained using this mode of vibration. Source: [3].

3.3.3 Crystal cut

The quartz crystal properties are strongly anisotropic, meaning depending of the crystal orientation one can observe significant differences in the physical properties. Quartz specialists use the term "crystal cut" to assign the orientation in which the crystal is cut.

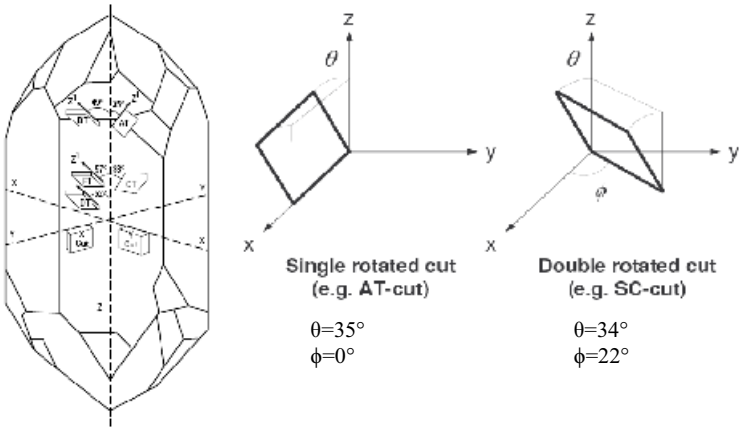

Figure 3.9: SC-cut and AT-cut representation. (Source: [21], [17])

There exist many cuts, but in this section the analysis will focus on two of the more popular ones: the SC-cut and the AT-cut. The SC-cut shows better performance compared to the AT-cut, but it's also far more expensive to manufacture. Referring to [26] and [21] one can list the major differences between the two, were relative performance Sc-cut compared to AT-cut is:

- better thermal transient compensated (allows faster warmup OCXO)
- better f vs. T repeatability allows higher stability OCXO and MCXO
- planar stress compensated
- less sensitive to radiation

- has higher Q (quality factor) for fundamental mode resonators of similar geometry
- less sensitive to plate geometry - can use wide range of contours
- is more expensive

3.4 Quartz oscillators type and behavior

The aim of this section is to present the different families of quartz oscillators available today and their standard characteristics. The term Crystal Oscillator is commonly abbreviated XO, the reason the more obvious term "CO" is not used instead, is that when this designator was chosen, the US Army was funding most of the research in that domain and in the US Military language CO means Commanding Officer. In order to avoid confusion, it was therefore not advisable to use the "CO" designation, resulting in the identification of "XO". One can represent a quartz crystal with an equivalent model using RLC components as follows:

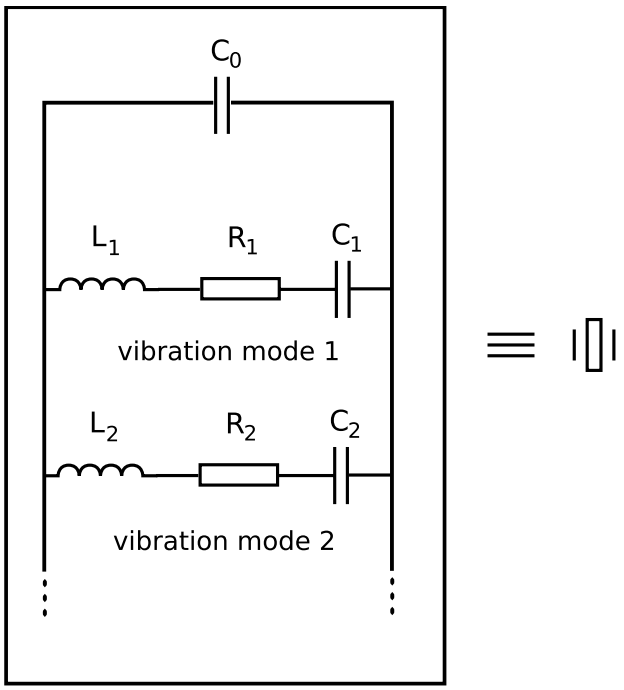

Figure 3.10: Equivalent RLC circuit of a quartz crystal

3.4.1 XO

This is certainly the simplest quartz based oscillator, being composed of only a vibrating part in quartz, and of an amplifier. Nevertheless the recent XOs use cuts that compensate

temperature and stress drift even though XO oscillators are often low cost products (less than 0.1 €), low power and their package size is less than $1cm^3$.

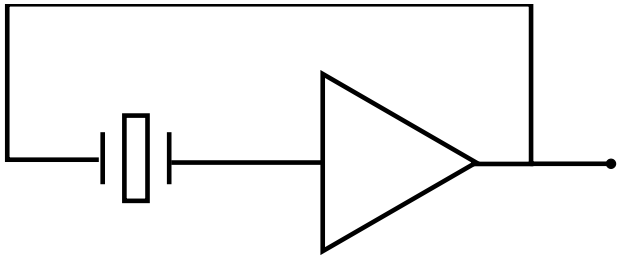

Figure 3.11: Scheme of a Crystal Oscillator(XO).

3.4.2 VCXO

The Voltage Controlled Crystal Oscillators (VCXO) are oscillators in which one can tune the frequency to a certain range by applying a voltage at the edges of a special diode called a varactor. This electronic device has the property of varying capacitance as a function of the applied voltage, so by introducing this in series with the resonator one is able to vary or tune the resonance frequency of the quartz resonator + varactor diode circuit. This feature is useful to calibrate the oscillator statically, or to dynamically compensate a known frequency drift[11] with an external compensation circuit.

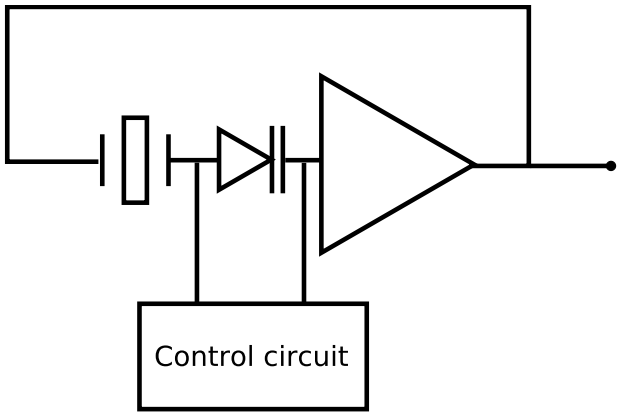

Figure 3.12: Scheme of a Voltage Controlled Crystal Oscillator (VCXO).

3.4.3 TCXO

The Temperature Compensated Crystal Oscillator (TCXO) is essentially a VCXO with an external compensation circuit. This circuit measures the environment temperature and

[11] Per example due to the temperature, acceleration,...

calculates what voltage to apply on the varactor diode in order to maintain the frequency output as close to the desired frequency as possible, using the frequency vs temperature model of the resonator.

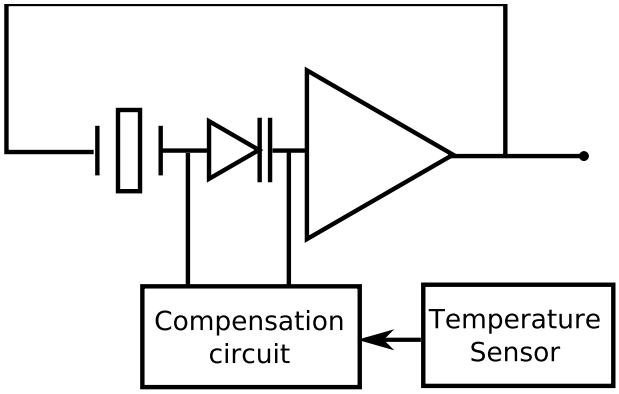

Figure 3.13: Scheme of a Temperature Compensated Crystal Oscillator (TCXO).

3.4.4 OCXO

With an Oven Compensated Crystal Oscillator (OCXO) the concept of operation is to maintain the crystal at a constant temperature, by putting it in an insulated oven. The temperature of the oven is constantly checked by an electronic circuit to shield the oscillator from temperature changes in the environment. The working temperature of the oven is set at the 'turn over' point of the curve of figure[3.18], in order to smooth the effect of residual oven temperature variation on the resonance frequency.

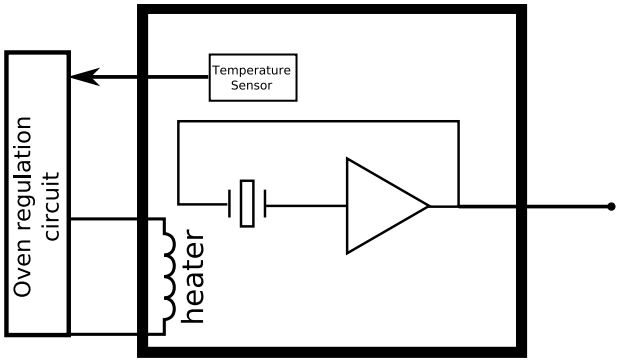

Figure 3.14: Scheme of a Oven Compensated Crystal Oscillator (OCXO).

3.4.5 DOCXO

For the Double Oven Compensated Crystal Oscillator(DOCXO) the idea is the same as that of the OCXO, with the addition of an outer oven around the first one. Through

this modification, better temperature control of the oven that contains the crystal can be achieved. One might also put the temperature sensitive electronics inside the external oven to avoid temperature dependences on the control circuits. In some DOCXO oscillators, thermal proof envelopes are also added (like in a thermos), to better isolate the oven from the environment.

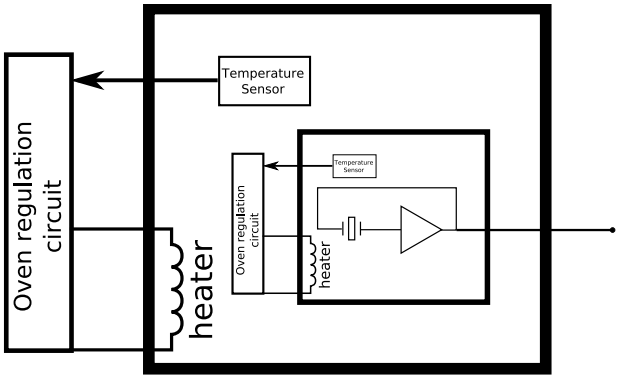

Figure 3.15: Scheme of a Double Oven Compensated Crystal Oscillator (DOCXO).

3.5 Output signal behavior and characterization

3.5.1 Aging-drift

Aging is the sum of all modifications to the output signal on a long term basis (minute/day/month/year/... scale) and due to the oscillator itself. Aging is essentially a predictable effect due to internal changes in the oscillator like:

- Stress relief in the bounding structures
- Molecule absorption and desorption from the crystal and walls of the oven
- Oven circuitry aging
- Pressure change in the chamber

Knowing that the mass of the quartz resonator is directly related to it resonance frequency leads to the realization that when there are mass variations, there will also be a resonance frequency change. A relevant rule of thumb for this is 1 monolayer of the quartz crystal corresponds to 1 part per million (ppm) frequency change, i.e. 5Hz for an 5MHz oscillator. Due to the importance of this issue, some solutions exist to avoid or limit such mass exchange, such as BVA technology (see 3.5.6) and placement of the quartz resonator under vacuum or ultra high vacuum conditions, in order to lower the number of gas molecule impinging on the quartz surface per unit of time (i.e. lower the surface interaction probability). One should note that the crystal and walls outgassing

can vary the pressure in the chamber which also participate in the aging process.
The oscillator warm-up time can be considered as an aging process, where the oscillator needs a certain time to stabilize its output frequency. This time is usually short (<1s) for low cost oscillators, but can reach several weeks for a state of the art DOCXO. Oven based technology is the slowest to complete the warm-up process because they need to reach the final to oven temperature set point very precisely, where the stabilization period represented in figure [3.16]. During this time ovenized oscillators usually draw more current than during normal work condition.

If one switches the oscillator power Off, and turns it On again, even shortly, one will have almost to start the entire stabilization period over to settle again to the data-sheet performance. As a result, it is very important to be sure that the stabilization period has been respected before beginning to use the oscillator, otherwise the performance could be much lower than expected. This phenomenon can be easily observed by taking a cold oscillator[12], turning it On, observing the output frequency one can observe that the frequency takes time to reach the oscillator nominal frequency. Once it's done, it doesn't mean the stabilization period is over, because other parameters has certainly not yet reached their data sheet values, including phase noise for example.
The term drift refers to all the effects of aging plus the effect of the environment on the oscillator like:

- Temperature variations.
- Shocks.
- Vibrations.
- G-force.
- Acceleration-deceleration.
- Humidity, water infiltration/diffusion.

3.5.2 Short term instabilities - Noise

In the proceeding section, one has seen the long term instabilities of the frequency represented by the red line in figure [3.16], those variations are mostly predictable for a given and known oscillator model. The short term (second scale or smaller), variations are however unpredictable ones, collectively referred as noise. These instabilities producing noise are essentially due to:

- Johnson noise, which is the fundamental limitation for the noise of oscillators [28].

[12] preferably a "big" OCXO

- Phonon scattering and quantum fluctuation. Phonons are quantized mode of vibration in crystal lattices. Their study explains some electrical and thermal behavior of the crystal.
- Electronic active and passive components of the oscillator.
- External vibrations.
- Stress relief at the interfaces (quartz, electrode, mount, board).
- Thermal effects.
- Fluctuations in the number of absorbed molecules at the quartz surface.
- Other unknown sources...

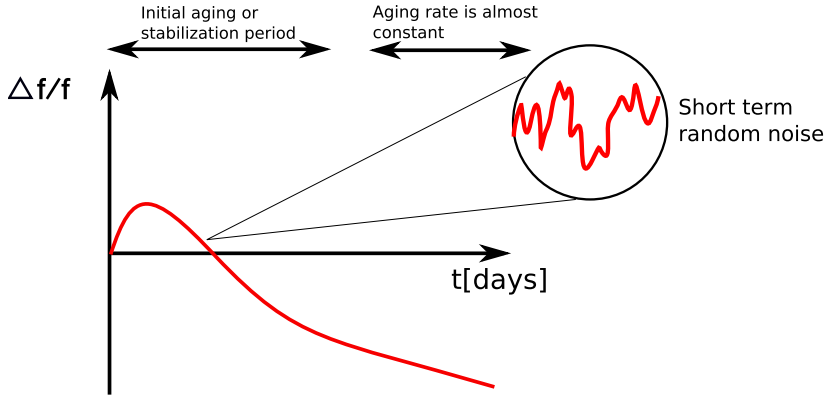

Figure 3.16: Oscillator aging is divided into two zones: the stabilization period and the zone where the aging rate is almost constant. On top of the long term variations there are short term instabilities also called noise.

3.5.3 Allan variance, deviation

One way to characterize the short term instabilities of an oscillator is the Allan variance ($\sigma^2(\tau)$)[2] or Allan deviation($\sigma(\tau)$). In the oscillator data sheet one will typically find either a plot as a function of τ or a set of discrete values to quantify oscillator stability. By definition one has:

$$\sigma_y^2(\tau) = \frac{1}{2}\langle (y_{n+1} - y_n)^2 \rangle \tag{3.3}$$

where y_n is:

$$y_n = \langle \frac{\delta f}{f} \rangle \tag{3.4}$$

$\langle \cdot \rangle$ denotes empirical average
n is the sample index

τ is the time interval between two samples
f is the nominal frequency
δf is the frequency error
y_n is the normalized frequency error over the time interval τ

The Allan deviation, equal to $\sigma(\tau)$, gives an idea of how stable on average an oscillator is over a given time interval, so theoretically to fully quantify the stability of an oscillator, one has to average over an infinite number of samples. In reality one takes a finite but large enough number of sample for analysis[13].

3.5.4 Phase noise

Ideally an oscillator should provide a sinus as output signal, but in reality one will observe the sinus at the nominal frequency plus other extraneous signals at different frequencies. On a phase noise diagram one represents the power of the signal relative to the carrier (nominal) frequency in dB:

$$N_{singleSideBand} = 10 \cdot log_{10}\left(\frac{P_{f0}}{P_{\Delta f}}\right) \tag{3.5}$$

The diagram (see figure [3.17]) is called single side band phase noise because one assumes that for negative Δf one will observe the same behavior than for a positive one, if one restricts consideration sufficiently close to the carrier frequency. As this approximation tends to hold well, phase noise is commonly represented as only the single sided quantity.
The close-in frequency is the most critical because due to the proximity of the nominal frequency it's difficult to filter any noise here out. Experience shows that the best close-in noise performance is obtained by using a 5th overtone AT-Cut or a 3rd overtone SC-Cut crystal.
Of prime importance is some application in the knowledge that the phase noise performances of an oscillator dramatically decreases when the oscillator is exposed to vibrations.

[13] typically 50 or more

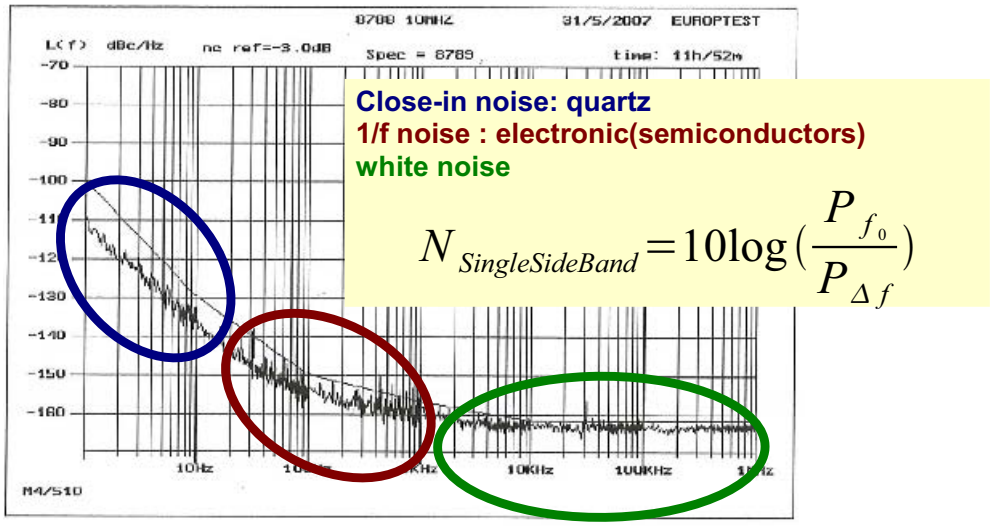

Figure 3.17: Phase noise diagram. (Source: Oscilloquartz SA)

3.5.5 Temperature behavior

Environmental temperature influences the crystal resonance frequency as shown in figure [3.18]. As the reader can observe, the curve of the resonance frequency vs temperature has two turning points where the curve is quasi flat for a certain temperature range. By exploiting this property, and working near these turnover temperatures, one is less sensitive to environment temperature variation. In the case of OCXO's one sets the oven to work at one of those temperatures, while one can also find crystal resonator exhibiting such flat temperature behavior at room temperature see [3.6.1]. In the case of the SC-cut one will observe a flatter curve at turning points than for a comparable AT-cut, which in turn means that SC-cut based oscillators will tend to be less sensitive to oven temperature variation than their AT-cut counterparts.

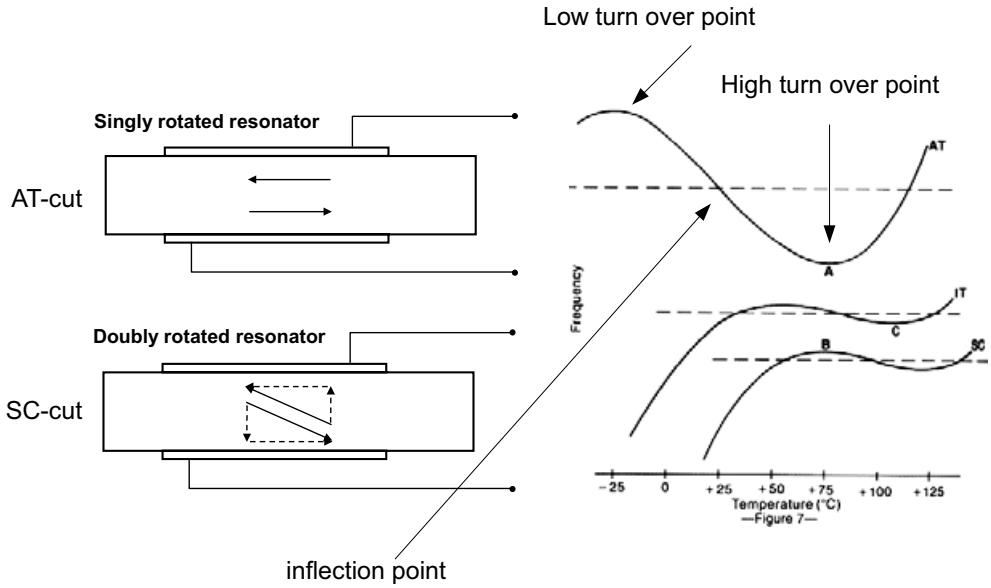

Figure 3.18: Resonance frequency vs temperature for AT and SC-cut. (Source: [26],[25])

3.5.6 BVA technology

The BVA[14] technology has been developed to avoid mass (atoms) migration between the quartz crystal and the oscillator circuit electrodes. Because the resonance frequency is dependent on the mass of the resonator, avoiding mass transfers offers better frequency stability in time. This technology was originally developed for AT-cut resonator by Prof. Dr. Raymond Besson (Laboratoire de Chronométrie Electronique Piézoélectricité, Besançon, France) in the 1970's. In 2006 Dr. Besson was recognized with the European Frequency and Time Award for his research on the BVA. In the 1980's Oscilloquartz SA bought the license for this technology and developed the SC-cut BVA which takes also advantage of the SC-cut crystal properties.

[14]French: Boitier à vieillissement amélioré, better aging case

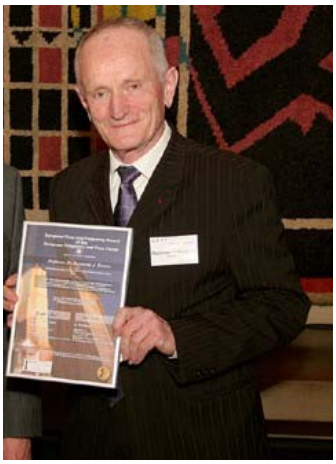

Figure 3.19: Prof. Dr. Raymond Besson was awarded at European Frequency and Time Award for is research on the BVA. (Source: http://eftf2006.ptb.de/award.htm)

The fundamental idea of the BVA technology is to avoid direct physical contact between the electrodes and the crystal resonator, and is basically accomplished by simply building a gap between the majority of the electrode and of the crystal structure. While conceptually simple, this is a complex manufacturing process which dramatically increases the price of such oscillators.

- + electrode generated stress vanishes
- + mount stress is lower
- + less atomic diffusion
- - difficult to produce
- - price

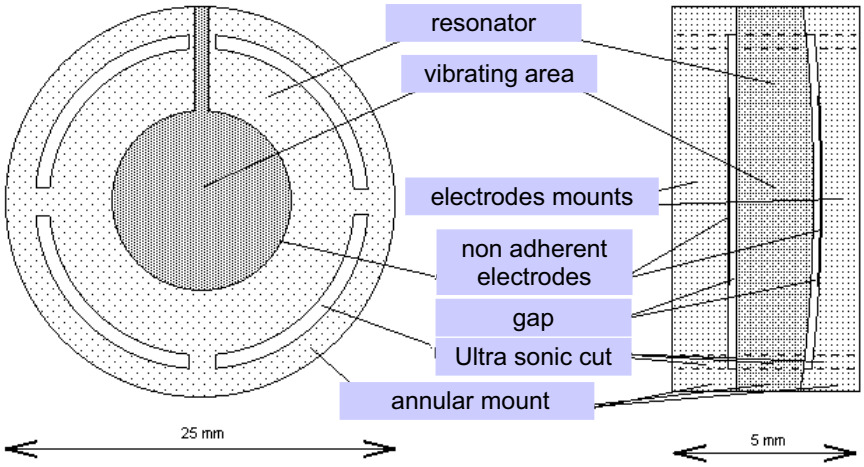

Figure 3.20: Scheme of the Oscilloquartz BVA technology [22].

The state of the art oscillator using the BVA technique is the Oscilloquartz 8607, which is a DOCXO, BVA, SC-cut 3rd overtone crystal. This oscillator achieves very good performances in: phase noise(-125dBc@1Hz), short term stability($\sigma(\tau) = 5 \cdot 10^{-13}$), temperature stability($2 \cdot 10^{-10}$) and aging($4 \cdot 10^{-9}$ per year)[15].

[15] value for standard option extracted from the 8607 datasheet: http://www.oscilloquartz.com/file/pdf/8607.pdf

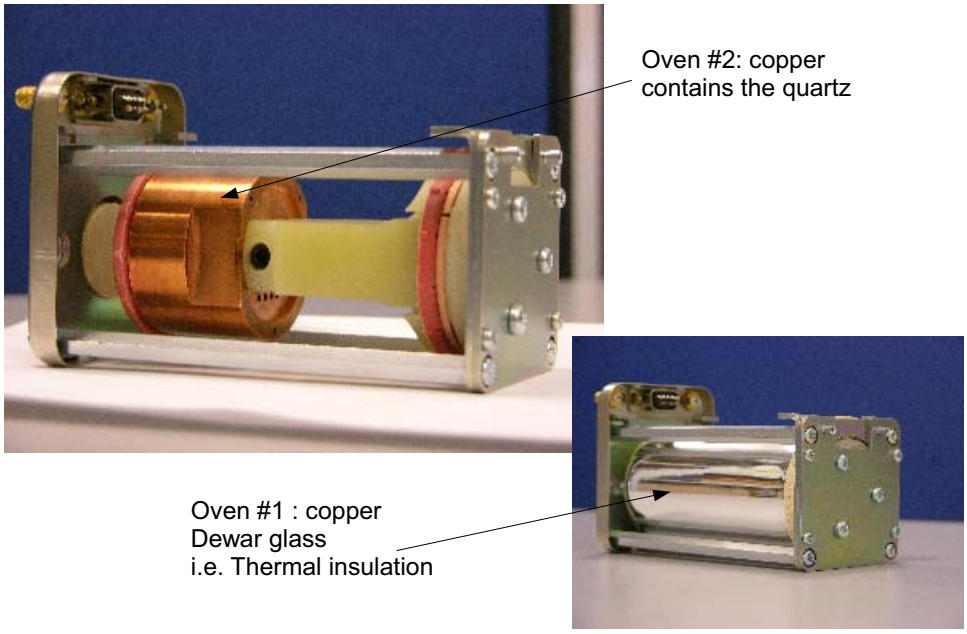

Figure 3.21: Pictures of the internal components of an 8607. (Source: Oscilloquartz SA)

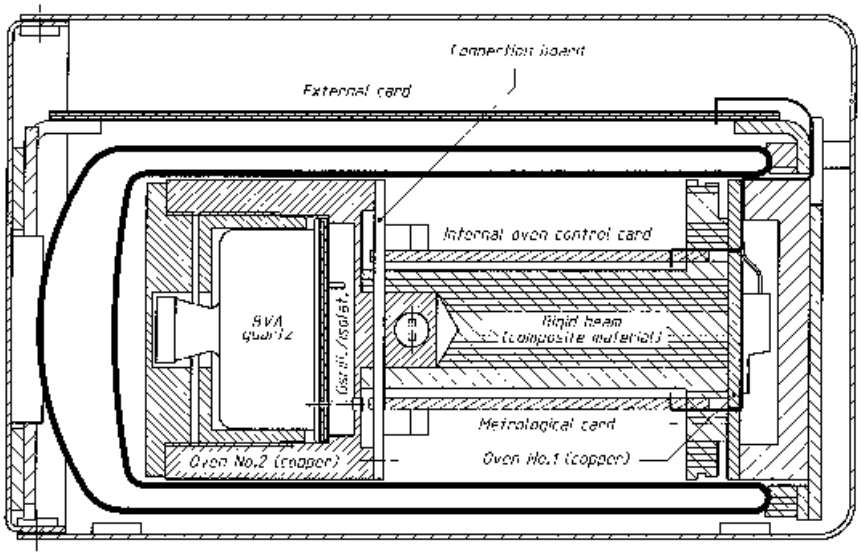

Figure 3.22: Cut view of an 8607. (Source: Oscilloquartz SA)

3.5.7 Fundamental limitation of XO's

Based on the discussion in article [29], the question of consequence is: can we in the future manufacture much better quartz based oscillators, or is there some fundamental physical limit? One assured limitation is the resonator resonance frequency, as it is given that thinner quartz leads to higher resonance frequency. Studies have shows that the physical limit to this thinning is approximately 15 quartz monolayer's which corresponds to a resonance frequency of 40 GHz.
Concerning the other parameters there is no knowledge or indication as to if there is a fundamental limit. Nevertheless a non-technical fundamental limit is the price that consumers are ready to pay for ultra high precision oscillators.

3.6 Other resonators types

The goal of this section is to present other oscillator families also available on the market today.

3.6.1 Tuning fork

Tuning fork oscillators use the same idea as that of the musical tuning forks, used to tune instruments. This kind of oscillator is principally used in the watch industry, due to their low cost, and low power operation. Figure [3.23] shows a representation of the resonance frequency vs temperature behavior of a typical tuning fork type oscillator, indicating that the flat zone of the curve is situated between 19°C and 35°C, corresponding to room temperature and human body skin temperature. Those temperatures reflect the normal operating conditions of a wrist watch, which will rest on the bedside table during the evening (room temp. 19°C - 22°C) and on a human (29°C - 34°C) during the day.

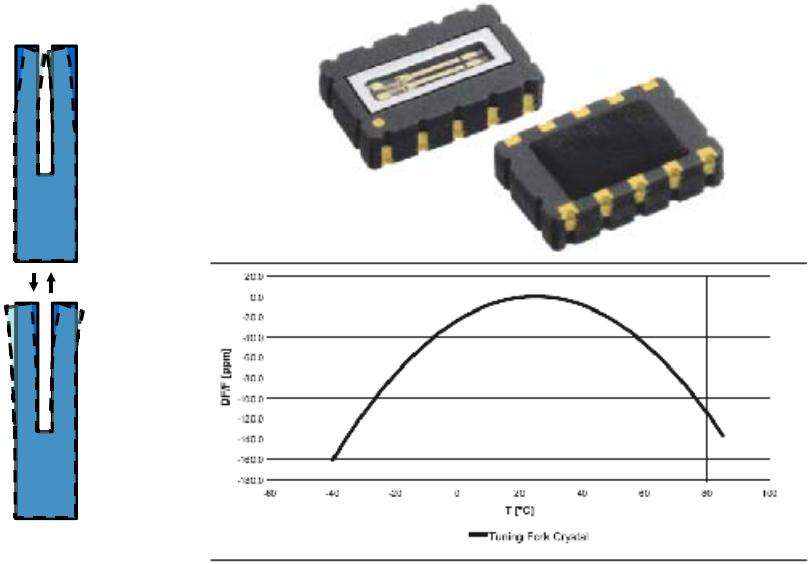

Figure 3.23: Tuning fork based oscillator[14].

3.6.2 Silicon oscillators

These oscillator types aren't a quartz based technology, as they are instead entirely made of silicon. The original idea behind this approach was that silicon also exhibited interesting piezoelectric behavior similar to that of quartz, combined with the fact that one can use Complementary Metal-Oxide-Semiconductor (CMOS) compatible technology to manufacture them, potentially allowing electronic Integrated Circuits (IC) and the Microelectromechanical Systems (MEMS) based oscillators on the some piece of wafer. This could in turn potentially save money, and decrease the size and power consumption of the circuits, but currently one is not able to produce the MEMS oscillators and the associated electronics with a sufficiently high yield[16] to be economically interesting. Nevertheless the manufacturers of this technology have stated these oscillators exhibit better performance than their equivalent quartz based counterparts see http://www.sitime.com for more informations. The better actual frequency stability performance of the Sitime MEMS oscillators are currently on the order of 50 to 100 ppm. This technology is for the moment not able to produce highly stable oscillators but in the future one can envision consequent performance increases.

[16]number of working device divide by the number of manufactured devices

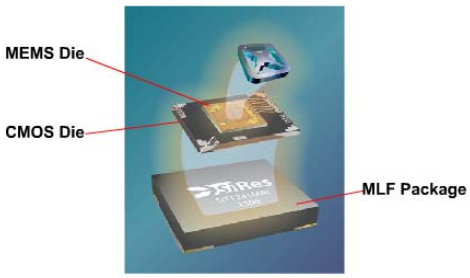

Figure 3.24: Silicon based oscillator. (Source: http://www.sitime.com)

3.7 Atomic clocks

The idea behind developing atomic frequency references is to get an absolute, unchanging frequency reference. Unfortunately for the moment this is possible only as an ideal case, nevertheless based on quantum mechanics, one knows that one can get an absolute energy reference, namely the atomic energy transition, and going from the energy reference to the photon frequency is straight forward using basic physics relations:

$$\nu = \frac{\Delta E}{h} = \frac{E_2 - E_1}{h} \tag{3.6}$$

ν is the photon frequency
ΔE is the energy difference between the quantum state ψ_{E2} and ψ_{E1}
h is the plank constant

Quantum mechanics law says that the atom can change from the low energy level E_1 to the higher energy level E_2, only if the energy of the photon($E_{ph} = \nu h$) exactly match the energy difference between the two levels, see figure [3.26]. The energy levels considered in the atomic clock technology are hyperfine transitions, which are spin related energy states. The lower energy state has nuclear spin "up" and the outer shell electron has the spin "down" state, a hyperfine transition occurs when the electron spin transitions from "down" to "up". To observe these useful hyperfine transitions, one has to use an element from the first column of the periodic table[17], as one requires that only one electron exists in the outer shell see figure [3.25]. Otherwise if one has two electrons, the Pauli exclusion principle[18] says if one particle is spin up the other has to be spin down.

[17] or ions
[18] two different particles can't be in the same quantum state

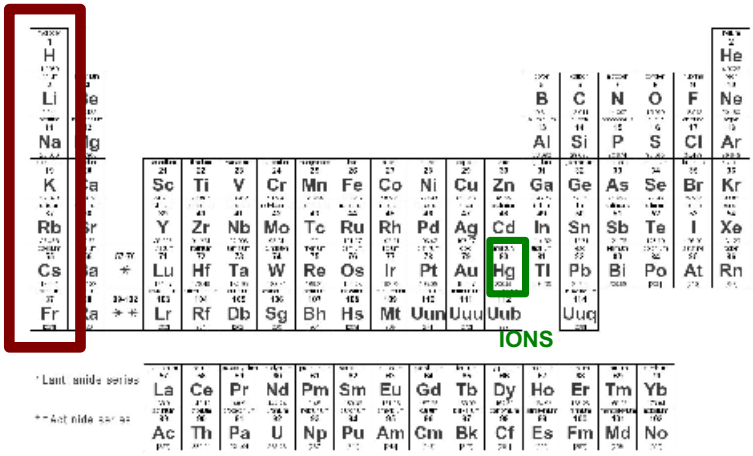

Figure 3.25: Elements used in atomic reference technology.

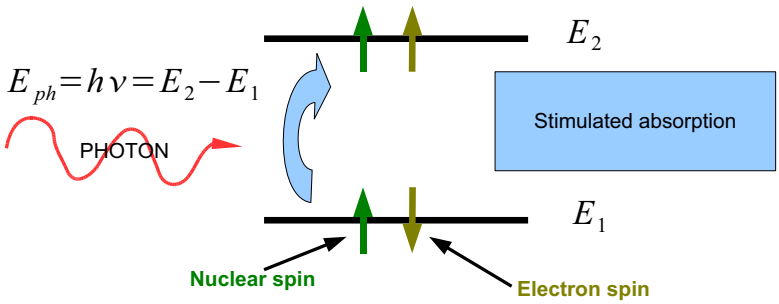

Figure 3.26: Stimulated absorption of a photon occurs only if the photon energy matches the energy level difference.

In the case of the cesium atomic reference, one produces Cs-vapour in a chamber, where this vapour contains the two atomic varieties i.e. a certain proportion of atoms have the quantum state ψ_{E1} and the rest ψ_{E2}. The spin is directly related to the magnetic properties of atom, so one forces the Cs atomic beam to pass through a magnetic filter (see figure [3.27]) which splits the atomic beam. One then selects the beam that contains the ψ_{E1} state, to enter a microwave cavity, wherein one generates an electromagnetic wave in the microwave range(i.e. photons energies are in the microwave range) in order to excite the atom to the quantum state ψ_{E2}. Only the photons with the right energy will be able to excite the atoms correctly, and once the atomic beam leaves the microwave chamber, one filters it one more time with a magnetic field, finally putting a detector to count the number of ψ_{E2} state atom at the output. The idea is to vary the excitation frequency to maximize the number of observed ψ_{E2} state atoms on the detector. Once one reaches this maximum, one uses the excitation frequency signal to feed the quartz oscillator correction circuit. One can note that since the output frequency of the oscillator

is also used to generate the microwaves, one has feedback system, see figure [3.28]. The consequence from the fact that every atomic reference uses a quartz oscillator at the output is that the short term performance of atomic references depend essentially on the quartz oscillator, rather than the underlying atomic transitions which dictate long term performance.

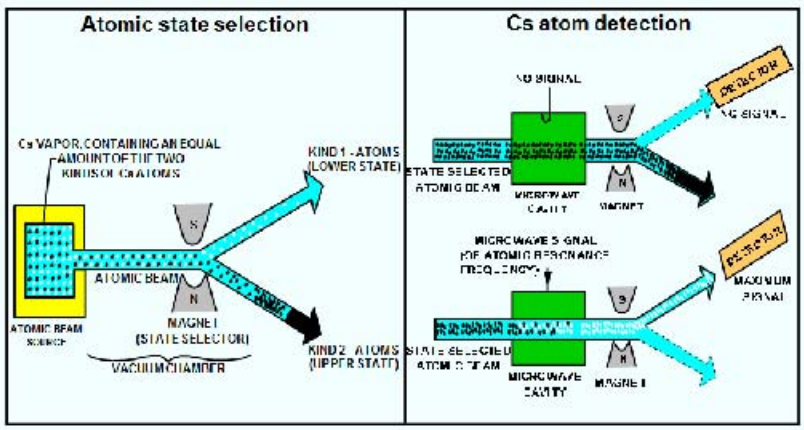

Figure 3.27: Schematic operating principle of a Cesium atomic clock[12].

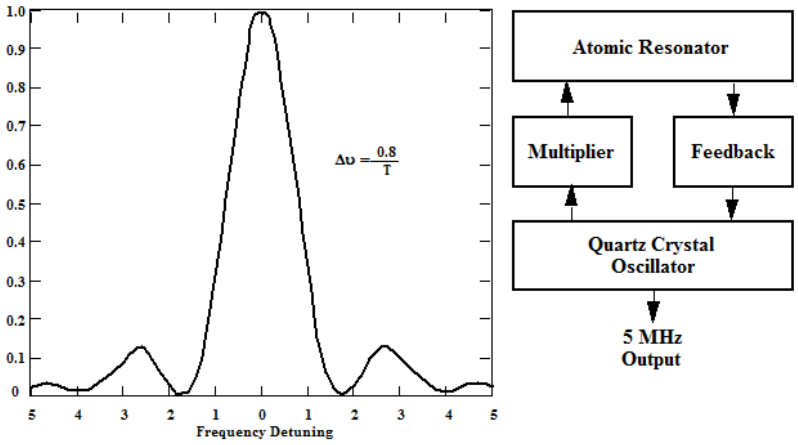

Figure 3.28: General working principle of an atomic clock[12].

Limits for the precision of an atomic clock:

- The Doppler effect: when the atoms enter the microwave cavity they are “hot”, meaning they randomly move around rapidly, such that if an observer would sit on a given Cs-atom he would not see the microwaves with the right frequency but slightly shifted due to the Doppler effect. To avoid this problem, one may

observe the atomic transition of atoms at lower temperature, which is the source of improvement in the so called Cs atomic fountains[19], which use laser cooling to slow the individual atoms.

- Resonance line width is inversely proportional to the coherent observation time.(Collisions with other atoms or apparatus walls interfere with this measure).
- Heisenberg: $\Delta E \Delta t \geq = \frac{\hbar}{2}$, where ΔE is the precision of measurement of the energy transition (i.e. the frequency) and Δt is the coherent observation time interval. So a smaller ΔE implies automatically a greater Δt. Generally speaking longer observation time means smaller frequency uncertainty.

[19]Cs fountains have the additional advantage of allowing increased observation time

Chapter 4

Experimental set-up

4.1 General principles

The main goal of this thesis is to explore and quantify the influence of oscillator on GNSS[1] signal processing. When speaking about oscillators, it is understood one is referring to both the oscillator in the receiver on the earth as well as those in the satellites. The general idea is that one uses a post-mission software receiver that is capable of predicting the Doppler shift, and compensating for the satellite motion. Assuming that the user (the remote antenna) is stationary, the atmospheric conditions are stable and that the other error sources are negligible, the only remaining error source in the frequency domain would be the one introduced by the oscillators them selves (local and satellite). Here one can then process the data and analyze the oscillator characteristics, by measuring the frequency deviations, and obtain the Allan deviation and the coherent integration time limits of the oscillator pair (satellite plus receiver) under test.
The next step is to test the integration time capabilities in a real indoor environment, with multipath and real attenuation which requires one to put an antenna indoors, for example in the corridor and then attempt to acquire a satellite from the recorded samples from the antenna. If one succeeds in finding this signal, it would be a sufficient proof one is able to integrate to a certain amount of time, and would also allow more information to be extracted on the given oscillator's capabilities.
To be able to integrate over durations several orders of magnitude over 20ms, one must use a data aided or AGPS technique, such as two receivers, with one reference receiver recording the broadcast data bits and the other one simultaneously recording the I and Q data, for later combination. For data synchronization purpose the two data sets are time tagged with a pulse signal generated by the reference receiver as it is better explained in section [4.4.4].

[1] here we consider only the GPS L1 signal, but this method can be conceptually generalized to other signals such as Galileo

4.2 Hardware

This section will present the different hardware configurations used for collecting data, and will also introduce the reader to the different experimental set-ups used in this study, as well as their justification. Please note that for clarity reasons the oscillators will be treated in a dedicated section hereafter (see [4.3]). The data collection methodology and the software for the data manipulation are detailed respectively in the appendices [C] and [E].

4.2.1 Open-sky mode

This setup collects data from an outdoor antenna situated on the roof, so the receivers connected to this antenna see no extra attenuation, and hopefully as little multipath as possible.

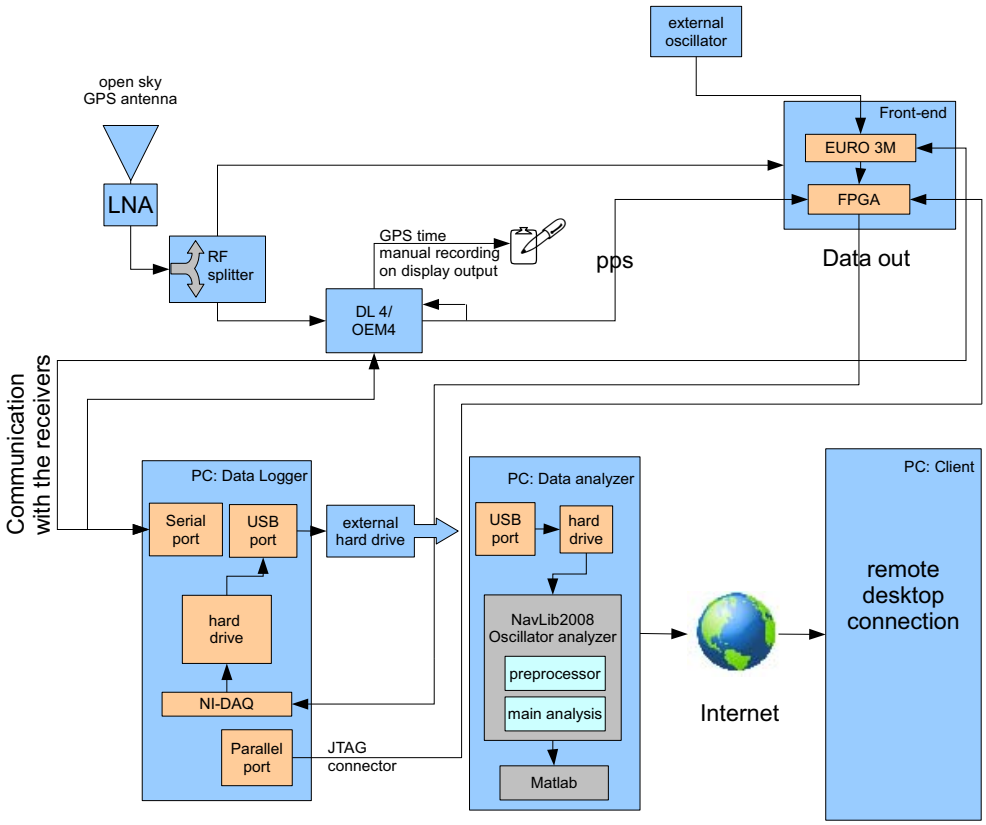

Figure 4.1: Experimental set-up used for open-sky test.

Hardware description:

- Note that the Pulse Per Second (PPS) cable is feed back to the reference receiver for logging purposes.

- The LNA is powered by the RF network, so no separate power source is needed for this purpose. In fact one has to make sure not to accidentally attempt to power the RF network, because this could damage the network or the power source.
- The RF splitter (splitter ZAPD-2)[2] from mini-circuit is used to distribute the GPS RF signal to both receivers.
- The reference receiver is a Novatel OEM4[3] card packaged in a DL4[4] box. The DL4 screen is used to get the GPS time, which is then used in the preprocessor software for the data synchronization process.
- The front-end is a PLAN Group custom hardware unit using a Novatel Euro3M[5] GPS receiver card and an Altera Field-Programmable Gate Array(FPGA) card.
- The data are collected into the front-end PC through a NI-DAQ card, which accepts the packaged data from the FPGA.
- These samples are then transferred to a PC, whose task is to analyze the data. This PC must be as powerful as possible in order to minimize the calculation time, preferably a Pentium 4 dual core or better.

[2]Data sheet: http://www.minicircuits.com/pdfs/ZAPD-2.pdf
[3]http://www.novatel.com/products/oem4g2l.htm
[4]http://www.novatel.com/products/dl4plus.htm
[5]http://www.novatel.com/products/euro3m.htm

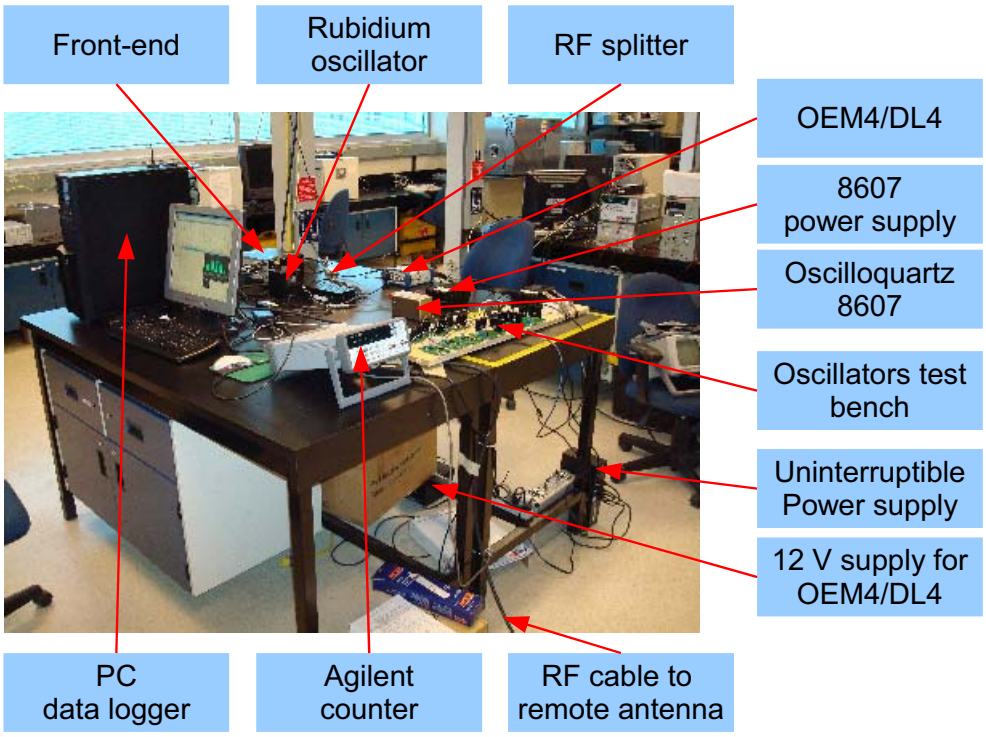

Figure 4.2: Picture of the experimental set-up, in the laboratory.

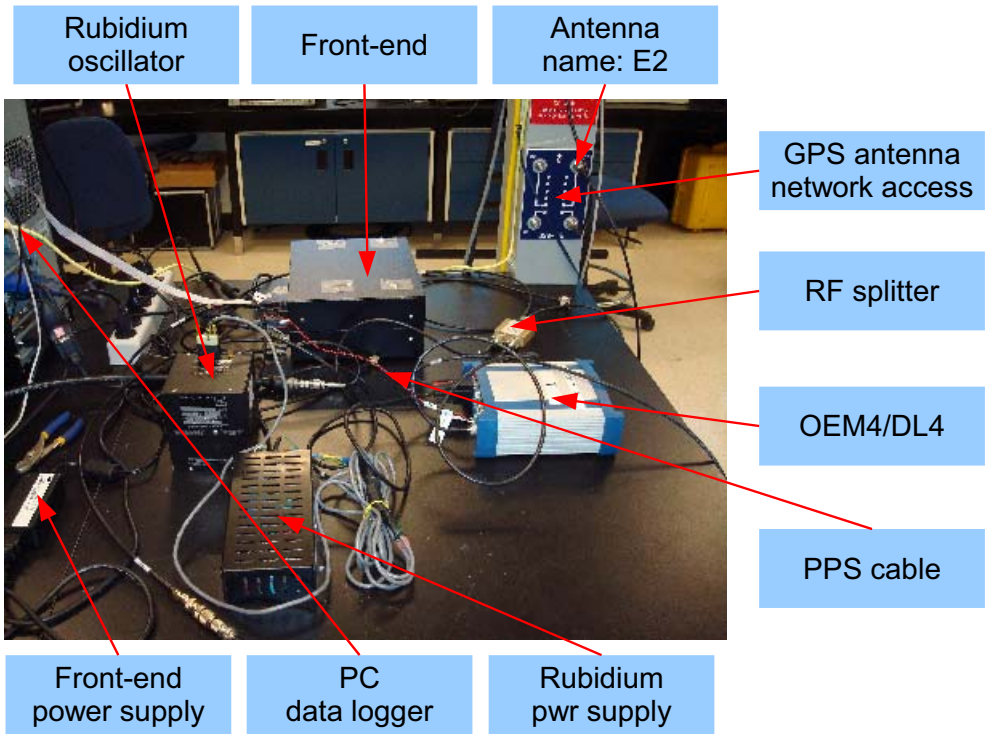

Figure 4.3: A closer view of the experimental set-up in the laboratory. For E2 antenna see[4.7].

4.2.2 Open sky attenuated mode

This set-up is the same as the preceding one, except for the variable attenuator placed on the RF cable that goes to the front-end, so one observes an attenuated signal with minimal multipath.

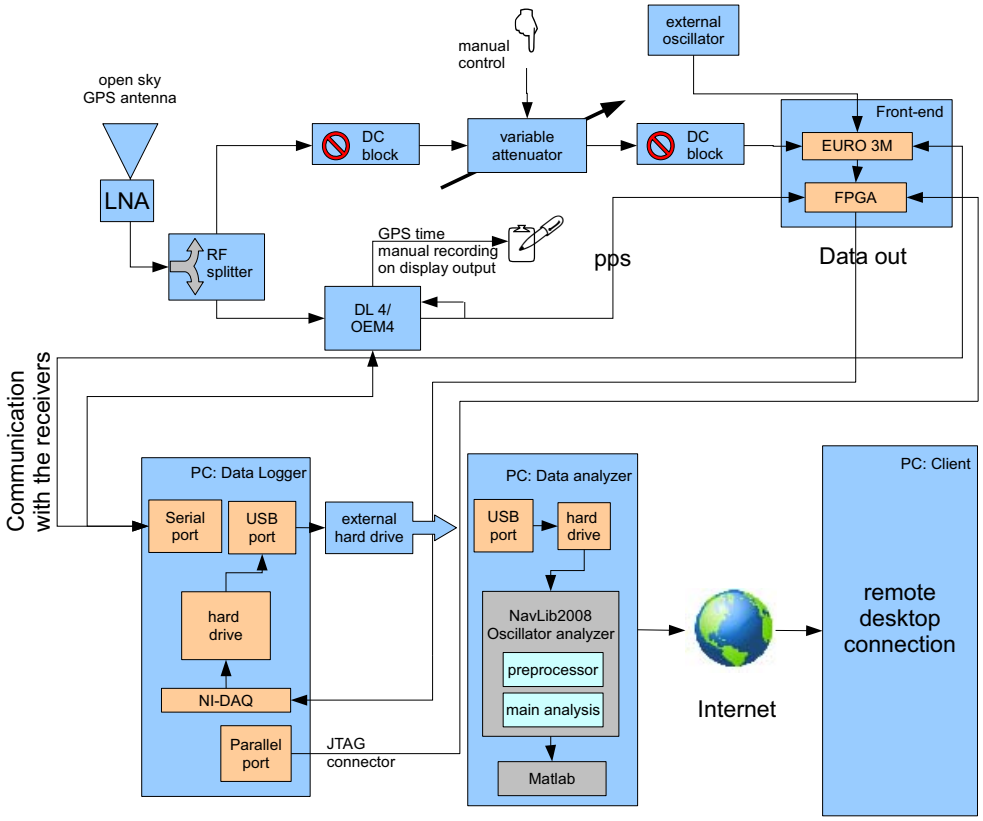

Figure 4.4: Experimental set-up used for open-sky, with attenuator.

This experimental set-up uses the same hardware as before except for:

- The variable attenuator manufactured by GPS Source[6].
- The two DC-blocks which avoid power flow from the attenuator to the RF network and to the receiver. This flow could potentially damage both the receiver and the network, and would prevent proper operation of the variable attenuator.

This set-up has been considered, but the results will not be presented since the tests failed to produce consistent results, likely due to the variable attenuator which seems not to function consistently due to past misuses. Due to these issues, the attenuator was not able to successfully perform the required -45 dB attenuation on the GPS signal[7],

[6] http://www.gpssource.com
[7] With stronger signals it operates as expected...

in addition one observed the presence of non-linearities in the attenuation. The use of passive attenuators was also investigated, which performed better, but due to time limitation the analysis was not completed. Nevertheless the general idea of this test set-up is still valid and could be further investigated in the future.

4.2.3 Remote indoor antenna mode

In this case one uses a mobile remote antenna (the same model and configuration as the one located on the roof), and collects data from an indoor location. In this configuration, the front-end receives an attenuated signal with relatively high multipath. The antenna (Novetel GPS-702[8]) is fixed on a 4-pod stable armature see figure [4.6].

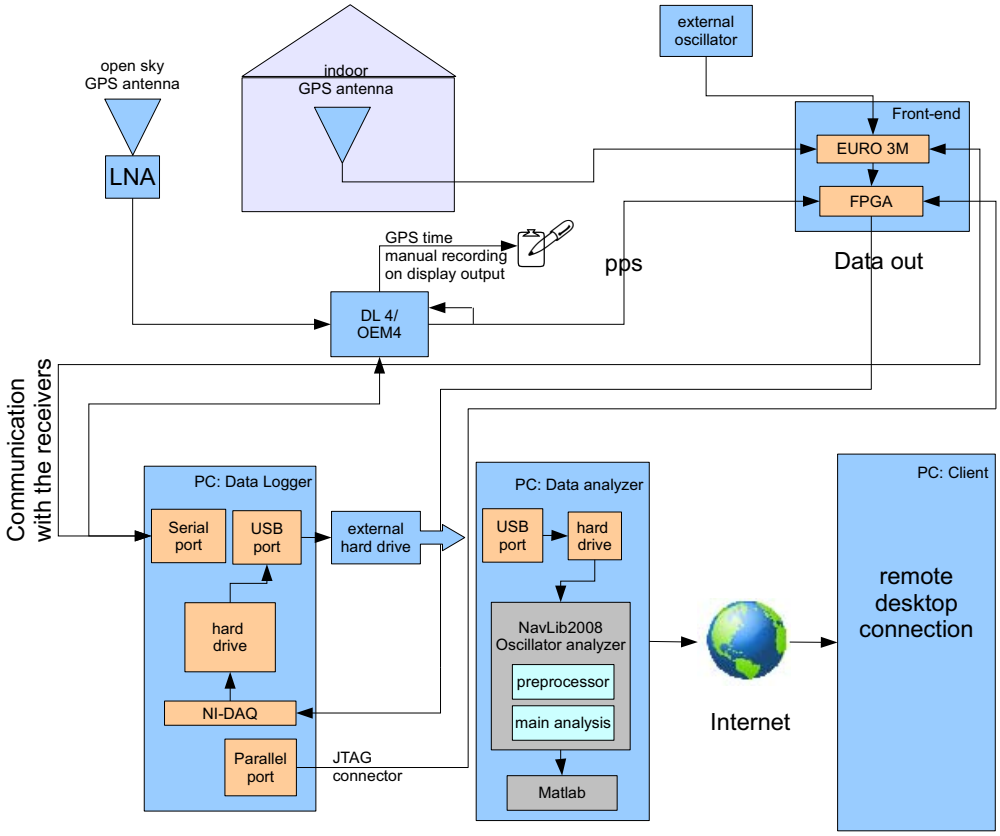

Figure 4.5: Experimental set-up used for indoor data collection.

4.2.4 Experiment locations

The aim of this section is to show the position of the antenna and the experimental environment. All experimental configurations described in this thesis take place on the 3rd

[8] http://www.novatel.com/products/gps_700.htm

floor of the Calgary Center for Innovative Technologies(CCIT) bulding on the University of Calgary campus. Figure[4.7] shows an external view of the CCIT 3rd floor, so the reader can gain an idea about the causes of the observed signal attenuation in the indoor configuration, and he can evaluate the position of the roof top antenna used as reference.

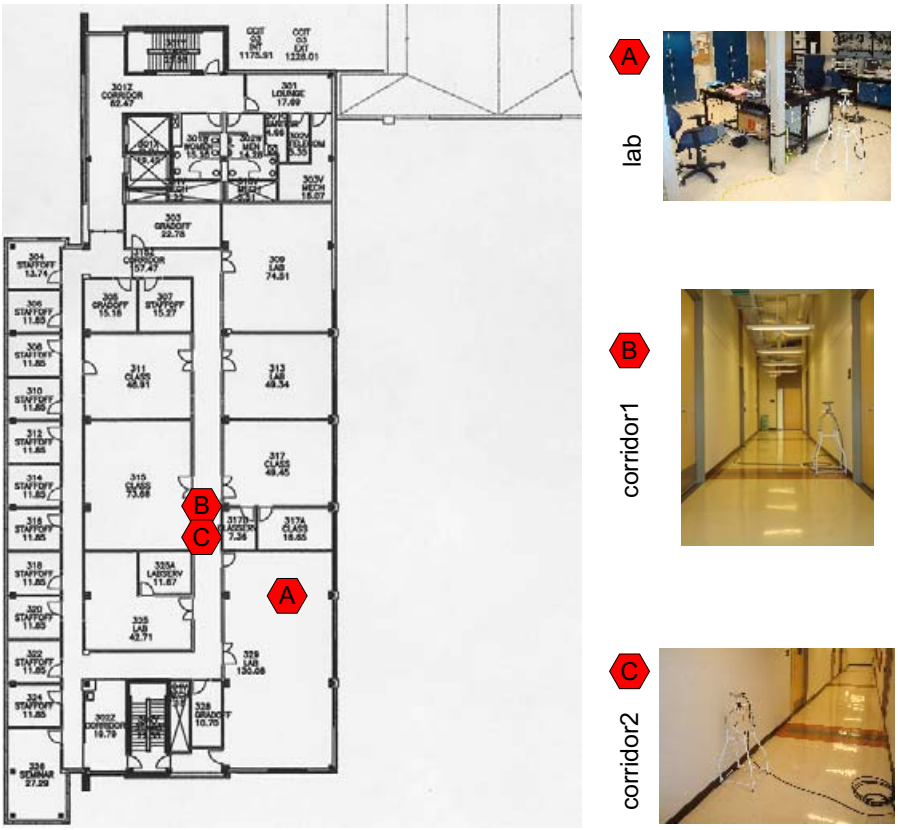

Figure 4.6: Shows the data collection points in the CCIT 3rd floor.

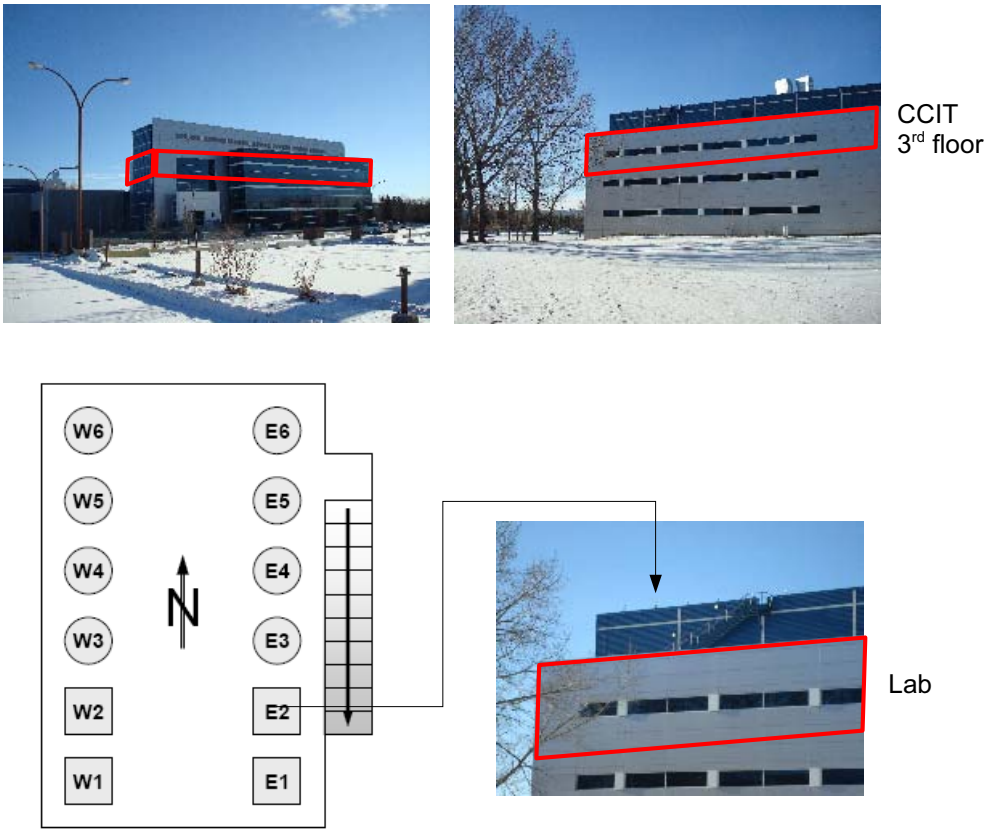

Figure 4.7: Outdoor view of the data collection environment.

4.3 Oscillators

4.3.1 Oscillator presentation

The oscillators used during this masters thesis are Swiss made oscillators[9], that have been freely provided by 3 different manufacturers as evaluation samples.

The specification of the different oscillators are reported in table [4.1] more in details:

- The warm-up time and power consumption are given as indicative values and will strongly depend on the environmental conditions where the unit is installed. These parameter are the temperature, temperature variations and the air flow around the oscillator. The given performance will be obtained only at room temperature in calm air conditions (similar to conditions found in the PLAN group NAVLAB).

[9] exceptions are the Symetricom and the Efratom rubidium already owned by the PLAN Group.

- The Allan deviation values are indicative of the minimum specification that the device is supposed to maintain, with the exception of the 8607 oscillator whose value has been expressly measured by Oscilloquartz engineers for this specific part.
- Frequency variation vs temperature value depends on the oscillator options selected by the consumer, where the values given in the table above are for oscillators operating under data sheet specified temperature conditions.
- more information and the data sheets for the oscillators can be found at the following manufacturer websites:
  - Oscilloquartz: http://www.oscilloquartz.com
  - Micro Crystal: http://www.microcrystal.com
  - Fordahl: http://www.fordahl.com

manufacturer	name	type	supply voltage [V]	nominal frequency [MHz]	volume $[cm^3]$	power(warm-up) [W]	warm-up time	short term stability $\sigma(\tau)$ @ 1s	temperature stability
Oscilloquartz	8626-AV5S	OCXO	5	10	2.1	0.35(1.25)	30s	$5 * 10^{-11}$	$1 * 10^{-6}$
Oscilloquartz	8712-ASH	OCXO	5	10	13.3	1.4(4)	7min	$5 * 10^{-11}$	$2 * 10^{-8}$
Oscilloquartz	8788-CS	OCXO	12	5	39.9	2.5(8)	72h	$1 * 10^{-12}$	$2 * 10^{-8}$
Oscilloquartz	8663-BS	OCXO	12	10	52.5	2.5(8)	72h	$1 * 10^{-11}$	$4 * 10^{-9}$
Oscilloquartz	8683-B2S	OCXO	12	5	64.5	2.5(8)	72h	$1 * 10^{-11}$	$4 * 10^{-9}$
Oscilloquartz	8607-BM	OCXO	12	5	886.5	3(10)	336h	$7.47 * 10^{-14}$	$1 * 10^{-10}$
Micro Crystal	OCXOVS-AV5	OCXO	5	10	2.1	0.35(1.25)	30s	$5 * 10^{-11}$	$1 * 10^{-5}$
Fordahl	0724 DFN S1-LHRZ	TCXO	3.3	10	0.79	0.033(-)	10ms	?	$1.5 * 10^{-4}$
Fordahl	0727 DFA S1-LHRZ	TCXO	3.3	10	0.79	0.033(-)	10ms	?	$5 * 10^{-6}$
Fordahl	0734 DFA S1-LHZ	TCXO	3.3	10	0.79	0.033(-)	10ms	?	$5 * 10^{-6}$

Table 4.1: Comparison of oscillators used.

4.3.2 Oscillator PCBs

The oscillators necessarily need a power supply, and some extra external discrete components to work properly, so it was necessary to implement the oscillators and external support components on a custom PCB, with one board for each oscillator. These designs were accomplished with the demonstration version of the commercial software Eagle[10]. The power supply needs to be as stable as possible in order to avoid negative influences on the oscillator stability[11], so a 2 stages linear regulator power supplies was adopted and fed by an external AC/DC converter. An $100\mu F$ electrolytic capacitor is used at the input of the first power supply stage to absorb irregularities. One also has a $20\mu F$ ceramic capacitor at the output of each stage for the same purpose. Two large heat sinks are attached to the power supplies IC's to properly cool them, and one can note that the thermal contact between the IC and the heat sinks is enhanced using a silicone based paste.
For the Oscilloquartz units the impedance matching is accomplished with a 50Ω resistance in parallel with the output, except for the 8626 and the microcrystal unit that requires 5pF and 1kΩ in parallel with the output. The frequency control input of each oscillator is fed with a potentiometer which provides a tension between 0V and Vcc.
The Fordahl oscillators output an HC-MOS compatible signal (i.e. square wave output) so one needs first to transform it in a sinusoid in order to meet the Novatel front-end specifications. In this implementation, one realizes this operation using a passive RLC filter at the output. The filter design as been provided by Fordahl SA, who have used it with their previous oscillators versions.
Certain Oscilloquartz oscillators also have a voltage reference output that can be used to adjust the operating frequency thought a potentiometer.
The Oscilloquartz 8607 requires no PCB since it is provided with its own hull that simply needs to be connected to the stabilized 24V power supply (ground and 0V together). In the future it may be useful to design an external circuit to provide the electronic frequency control reference voltage to the 8607 oscillator.
To avoid track to track cross talk (see figure [4.9]), one adds two ground plates one on each side of the PCB. If no ground plate is present the equivalent circuit of two nearby PCB tracks is a single capacitance. So, if the voltage rises in one line, a transient appears in the other one via the capacitive coupling between them. Adding the ground connection in between destroys the capacitive coupling between the tracks. Moreover this offers a certain level of shielding against outside world Electro Magnetic Interference (EMI) perturbation. The EMI emissions of the PCB are also reduced. Figure [4.8] shows an extract of the top and bottom layer of a PCB. One can note the vias connecting the top and bottom ground plates. For more details the electronic scheme and part list are detailed in appendix [B]

[10] This version is fully capable and only limits the PCB size. For more informations see:http://www.cadsoftusa.com.

[11] See oscillators datasheets for more information.

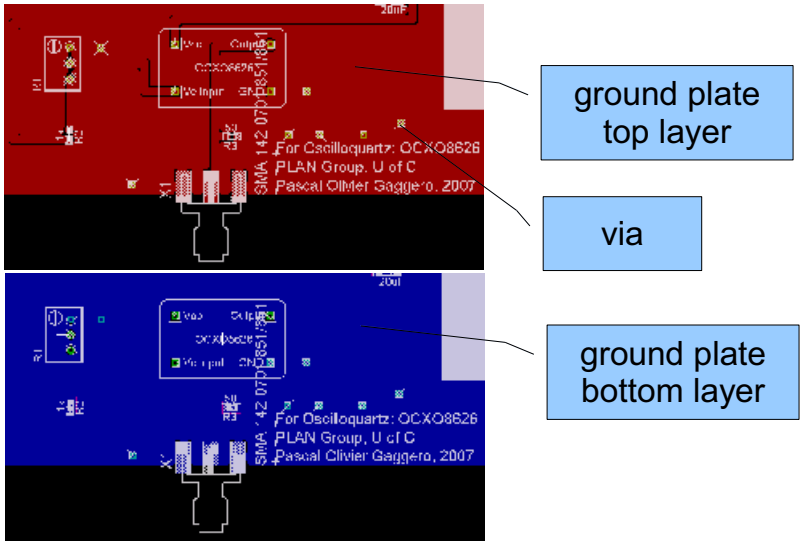

Figure 4.8: PCB top (red) and bottom (blue) layers, view of the design software Eagle

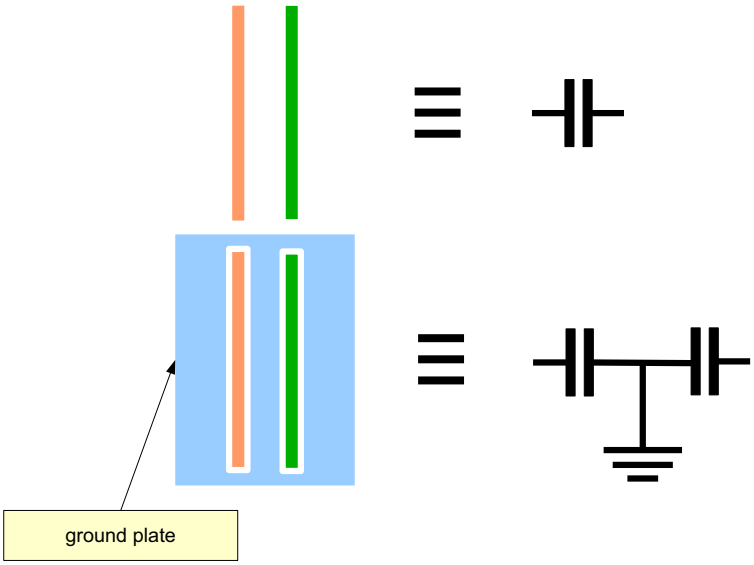

Figure 4.9: Equivalent circuits are represented with and without the ground plane. One can demonstrate that designing ground planes avoids cross-talk effects between lines.

4.3.3 Oscillators test bench

The oscillator test bench is a wood plank where the oscillators and their respective AC/DC converters are fixed together. The motivation behind this was to create a convenient test platform to work with. An external Uninterruptible Power Supply (UPS), which is a battery based power backup that maintains, for a limited time the power of the

oscillators in the event of an AC failure is also included in the set-up. As explained in chapter [3] switching ON and OFF the oscillators would force the user to wait the entire stabilization period before using them with the expectation of meeting specified performance. The UPS also allows the oscillators to be moved between the lab and the storage area without being deprived of the required power supply. This feature was important as, for security reasons due and the high oscillator value, the units were stored in a separate locked room when not in use. Thanks to the UPS, one also avoids someone perturbing the system by intentionally or involuntary switch ON and OFF the oscillators.

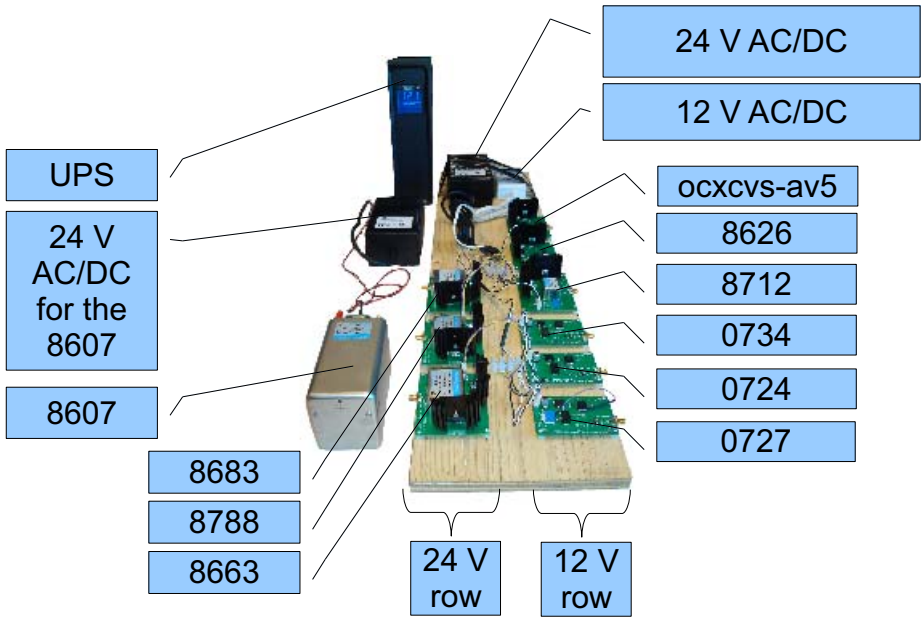

Figure 4.10: Oscillator test bench.

4.4 Software

This section will introduce the reader to the different software used and developed to process the collected data. These packages are exclusive propriety of the PLAN Group of the University of Calgary, and their use is subjected to prior consent of the head of the PLAN Group, Prof. Gerard Lachapelle.
Certain software components have been previously developed by PLAN Group developers (pale green round rectangle in and [4.11], [4.12] and [4.13]) while the rest have been developed in the conduct of this thesis.[12]
The developed software package has been named NavLabInterface2008 which also includes a Matlab toolbox. The main idea behind developing this GUI was to automate the

[12]The previously developed software has been also modified in order to be interfaced with modern c++ standards and GUI requirements.

data processing and to be able to add advanced and complex data processing options and features. GUI also offers a more user friendly and intuitive environment that reduces the software learning time.
The software user's manual has been reported in appendix [E].

4.4.1 Data processing flow

The first step is to download the daily[13] ephemeris from http://garner.ucsd.edu[14] see (figure[4.11]). The required file is located in pub/nav/aaaa/ddd/autoddd0.0aa.Z, for example for January 1st 2007 would the file location be: pub/nav/2007/001/auto0010.007.Z. Then one uses an decompression software[15] to unpack it. At last the program Rin2eph.exe[16] transforms the obtained files to the PLAN Group internal ephemeris format.

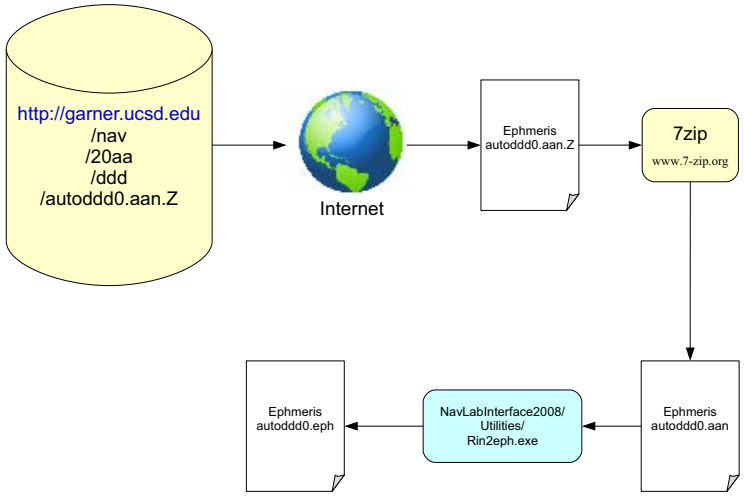

Figure 4.11: Ephemeris processing flowchart.

The second step (see figure [4.12]) of data processing is to go through the pre-processor, where one has to manually enter the files names, the antenna coordinates (X,Y,Z) and the approximate time of the data collection start[17] in the OscillatorAnalyzer GUI, under the pre-processor tab. During the processing the user will have information on the actions undertaken by the program in the log window situated in the "control panel" tab. As soon as the pre-processing work is over, incomplete data (for example relative to satellite that are not in view during the whole experiment) are removed from the SVInfo and Navdat file. The final data are saved under the files named SVInfo_OK and NavDat_OK.

[13] Day on which the data has been taken
[14] Other orbit products can be found here: http://igscb.jpl.nasa.gov/components/prods.html
[15] Recommended is the open-source product from: http://www.7-zip.org
[16] Distributed in the NavLabInterface release
[17] within 20 seconds

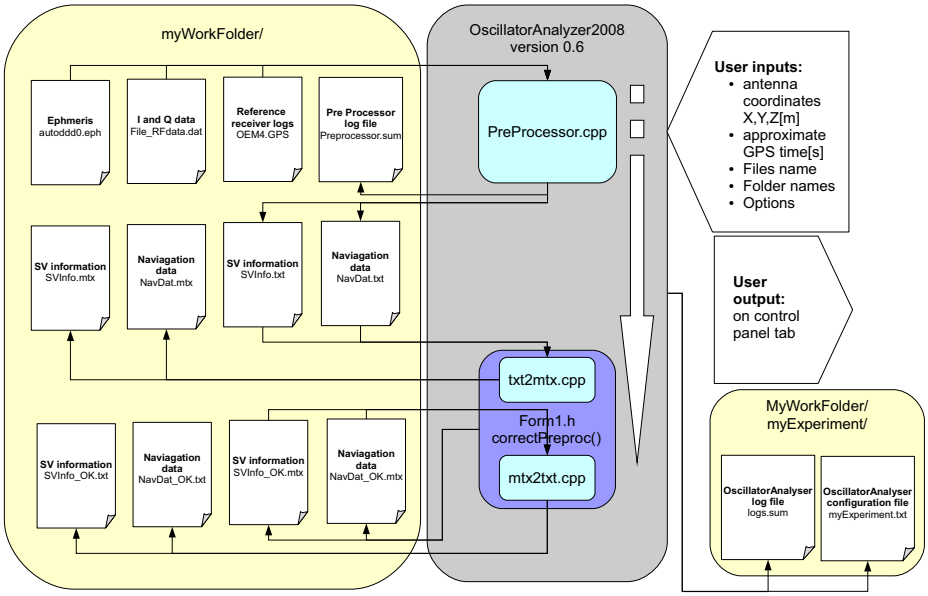

Figure 4.12: Preprocessor processing flowchart.

The third step (see figure[4.13]) is to calculate the correlations in the search space. This is done with the mainAnalysis.cpp program. the program results are saved in the I, Q and Pow files (see [4.4.2]). Also, this program automatically creates the Matlab scripts with the right options to analyze the data.

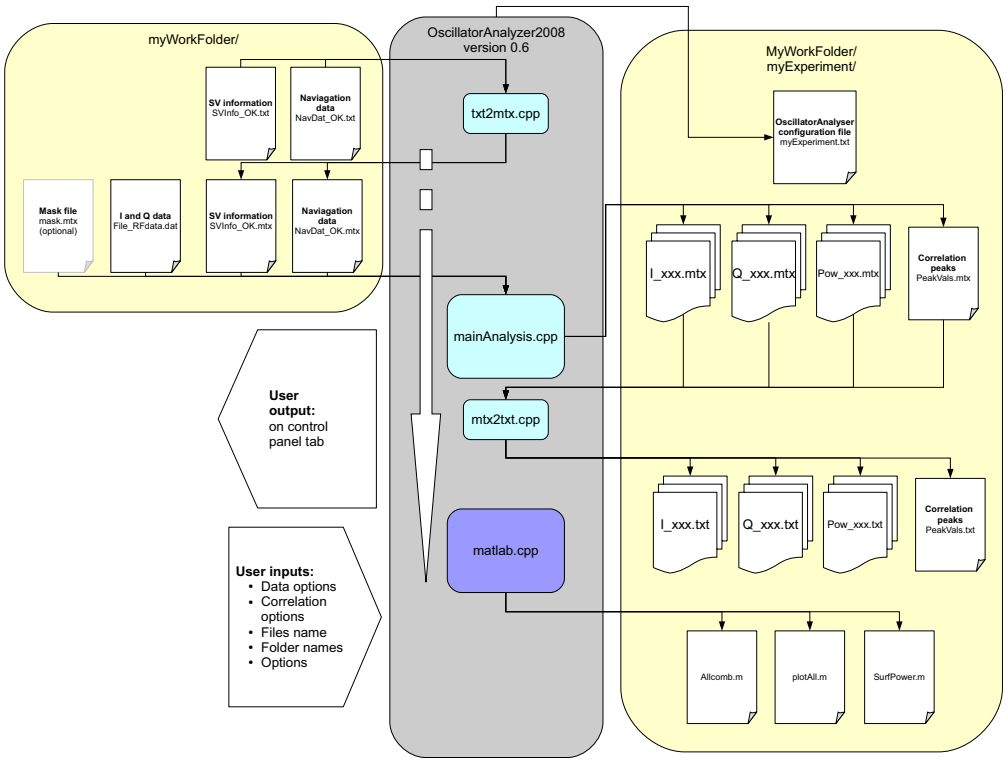

Figure 4.13: Main analysis processing flowchart.

4.4.2 I,Q,Pow files

The I and Q file contains the in-phase and quadrature correlation outputs evaluated for a coherent integration time equal to 1 epoch[18], for different values of code delay and Doppler shift. The I, Q and POW files are automatically created in text format (.txt) by the OscillatorAnalyzer, which uses the generic names I_xxxx, Q_xxxx and Pow_xxxx for file reference, with the xxxx indicating the epoch number. For example, the I data file name of the first epoch would be I_0000.txt. Each file contains on the first line and column the axis with the remainder of the fields holding values for each matrix element see figure [4.14]. The Pow_xxx file contains values for each epoch, representing I^2_xxxx+Q^2_xxxx.

[18]Fundamental coherent integration time chosen by the user.

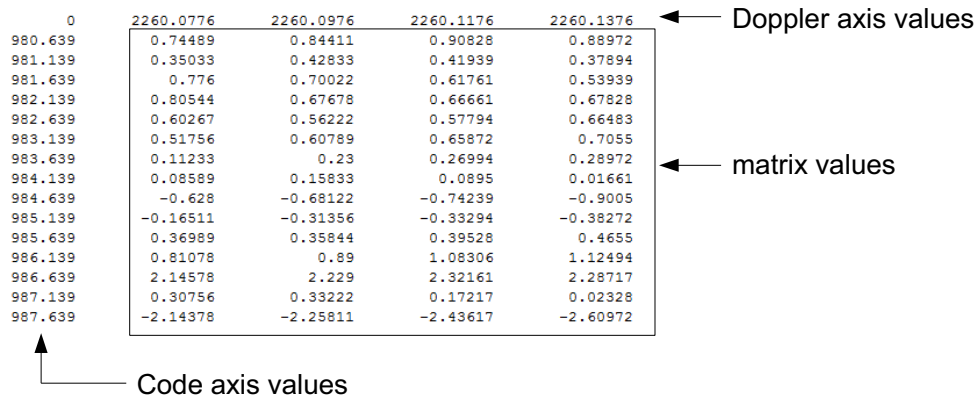

Figure 4.14: Detailed view of an I,Q,Pow file.

4.4.3 PeakVals file

The peak file is produced by the mainAnalysis program. It contains the peak position within search space defined by the code delay and Doppler shift and the peak magnitude for each epoch.

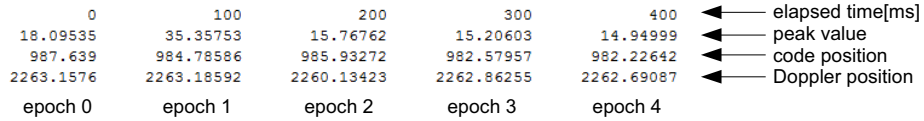

Figure 4.15: Detailed view of the peakvals file.

4.4.4 Pre-processor

The pre-processor tasks are the following:

- To synchronize the reference receiver data with the recorded I and Q data (in other words to find the exact GPS time of the first recorded I and Q sample).
- Calculate the 2nd order Doppler prediction model parameters, using the ephemeris, user position and the synchronization time. This operation also calculates the predicted code delay as a useful byproduct.
- Produce a file named SVInfo.txt containing the PRN number, Doppler model parameter, predicted code delay, SV elevation and azimuth.
- Produce a file named NavDat.txt containing coded navbit transition information.

Data synchronization

To perform the synchronization the preprocessor uses a pseudo random pulse signal produced by the reference receiver and recorded by the remote receiver[19]. After performing a correlation of the both recorded pulse data the result is a sequence of correlation peaks, within which to solve the ambiguity and decide which peak is the right one, the program uses the manually entered time. Then the preprocessor simply has to examine the reference receiver data for the corresponding time mark. This founded time corresponds to the time at which the data collection starts. This time is used to correctly compensate the GPS data bits.

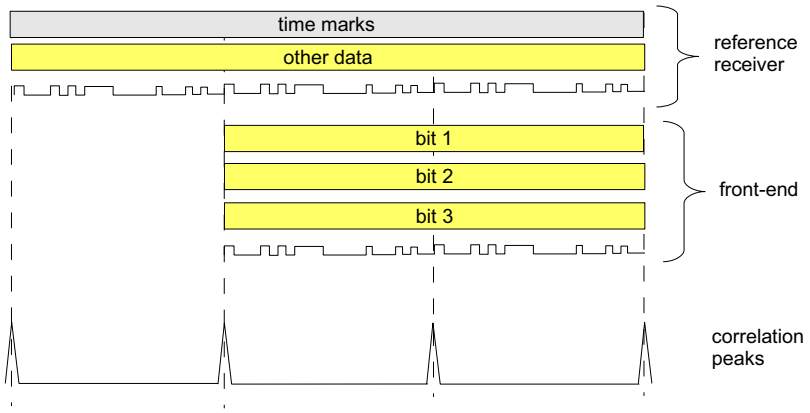

Figure 4.16: Data synchronization.

There exists also a manual method using a one second pulse signal and precise manual time entry[20], this has not been used in this work, but for more information about this method please refer to Rob Watson's documentation distributed in the full release of this thesis, and to his master thesis [30]. More information about Watson's previous studies and results can be found in [4] and [5].

SVInfo.txt

The SVInfo file contains all the visible satellite information such as PRN number, Doppler model parameter, predicted code delay, SV elevation and azimuth.

[19] The reference receive also record its own signal.

[20] One inhibits some of the pulses manually so there will be missing pulses. The time of the first missed pulse is then given to the software.

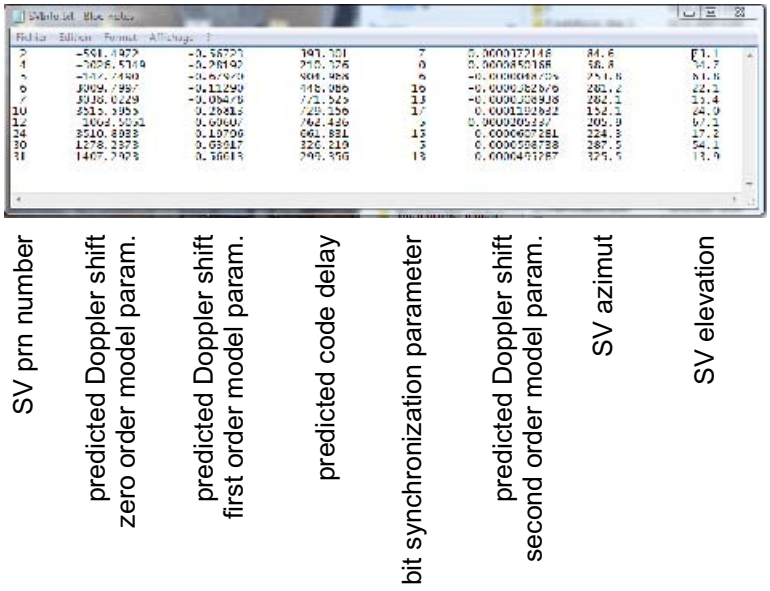

Figure 4.17: Detailed explanation of SVInfo.txt file.

NavDat.txt

In the NavDat.txt file each column represents a satellite, such that the listing in column 1 corresponds to the SV into row 1 of the file SvInfo.txt (see figure [4.18]). The first line of each column is the first data bit value of the data set. Then the transition time of the data bits are recorded in unit of samples (sampling frequency of 20MHz). Each column ends with an ”-1” tag with other fields filled with zeros, representing empty matrix position. As represented in figure [4.18], it is possible that some SV data sets are corrupted because of an error, or because the satellite is not visible anymore. These columns can only be used to the point the data disappears. The OscillatorAnalyser2008 will apply a correction algorithm to be sure to work with non-corrupted data sets. The option to disable this feature is provided for who is interested to work with incomplete data sets.

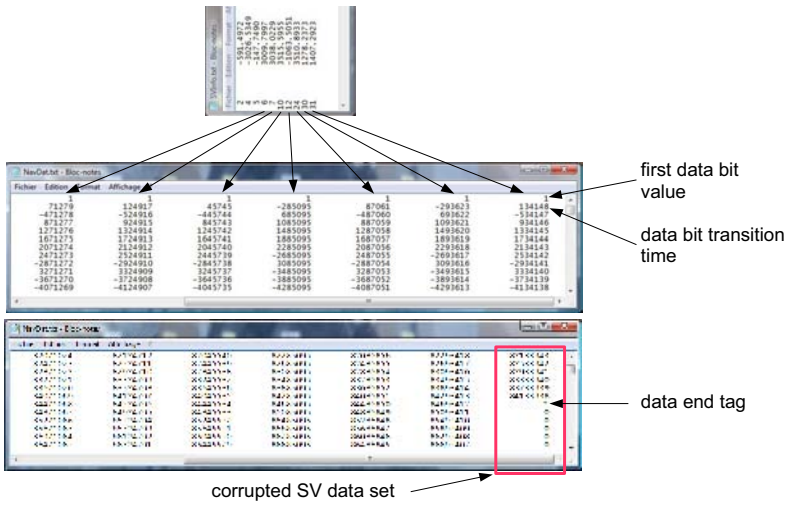

Figure 4.18: Detailed explanation of navdat.txt file.

4.4.5 Main analysis

The main analysis program uses the preprocessor output file, SVInfo and NavDat to calculate the correlation across the user defined search space and outputs the different I_xxxx, Q_xxxx and POW_xxxx epoch files, where an epoch is the fundamental coherent integration time chosen by the user. Subsequently one can coherently combine the epochs using the developed Matlab toolbox.
The program will, for each epoch, calculate the correlation as explained in figure [4.19]. In the given figure, the green arrow represents the calculation direction, while the search space dimensions are defined by the user with the code and frequency steps sizes as program inputs. The calculation time is directly related to the size of the search space.
One knows that a GPS L1 code length is 1023 chip so with a chip step of 0.5 chip one gets a maximal search space of 2046 code bins[21]. The maximal observed Doppler shift is typically considered to be ±5kHz[22], so using a Doppler step of 125Hz and 81 bins one is able to cover the whole frequency search space. Of course, if one is careful enough, one can avoid searching the whole space. For more information about that see the software user manual [E].

[21] 2047 as to be introduce in the program because this parameter must be an odd number

[22] Maximal Doppler shifts are observed when satellite are at the horizon. However commercial receiver will take $\pm 10kHz$ in order to take into account for real dynamic and cheap oscillator imperfections.

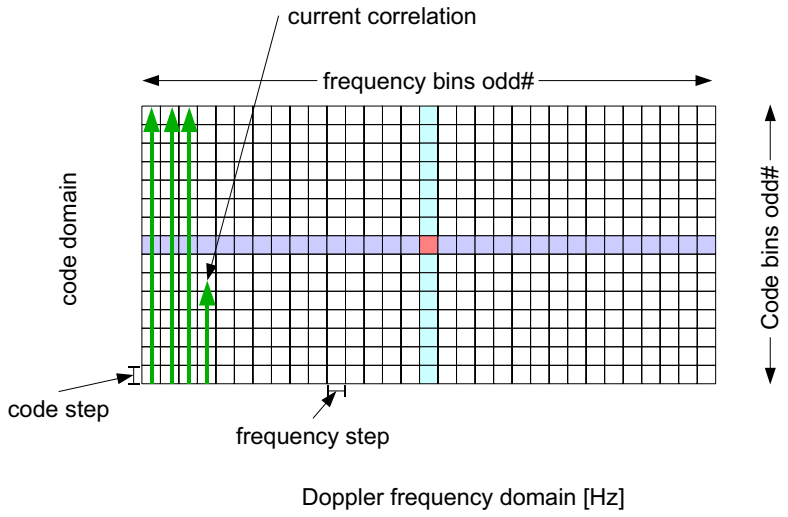

Figure 4.19: Schematic representation of the search space, the coloured squares represent the Doppler and code predicted value, the peak predicted position is the red square.

The choice of the frequency step value depends on the integration time T_{coh}[23], as it is known that increasing the integration time will decreases the peak width in the frequency domain. It is interesting to note that the peak shape in the frequency domain is a squared sinc function and a triangle in the code domain. A rule of thumb formula says that the maximal step size should be:

$$f_{maxstep} = \frac{2}{3 \cdot T_{coh}} \tag{4.1}$$

Using equation(4.1) the maximal integration time that is possible to calculate in order to be sure to see the peak in the case of the whole search space parameters described above is $T_{coh} = \frac{2}{3 \cdot f_{maxstep}} = \frac{2}{3 \cdot 125Hz} = 5ms$.

4.4.6 Matlab toolbox

Allcomb.m

Allcomb.m is the main Matlab script used herein, and is represented by the top level scheme depicted in figure [4.20]. To expand on this general overview, the reader can refers to the NavLabInterface User's manual in appendix [E].

[23] here one means the final coherent integration time not the epoch length

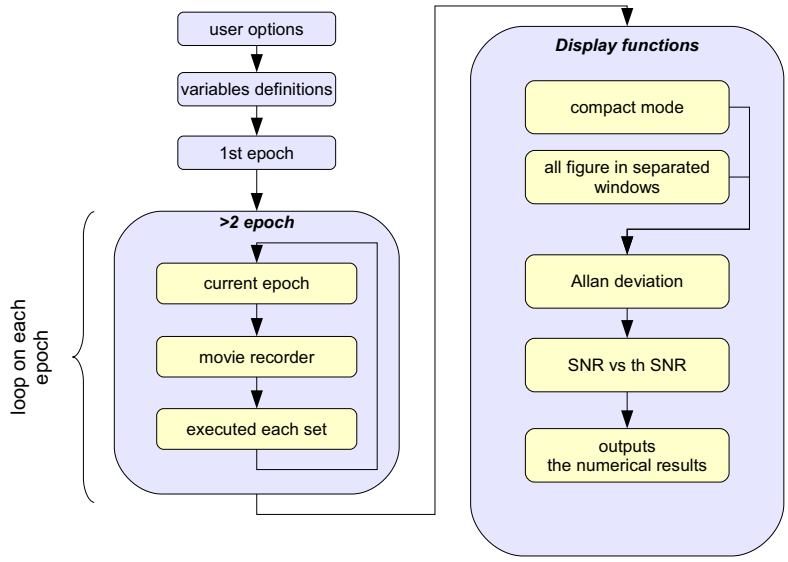

Figure 4.20: Top-level representation of the main Matlab tool Allcomb.m.

Once the data has been processed by the oscillatorAnalyzer software, one obtains the I and Q files for each epoch, which can be further combined using the Allcomb.m tool, where the first task of the Allcomb.m code is to combine the I and Q data coherently. As explained in [2.3.5] one compensates the obtained value for the noise floor, as this compensation is necessary to be able to compare the result of the different integration times with each other, as one will then have the same noise floor in each case. The axis values of the code and Doppler shift are respectively in the first column and the first row. The value of the first epoch is used for the entire integration time, and consequently if one would use the resulting code delay to calculate a position, one would get the position of the antenna where the first epoch has been recorded.
The Allan variance measurement[24] of the utilized oscillator comes for free with the collected data. This measurement is based on the assumption that the Doppler prediction model is precise enough to predict the frequency shift without introducing extra noise into the signal. This is a quite reasonable assumption, because the model used is of the second order, i.e. a parabola. While the trajectory of the satellite also is a parabola like curve over a short time period (less than a few minutes). So even if the model of the satellite trajectory is not precise it would not contribute to the Allan variance for small τ[25] (Doppler short term variations) in the transmitted GPS signal see figure [4.21].

[24] Of the worst oscillator or a combined result between SV and receiver frequency reference(s).
[25] Smaller than 1 30 seconds.

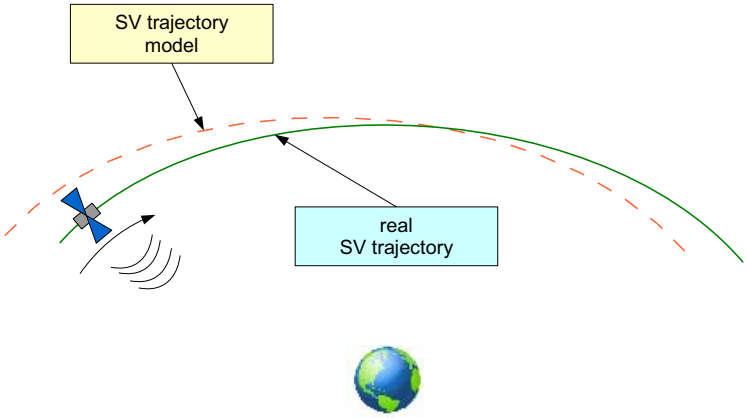

Figure 4.21: The represented real SV trajectory can be modeled by fitting it with a 2nd order model. If the model is not perfect it would not introduce short term variations over Allan deviation averaging time periods τ less than 30 seconds.

The mainAnalyzis program will use the previously mentioned Doppler prediction to center the search space, i.e. the central matrix index will always represents what the model thinks the Doppler shift will be for this epoch. But in reality the oscillator instabilities in the satellite and in the receiver will produce a slightly shifted peak compared to the predicted one, so by taking the difference between the measured peak position and the predicted one, and applying the Allan deviation formula, one is able to plot the Allan deviation of either the receiver oscillator or the satellite or a combination of both if both exhibit the some characteristics. It is important to note however that the formula of the Allan variance given in section[3.5.3], can't be directly applied, as the averaging over the time period τ is replaced by a coherent integration length τ. The fundamental reason for that is that one has to integrate over a certain time to get the GPS peak, which is usually at least 2 ms, and as a result one will not get enough samples to make a valid average. Moreover in order to save calculation time one focuses the search space on the peak position so if the coherent integration time is too small, one is looking too closely at the peak in order to decide where the center is. In other words observing only the peak region does not allow one to determine the shift to the central index, due to the noisy signal see figure[4.22]

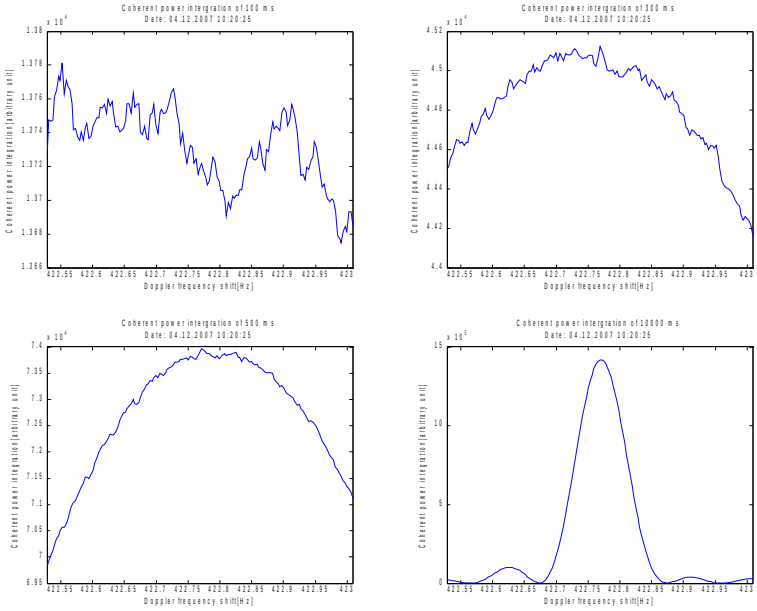

Figure 4.22: This figure demonstrates the fact that looking too closely to the peak by selecting inappropriate search space parameters and too small coherent integration time will inhibit performing the Allan variance calculation. In this case the minimum integration time needed is 0.5 second, in order to get a sufficiently smooth peak for evaluation.

plotAll.m

This function plots in separate figures the different individual epochs.

SurfPower.m

This is a function used by Allcomb.m to plot the search space.

Chapter 5

Experiments

In this chapter the methodology used to collect the data is explained in detail. A step by step tutorial is also provided in appendix[C]. Concerning the software manipulation, the reader could refer to the NavLabInterface user manual in appendix[E]
One of the most important issues in data processing is that the time needed is very long, strongly impacting the work organization.
While going through this chapter the reader has to keep in mind that when talking about oscillators, one refers to either the local oscillator in the receiver or the one on the satellite. Moreover combined effects of both oscillators can be also considered. Here the potential of the experimental set-up presented in chapter [4] is explored, the results will be presented as follows:

- **Long integration time [5.1] :** Comparison of the different oscillators in open-sky condition. The goal is to execute a first coarse test over the whole oscillator selection in order to get an idea of their performances including the analysis in open-sky conditions over long coherent integration time periods. The maximal coherent integration time that can be obtain by each oscillator is also investigated. The position obtained using indoor data measured is calculated.

- **Indoor acquisition [5.2] :** Working with indoor measured data set, one will try to execute some long integration in real weak signal condition.

- **Oscillator behavior modeling [5.3] :** The goal is to obtain a predictive model of the oscillator under test.

- **Oscillator Allan deviation [5.4] :** Determination of the oscillators Allan deviation using open-sky data sets.

Parameter	value
Num Correlators	1
Correlator Spacing [chip]	1
Num Frequency Bins	161
Frequency bin spacing [Hz]	0.002
Coherent Correlation Length [ms]	100
Number of epochs	999

Table 5.1: Parameter used for search space fine acquisition for open-sky measurement.

5.1 Long integration time

In this section the coherent integration times that can be achieved by each oscillator have been investigated. The data presented next have been processed according to the following steps:

- Preprocessor.
- The 9 first default autofocus steps.
- Main analysis using the parameter described in table [tab:param0].

5.1.1 Fordahl 0727

The Fordahl TCXOs were not equipped with voltage controlled frequency regulator[1]. Thus it was not possible to exactly match the frequency required by the front-end. Nevertheless the frequency reference produced by the Fordahl TCXO 0727 was precise enough to correctly down-convert70 the GPS signal and allow the data analysis. Other TCXO oscillators were not precise enough to allow the front-end PLL to be locked to the right frequency.

The graphs in figure[5.1] have been obtained by coherently accumulating several 100ms epochs. In the left side of the figure [5.1] the evolution of the correlation peak as a function of the coherent integration time has been reported. One clearly observes that after 12.6 seconds of coherent integration the accumulated peak value begins to decrease. The peak value alone is a numerical value given in arbitrary unit. The ratio between the peak value (in arbitrary unit) and the noise value (also in arbitrary unit) represents an estimation of the SNR. On the right side of figure [5.1] a zoom of the maximum integrated power is reported. One can note that, due to the time quantization in 100ms epochs, it is not possible to determine the maximal integration time within a precision better than $\pm 50ms$. This precision is enough for the work developed in this thesis. More precise

[1]Those TCXOs didn't have the voltage frequency control option. This option is essential and should be purchased for each future new oscillator.

measurements would require processing the data with smaller integration time epochs. For this purpose starting with version 0.6RC3, the OscillatorAnalyzer software is able to process up to 9999 epochs. One of the problems is that the use of this number of epochs and files dramatically increases the processing time. Especially burdensome is the files conversion(.mtx to .txt).

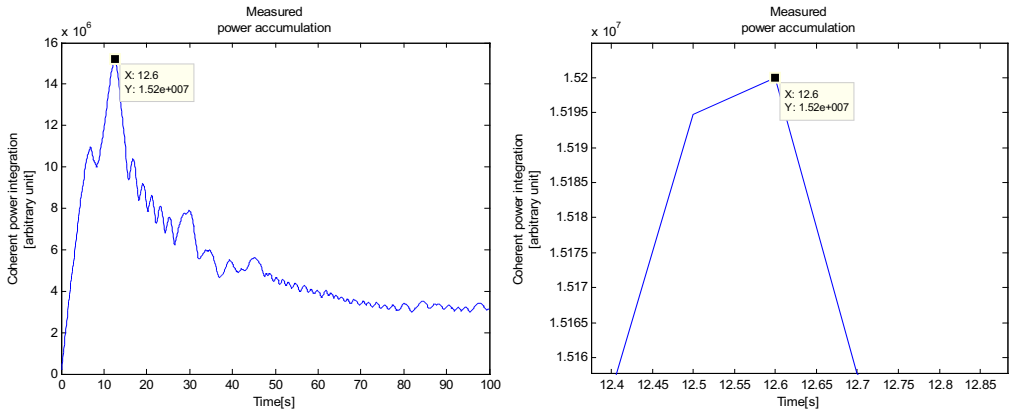

Figure 5.1: Left: Peak accumulated power vs. coherent integration time; Right: A zoomed view.

Figure [5.1] displays a bump in the accumulated power at about 6.8 seconds. This is due to the absorption of a portion of the useful signal power by a side lobe. This phenomenon is better highlighted in figure[5.2] where the correlation peak is reported for different integration times. A secondary peak appearing in the frequency domain absorbs part of the main peak power causing the first bump in figure [**??**f:0727int]]. This phenomenon can be probably explained by a signal degradation due to a small frequency change that is not completely compensated during the accumulation process. This frequency deviation makes the secondary peak grown with respect the main one. This frequency error seems to behave more as a small jump than as a continuous drift. In fact a continuous drift would cause the main lobe ti widener. A small frequency jump can justify the growth of the side peak. A frequency jump in the signal or in the local carrier can be caused by:

- An error in the model predicting the Doppler profile used to compensate the effect of the satellite motion.
- An error caused by the front-end and causing a distortion in the signal.
- A micro-jump in the carrier generated by the local oscillator [27].

Using the video analyzer[2] it is very easy to observe the curve behavior frame by frame. Video files are distributed in the electronic version of the thesis in \public\video\ folder. The video relative to this phenomenon is named "0727OpenSky60secondsPowerAccumulation.avi". The movies are created using the developed Matlab script allComb.m.

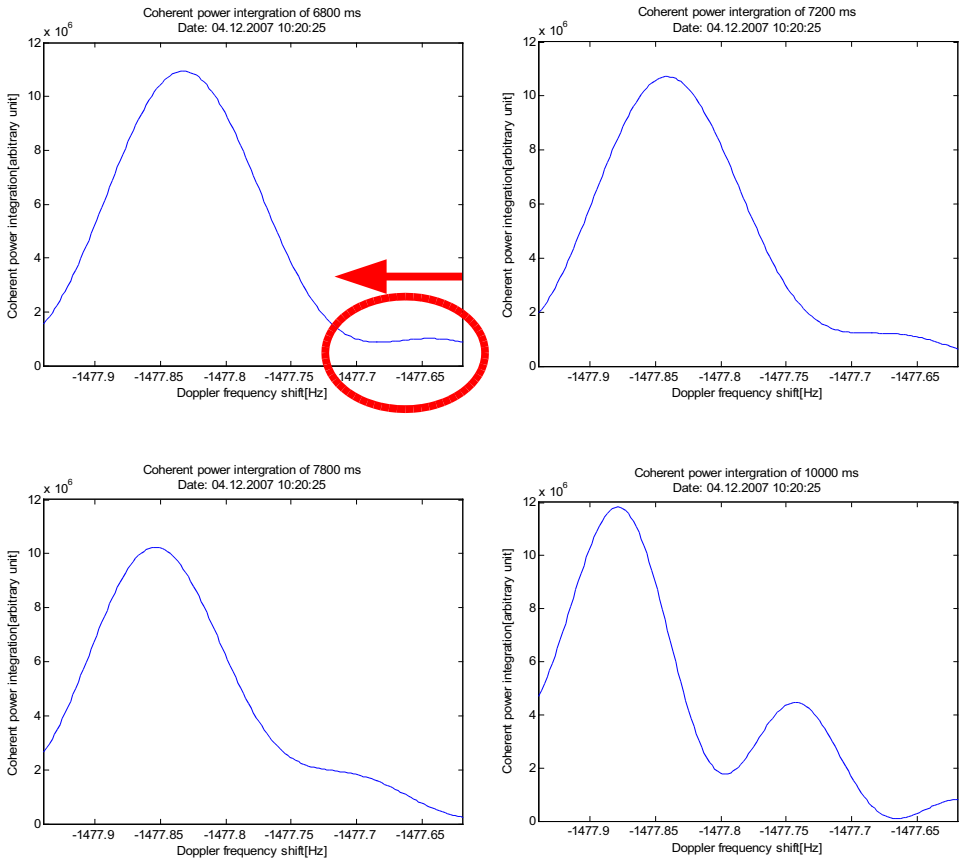

Figure 5.2: Power absorption from a side lobe.

Starting the coherent accumulation at epoch 400 (40 s), one observes the same phenomenon (see figure [5.3]). By using prn6 data instead of prn 30 data (see figure [D.1]), a similar artifact can be observed after exactly the same elapsed time. This suggests that the phenomenon is caused by an event (related to the receiver) that affects all the GPS signals at the same time and can be possibly explained by the three causes listed above.

[2] http://www.virtualdub.org

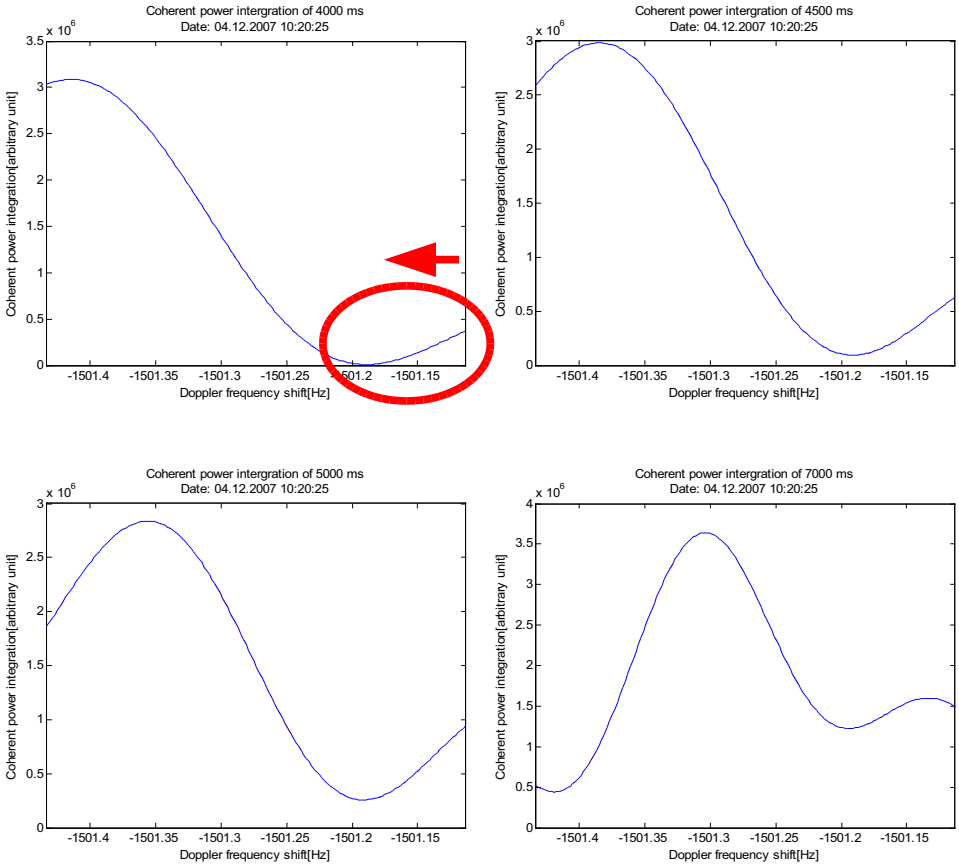

Figure 5.3: Absorption of a side lobe starting the coherent accumulation at epoch 400.

Plotting the coherent power accumulation starting at epoch 400 (see figure [5.4]), it is interesting to see that depending on the accumulation starting time (in epochs) the error accumulate differently and thtat the accumulated power can start growing again. In this context only the maximum of the correlation functino is used ti measure the accumulated power. Thus the behavior of the power profile in figure [5.4] can be possibly explained by the presence of secondary lobes that after, a certain integration time, can result more powerful than the main correlation peak. Further investigations should be devoted to these aspects.

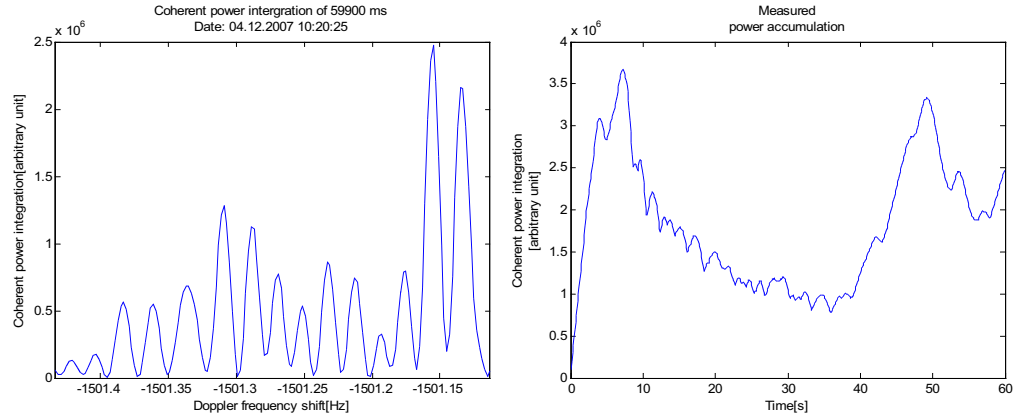

Figure 5.4: Power absorption from a side lobe starting at epoch 400.

An estimate of the theoretical power accumulation evolution can be obtain by simply summing the maximal peak value of each individual epoch. This estimation technique is based sensitive to peak estimation errors that can explain the change in slope clearly appearing in figure[5.5]. The ratio between the theoretical and measured coherent power accumulation is displayed on the right hand side of the same graph. On the ratio graph the effect of the previously discussed artifact is visible, by introducing a bump in the curve.

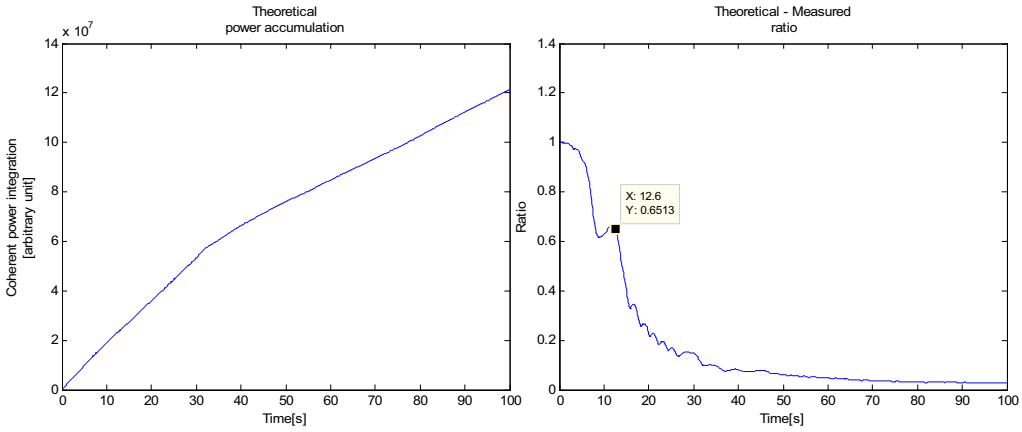

Figure 5.5: Left: Theoretical coherent power accumulation peak value evolution in function of the accumulation time; Right: Ratio between theoretical and measured coherent power accumulation peak value evolution.

In figure[5.5] in the theoretical power accumulation evolution one see that after about 32 second the line takes a smaller pitch. This is due to the fact that after 32 seconds the peak value of each individual epoch is in average smaller than previously.

All the data sets processed with the same parameters exhibit the same change in slope in the theoretical power profile. All those data sets have been taken with different satellites, oscillators and at different times. Although the exact source of the problem has not been determined yet, it could be probably caused by a problem in the data collection hardware[3], such as memory saturation, or by errors in the program producing the 100 ms accumulation blocks.

In figure [5.6] the peak value (non-accumulated power) obtained for each epoch (100 ms coherent integration) is reported. Interestingly it is possible to observe a big jump in the non-accumulated power occurring after 32 s. Although the reasons for this phenomenon are not clear yet, for each epoch the peak value should be fairly constant, this trend explains the change in slope of the theoretical accumulated power: the peaks before 32 s contribute more to the accumulated power growth than the ones after this instant.

In the right side of figure [5.6] the position of the main correlation peak in frequency domain has been reported. Three different zones can be observed:

- Zone 1: from 0 to 8.2 s, it is shown that the main peak is in the considered search window. One can note the noisy behavior of the peak position is due essentially to the fact one is looking to closely to the peak.
- Zone 2: from 8.2 to 32s, the peak maximum is on the right part of the search window.
- Zone 3: from 32 to 99.9s, the correlation maximum is on the left part of the search space windows.

The fact that the position of the correlation maximum saturates on the border of the search window can indicate that the true correlation maximum is not included into the search space. A possible explanation of the observed phenomena is presented in figure [5.7]. The search window is supposed to be tight with respect to the main lobe of the signal spectrum and only a portion of its main lobe is explored. In Zone 1 corresponding to part a) of figure [5.7], the signal spectrum is centered with respect to the search window and the noise contributions randomly move the position of the maximum. Due to a frequency drift in the signal and in the local carrier the signal spectrum is moved and the position of maximum saturate on one border of the search window. This corresponds to Zone 2 and to part b) of figure [5.7]. The power fluctuations observed in the left side of figure [5.6] can be caused by this frequency drift. This frequency drift progressively move the signal spectrum, at first reducing and then increasing again the signal power contribution.
If a frequency jump occurs, the position of the peak observed in the search window can

[3]The front-end got “clockadjust disable” command.

change from one side to the other. If a secondary peak is locked, a drop in the non-accumulated power can be observed. This situation is described in part c) of figure [5.7] and can probably correspond to Zone 3 of figure [5.6]. A sudden jump is the signal/-carrier frequency can be possibly explained by a hardware problem that caused the loss of some portions of the incoming signal. A second hypothesis consists in presence of discontinuities in the model used for predicting and compensating the satellite Doppler shift.

Further analyses should be carried on in order to better verify the proposed explanations and possibly solve the problem.

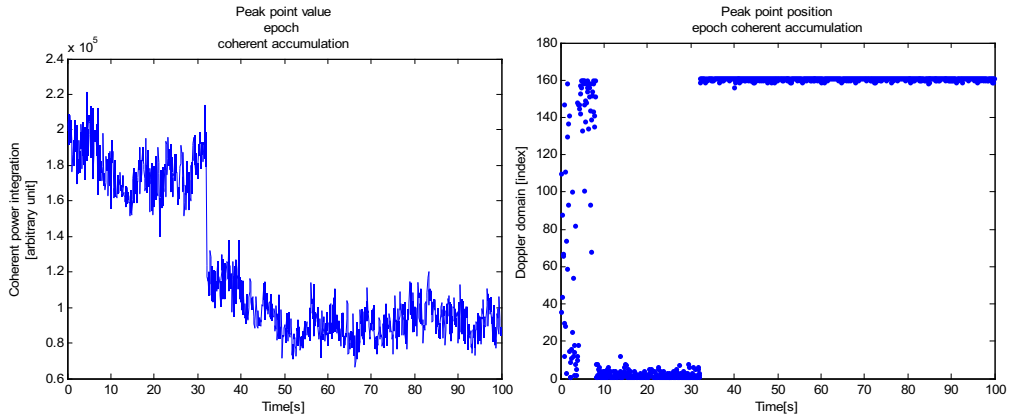

Figure 5.6: Left: Peak value of each individual epoch, a clear jump is observed after 32 s; Right: Peak position in frequency for each individual epoch as function of the time.

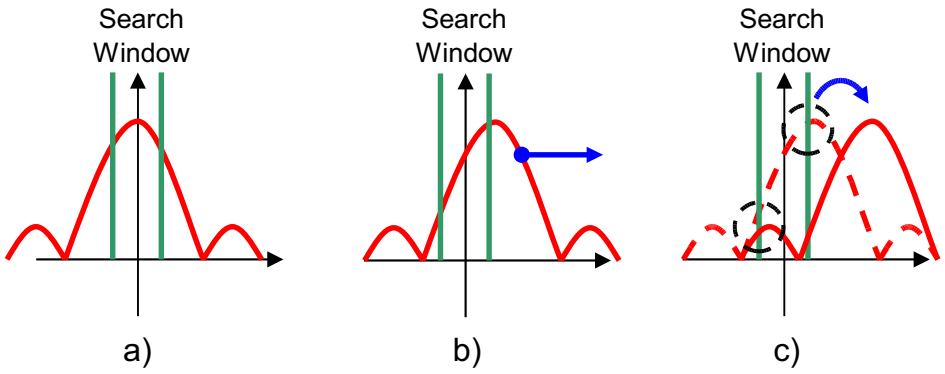

Figure 5.7: Possible explanation for the phenomenon observed in figure [5.6]; a) The search window is well centered on the signal main lobe.; b) A frequency drift progressively makes the signal component shift with respect to the search windows; c) A frequency jump can move the peak position from one side to the other. If a secondary lobe is locked a drop in power is observed.

A similar phenomenon is observed by using the oscilloquartz 8607. A drop in power, occurring after 32 s is clearly observable, as reported in figure [5.8]. Since the same phenomenon occurs with different oscillators, it is possible to assume that its cause is not related to the local carrier generation.

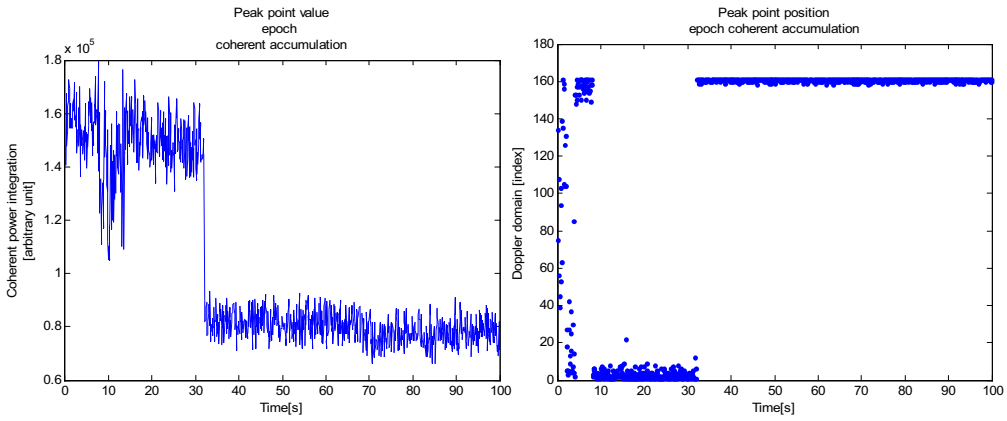

Figure 5.8: Left: Peak value of each individual epoch, one clearly observe the jump after 32 second; Right: Displays the peak position in matrix index unit for each individual epoch in function of the time.

Different snap shots of the accumulated power frequency distribution are reported in figure [5.9]. After 99.9 s the main signal peak is completely lost and coherent integration results completely ineffective.

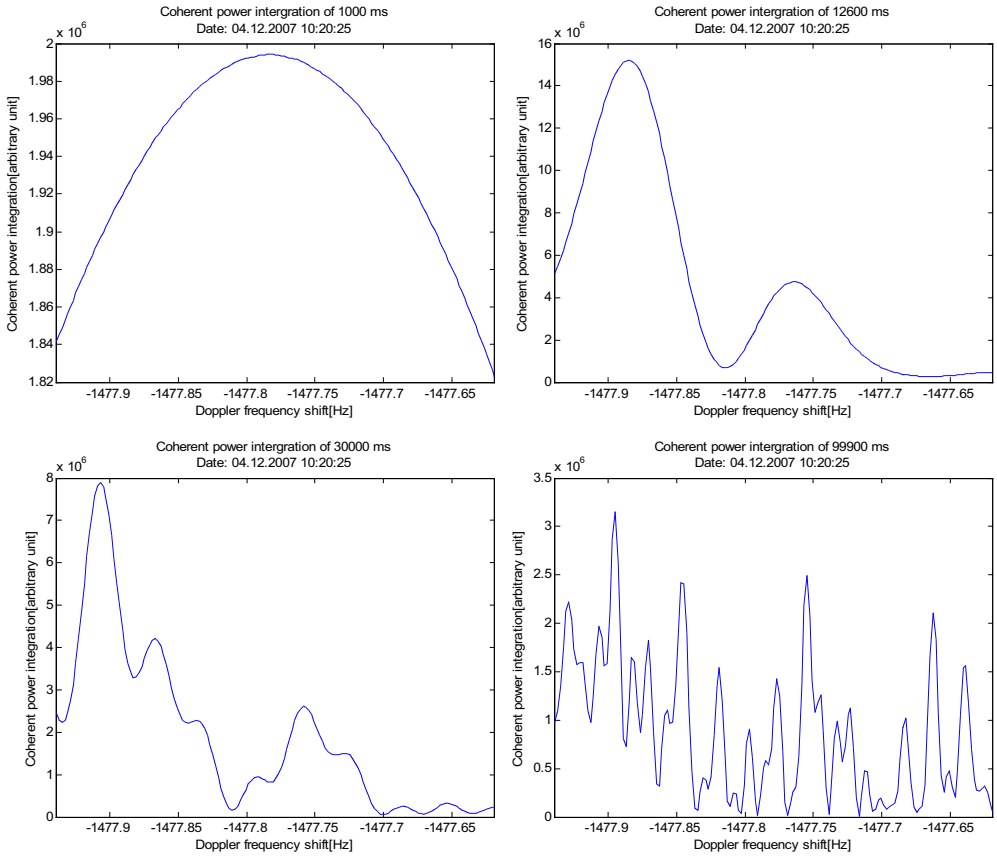

Figure 5.9: Snap shots of different coherent accumulated power frequency distribution. A strong degradation of the signal peak can be observed after 12.6 s. After 99.9 second no peak can be observed.

Figure [5.10] reports a zoom of the accumulated power frequency distribution. It is important to note that, due to the quantized Doppler step, it is not possible to exactly determine the maximum of the accumulated power distribution. A smaller frequency step should be used in order to obtain a more precise estimation of the peak position. Nevertheless the error in estimating the power maximum can be upper bounded. Since the position of the maximum has been estimated with a finite step, if the selected frequency bin is correct, the frequency value results in the range:

$$f_{peakmeasured} - \frac{\Delta f_{bin}}{2} < f_{peaktrue} < f_{peakmeasured} + \frac{\Delta f_{bin}}{2} \tag{5.1}$$

where in this case $f_{peakmeasured}$ is the measured peak position in the frequency domain, f_{bin} is the frequency step and $f_{peaktrue}$ is the real peak position.
Knowing that the shape of the power distribution along the frequency dimension is a square sinc, it is possible to evaluate the maximum loss affecting the peak power. In particular the measured peak value is, in the worse case $\frac{\Delta f_{bin}}{2}$ shifted compared to the

true position, so the corresponding loss is:

$$L_{oss} = \frac{sin^2\left(\pi\frac{\Delta f_{bin}}{2}T_c\right)}{\left(\pi\frac{\Delta f_{bin}}{2}T_c\right)^2} \tag{5.2}$$

where T_c is the coherent integration time. Thus, by denoting the measured peak magnitude value by $\hat{c}$ the following interval is obtained:

$$\hat{c} < c_{true} < \frac{1}{L_{oss}}\hat{c} \tag{5.3}$$

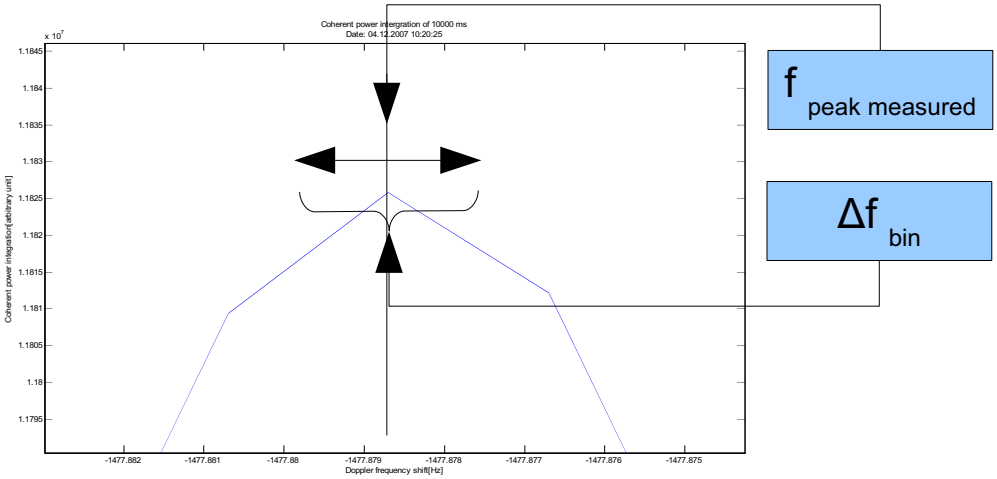

Figure 5.10: Zoom on the peak maximum.

5.1.2 Oscilloquartz 8626

This oscillator is a OCXO with Allan deviation of typically $5 \cdot 10^{-11}$. This is the cheapest OCXO tested during this project. The analysed data as reported in figure [5.11] shows that the coherent integration time is limited to about 3 s.

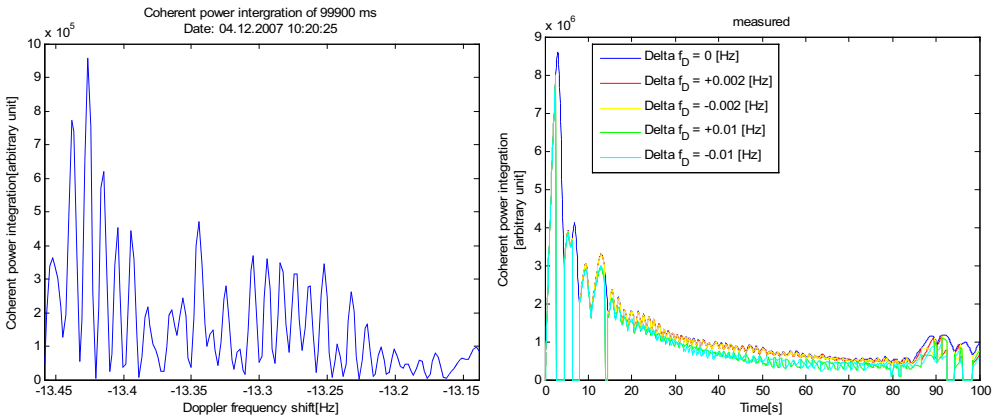

Figure 5.11: Left: Ratio between the theoretical and measured accumulated power; Right: Peak accumulated power vs coherent integration time.

This kind of oscillator was supposed to perform better than the Fordahl TCXO 0727, that can potentially integrate over 10 seconds. The advantage of the Oscilloquatz 8626 consists in the additional oven that should harden the oscillator against temperature variations. The obtained result can be explained by the fact the tests were run under the following conditions:

- Stable room temperature.
- No extra vibration.
- Calm air condition.

that nullify the technological advantage of the OCXO8626.

The TCXO 0727 performs better than the OCXO8626 under the above listed conditions, but in real applications the performance of both oscillators will be affected by temperature changes and vibrations. For example it is likely that under quick temperature changes the OCXO8626 would outperform the TCXO 0727.

5.1.3 Oscilloquartz 8712

This oscillator is a OCXO with Allan deviation less than $5 \cdot 10^{-11}$ for τ between 0.2 and 10s. Figure [5.12] gives an overview of the evolution of the correlation peak along the frequency dimension as function on the coherent integration time. It is worth to note that after 99.9 s coherent integration the correlation peak is still clearly observable.

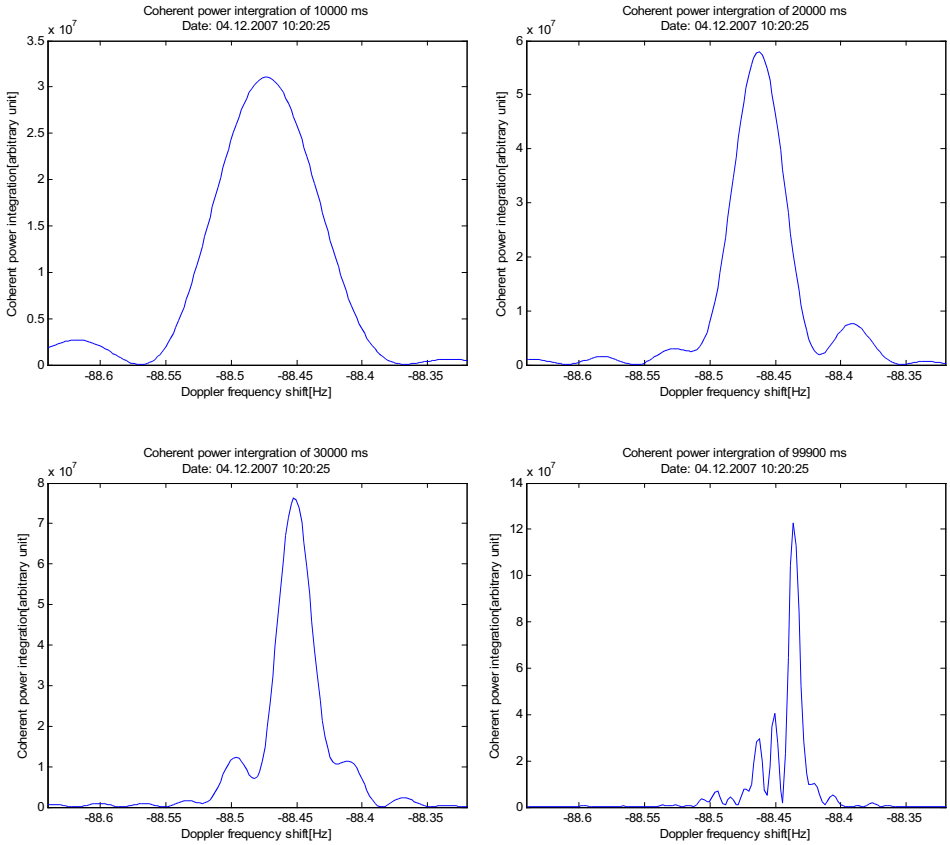

Figure 5.12: Correlation peak evolution as function of the coherent integration time, OCXO8712, SV30.

In figure [5.13] the peak power accumulated over 300 ms (3 x 100 ms epochs) has been plotted as function of time. As for the previous oscillators a jump occurs after 32 seconds. This plots show a behavior consistent with the one observed in figure [5.6] and explained in previous sections.

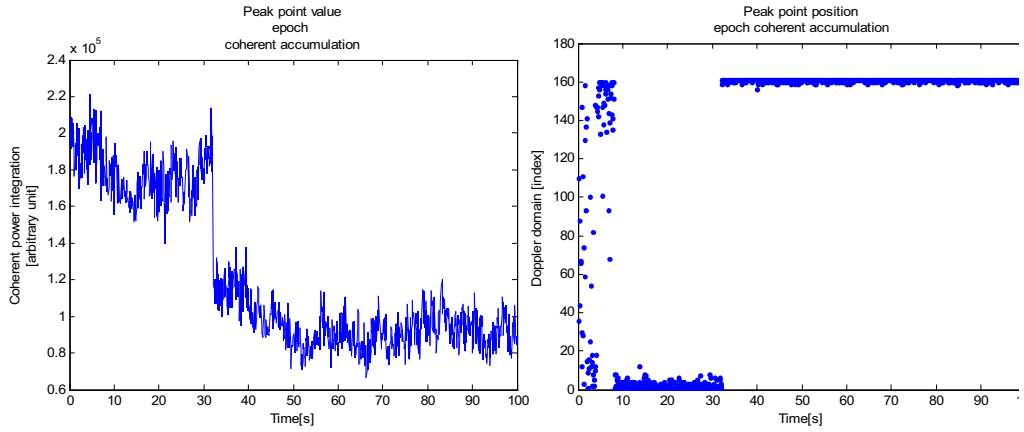

Figure 5.13: Left: A clear jump is observed after 32 s Right: The some behavior shape that for the 0727;

The effect on the accumulated peak magnitude is depicted on figure[5.14]. After 32 s a clear drop in the accumulated power is observed. This phenomenon is due to the peak magnitude variation. After 40 s the accumulated power starts growing again. In this case there is no evidence of limits for the integration time.

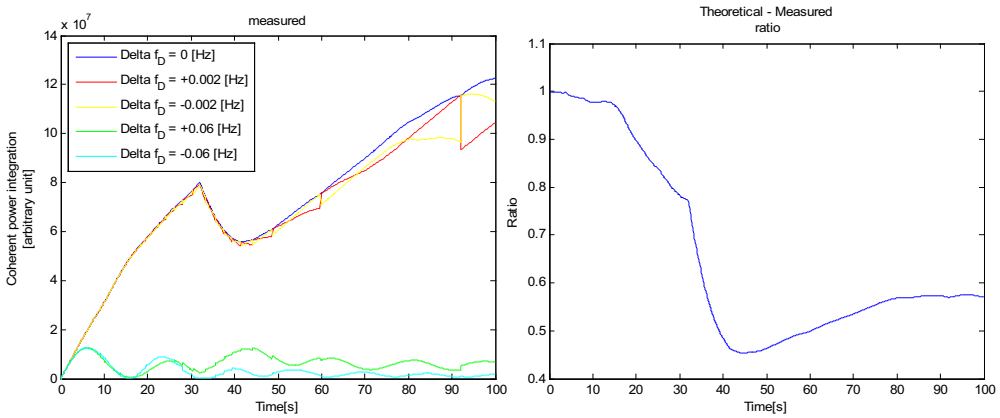

Figure 5.14: Left: The peak magnitude time evolution ; Right: Ratio between the theoretical value peak and the measured one

The different plots, reported in different colors in figure [5.14], refer to the accumulated power of frequency cells located at Δf_D Hz from the main peak. The accumulated powers of these cells provide an intuitive perception of the width of the main peak: for $\Delta f_D = \pm 0.06$ Hz the accumulated power is extremely reduced, probably corresponding to secondary peaks.

By ignoring the first 40 s integrated in figure[5.14], it is possible to observe a coher-

ent integration time of 60 seconds is realized with only 12% peak magnitude difference between the theoretical expectation and the measurement. This result is depicted in figure [5.15]. None 32 s effect are observed.

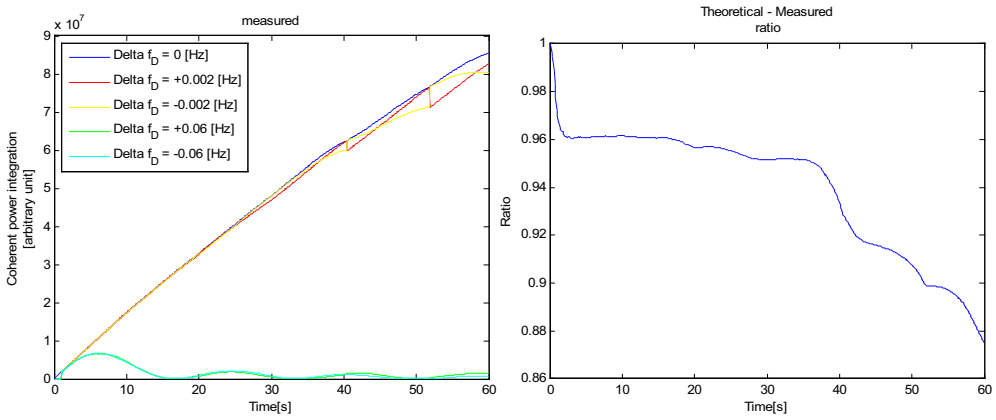

Figure 5.15: Data starts at epoch 400, Left: The peak magnitude time evolution; Right: Ratio between the theoretical value peak and the measured one;

The 32 s artifact has been observed in all the performed tests and for all oscillators. Also the early bump observed with the with 8626 and the 0727 do not appears anymore. Which gives the indication that this phenomenon of “early bumps” in the accumulation power raise is visible for lower quality oscillators only.

5.1.4 Oscilloquartz 8663

The results for the Oscilloquartz 8663 are depicted in figure [5.16]. These results are comparable with the ones previously obtained. A change in slope of the accumulated power can be observed in correspondence of a 32 s integration time. In picture caption clk refers to the satellite clock and osc to the local oscillator.

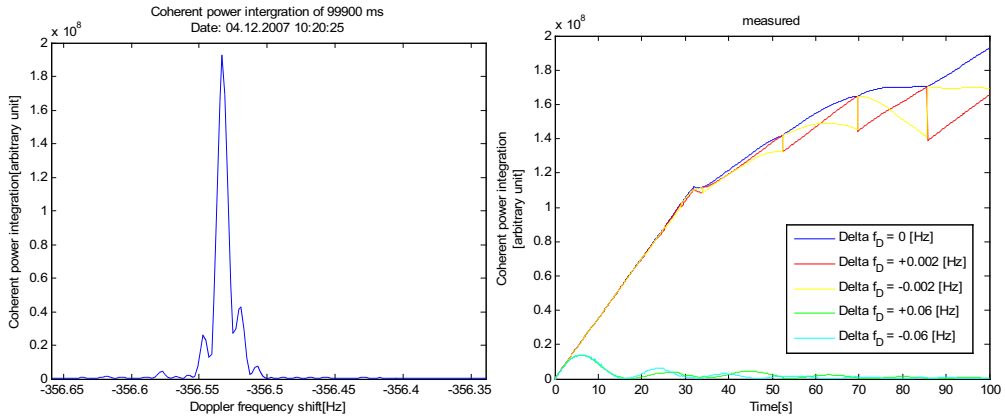

Figure 5.16: SV30(prn30) clk:Cs osc:8663, Left:The peak magnitude time evolution; Right: Ratio between the theoretical value peak and the measured one;

5.1.5 Oscilloquartz 8683

The results for the Oscilloquartz 8683 are depicted in figure [5.17]. These results are comparable with the ones previously obtained. A change in slope of the accumulated power can be observed in correspondence of a 32 s integration time.

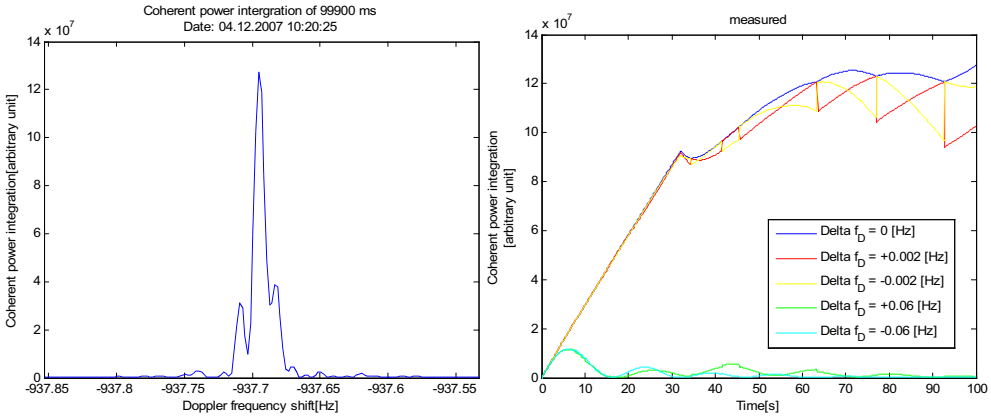

Figure 5.17: SV30(prn30) clk:Cs osc:8683,Left: The peak magnitude time evolution; Right: Ratio between the theoretical value peak and the measured one;

5.1.6 Oscilloquartz 8788

The results for the Oscilloquartz 8788 are depicted in figure [5.18]. These results are comparable with the ones previously obtained. A change in slope of the accumulated power can be observed in correspondence of a 32 s integration time.

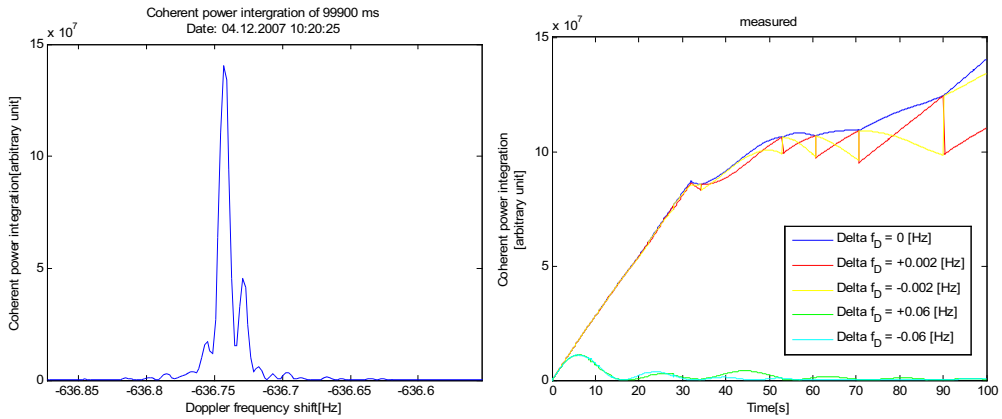

Figure 5.18: SV30(prn30) clk:Cs osc:8788,Left: The peak magnitude time evolution; Right: Ratio between the theoretical value peak and the measured one;

5.1.7 Oscilloquartz 8607

The results for the Oscilloquartz 8607 are depicted in figure [**??**]. These results are comparable with the ones previously obtained. A change in slope of the accumulated power can be observed in correspondence of a 32 s integration time.

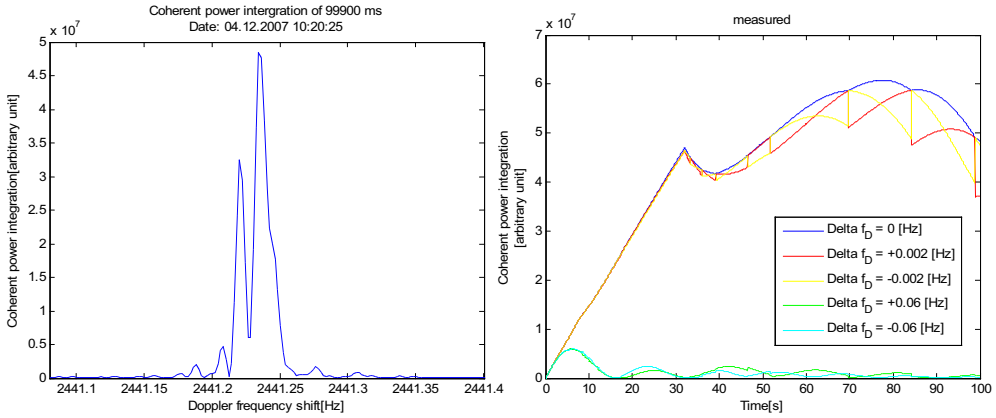

Figure 5.19: SV30(prn30) clk:Cs osc:8607, Left: The peak magnitude time evolution; Right: Ratio between the theoretical value peak and the measured one;

5.1.8 Efratom Rubidium

The results for the Efratom rubidium are depicted in figure [5.20]. These results are comparable with the ones previously obtained. A change in slope of the accumulated power can be observed in correspondence of a 32 s integration time.

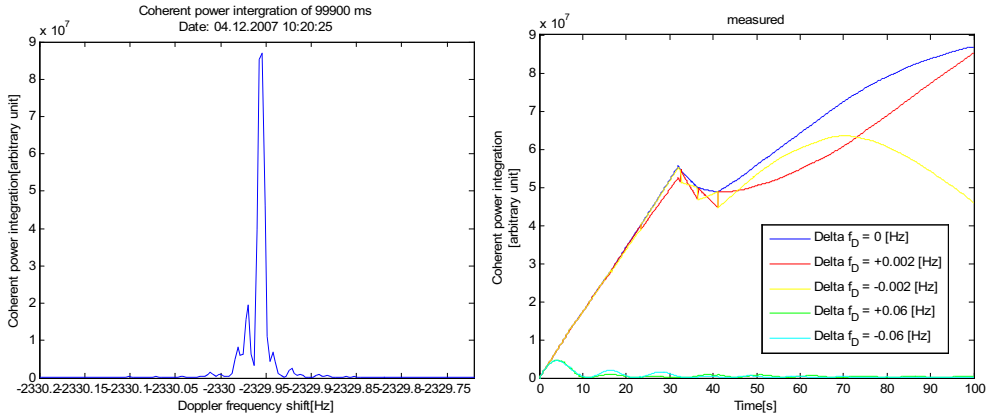

Figure 5.20: SV30(prn30) clk:Cs osc:rub, Left: The peak magnitude time evolution; Right: Ratio between the theoretical value peak and the measured one;

5.1.9 Conclusion

Additional material regarding the oscillator performance is reported in appendix [D] where graphs similar to the ones displayed in this section are provided. The following conclusions also include those results. The observed phenomena can be summarized as follows:

Early bumps

Early bumps can appear in the plot of the accumulated power evolution vs. coherent integration time for lower quality oscillators, characterized by an Allan deviation $\sigma = 5 \cdot 10^{-11}$. This phenomenon is characterized by a drop in the coherent power accumulation as shown in figure [5.21].

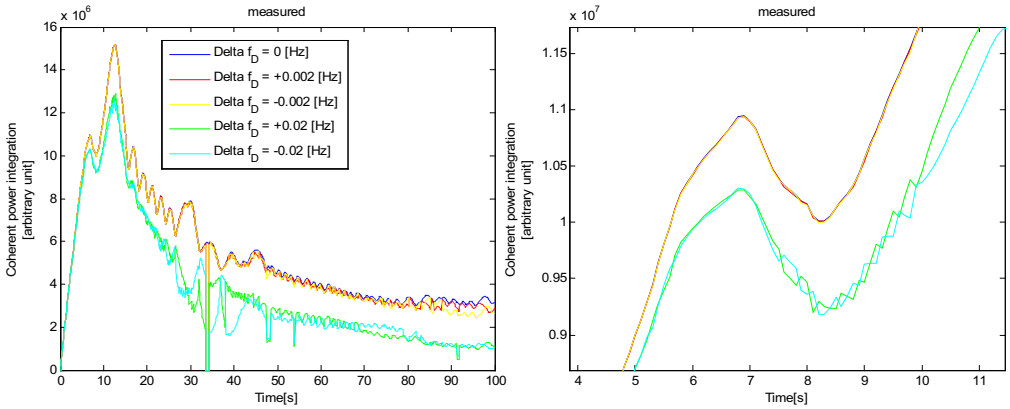

Figure 5.21: SV30(prn30) clk:Cs, osc:0727, Left: Coherent power accumulation; Right: Zoom on the “early bumps”;

As explained in figure[5.2] this artifact appears exactly at the some time a side lobe begins to appear. Early signal degradation is probably at the origin of the effect.

Side index jumps

Side index jumps are essentially due to the fact that the main peak moves in function of time in the frequency domain (see figure [5.22]). he consequence is that the peak suddenly appears on one of the frequency side indexes. Keeping in mind that the frequency domain is divided in several discrete frequency bins explains the discontinuous nature of the transitions. Considering a larger number of bins would smooth the transitions.

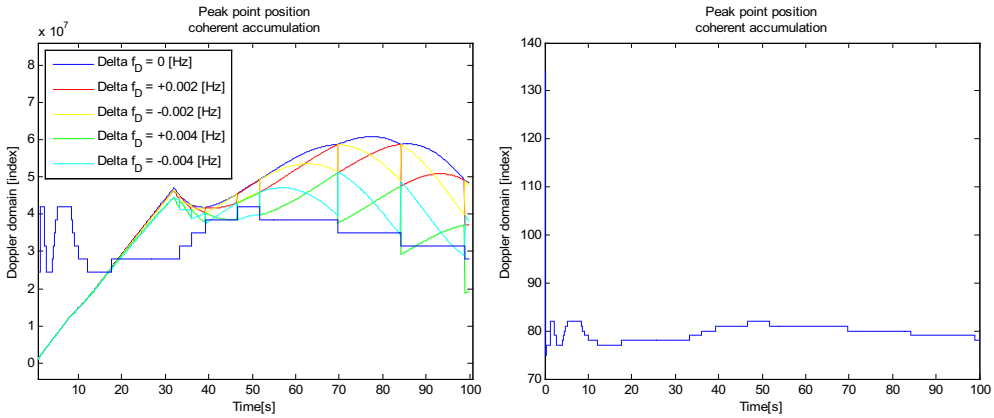

Figure 5.22: SV30(prn30) clk:Cs, osc:8607, Left: Coherent power accumulation and superposed peak position in frequency domain; Right: Peak position in frequency domain;

Regular peak magnitude drop

Regular peak magnitude drop effect refers to the phenomenon appearing after 32 seconds on each analyzed data set. The shape of the artifact is different from the “early bumps”. It is possible to observe a quick power drop followed by a smooth raise; on the contrary, in the case of early bumps, a quick drop and a quick raise of the accumulated power is observed. This suggests that the two phenomena have different causes. It is also possible to observe that accumulated powers of contiguous frequency cells behave similarly as the main peak power. Thus, this phenomenon can hardly related to a smooth and continuous frequency drift. Figure [5.23] highlights the correlation between frequency peak position and changes in the accumulated power.
Further analyses are required to better explain the dependence between the two phenomena.

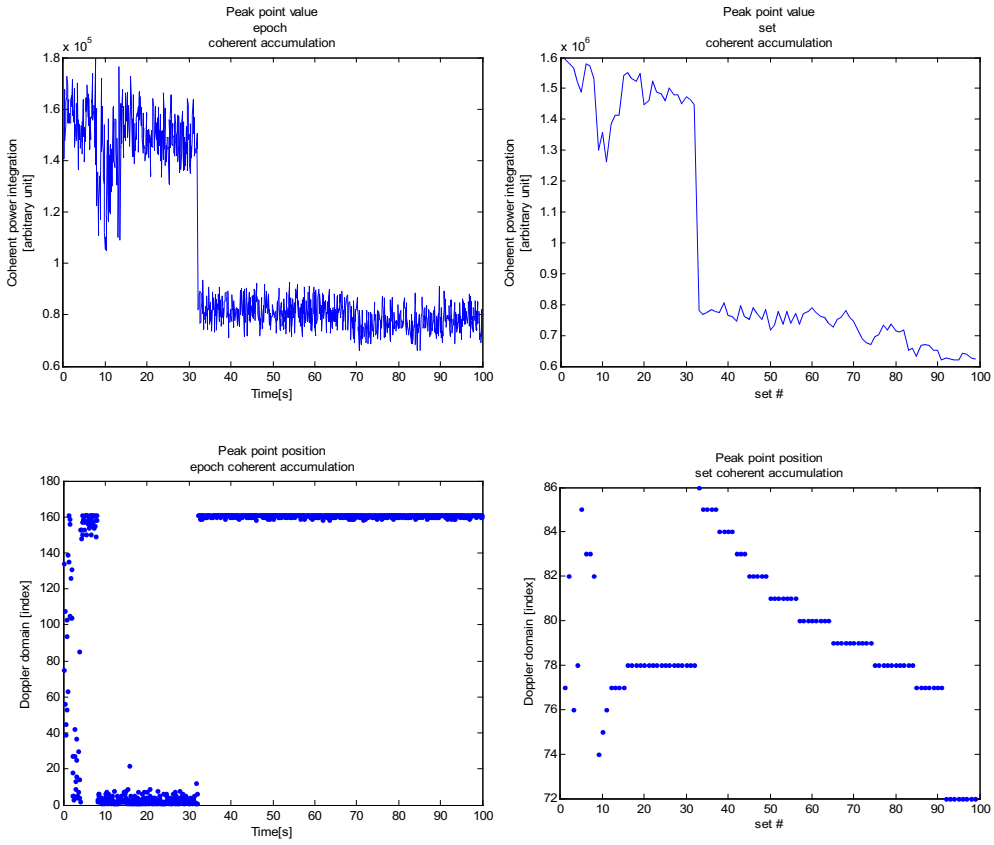

Figure 5.23: SV30(prn30) clk:rub, osc:8607, Other phenomenon appearing at 32 second on each open-sky data sets considered in this study. The left images represent data for each epoch; the right images represents data for set of 10 accumulated epoch(i.e. 1 second)

Double peak

On all data sets considered in this study double peak appears after passing a certain time of coherent integration, typically between 45 and 60 s. Depending on the considered data set the secondary peak is more or less visible. No strong dependence relating the local oscillator quality, the secondary peak amplitude and different satellites has been observed. In certain data sets [5.24] and [D.25] it is also possible to observe the secondary peak becoming stronger than the original peak.

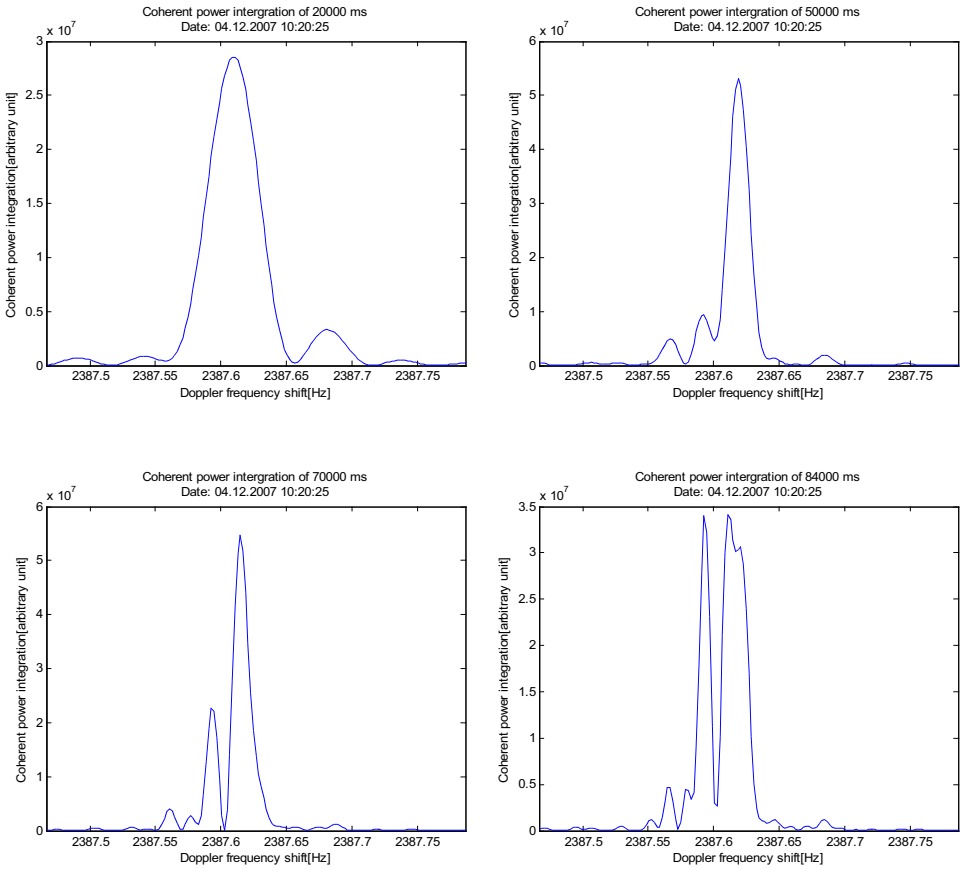

Figure 5.24: SV36(prn6) clk:Rub, osc:8683, Search space time evolution.

5.2 Indoor signal acquisition

In this section the results based on the set-up depicted in figure [4.5] are presented. The general idea is to have a remote indoor antenna and an open-sky reference receiver. In this way the front-end is fed with a strong attenuated signal and corrupted by multipath, whereas the reference always receives a clear GPS signal. The basic idea is to show that the results obtained for open sky-measurements are still valid when working under real conditions.

Since the signal has to be acquired using integration time longer than 1 second, it is impossible to use efficiently the autofocus function of the software. The general processing methodology consists in executing a coarse acquisition of the search space using the parameters described in table [5.2][4].

[4]Those parameters are pre-programmed in the software and can be loaded by click on the “weak signal 1” button.

Parameter	value
Num Correlators	15
Correlator Spacing [chip]	0.5
Num Frequency Bins	161
Frequency bin spacing [Hz]	0.02
Coherent Correlation Length [ms]	100
Number of epochs	300

Table 5.2: Parameters used for the search space coarse acquisition for indoor measurement.

The consequence is that if the nominal output frequency is not calibrated precisely enough or not stables enough to be in the considered coarse search space, it will not be possible to acquire the signal. Of course it is conceptually possible to increase the search space size, but the problem will be the increased processing time. The oscillators which were not able to comply with those constrains were the Fordahl 0727, the Oscilloquartz 8626 and 8712. These three oscillators are the cheapest ones belonging to the tested collection. So no successful signal acquisition has been demonstrated using those medium cost (less than 100 Euro) frequency generators.
If a finer acquisition is needed, a second step can be computed using the parameters described in table [5.3] [5].

[5]Those parameter are pre-programmed in the software and can be loaded by click on the “weak signal 2” button.

Parameter	value
Num Correlator s	1
Correlator Spacing [chip]	1
Num Frequency Bins	161
Frequency bin spacing [Hz]	0.003
Coherent Correlation Length [ms]	100
Number of epochs	999

Table 5.3: Parameters used for the search space fine acquisition for indoor measurement.

Acquiring at least 4 different satellites and determining their respective code delay, would allow using the ephemeris and the reference antenna position to calculate the remote antenna position (user position). Due to time constrains only one set of data have been processed to obtain 5 satellites and a reasonably good precision in the code domain.

5.2.1 Oscilloquartz 8607

Here the Oscilloquartz 8607 is used to acquire strongly attenuated signal taken in point "C"of figure [4.6]. If one wants to know the minimum integration time needed to acquire the signal, a possibility is to look at the peak position in the code domain. If the correlation peak stays at the same position for sufficiently long time (see figure[5.25]), it would be considered that the GPS signal has been successfully acquired. In other words this means that the required detection SNR threshold has been reached. If the peak don't comes out of the noise floor the peak position in the code domain will randomly vary.

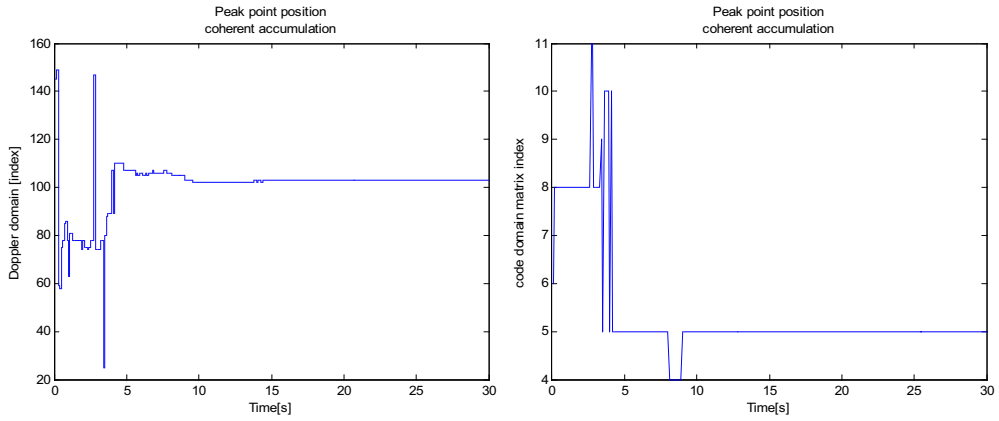

Figure 5.25: SV54(prn18) clk:Rub, Left: The time variation of the peak position in the frequency domain; Right: in the code domain.

Using a coherent integration time of 30 seconds allows a clear signal acquisition as shown in picture[5.26]. One can measure the SNR taking the peak maximum value expressed in arbitrary unit and divide it by the mean noise floor value. The noise floor value is estimated by averaging the noise value in a search space area where no GPS signal

is present. The measured SNR value measured after a 30 seconds coherent integration time is, in this case, 18.3 dB.

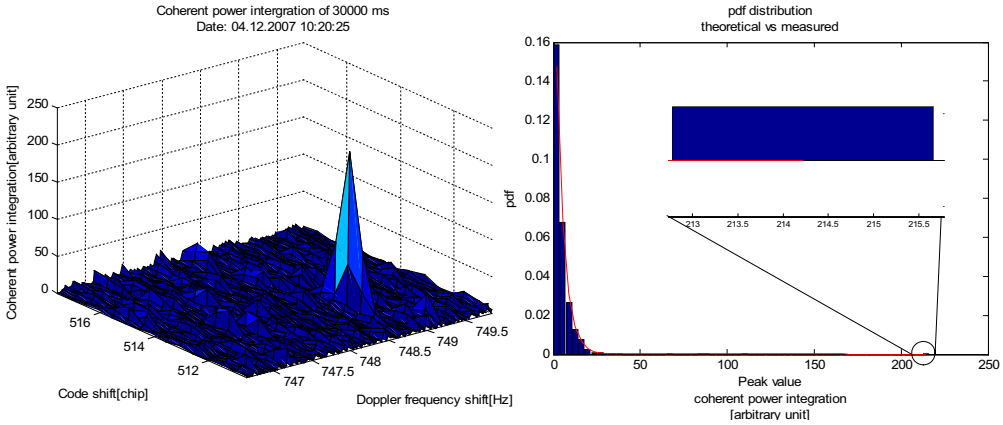

Figure 5.26: SV54(prn18) clk:Rub, Left: Search space view, with a strong peak coming out of the noise floor; Right: In the histogram the signal peak appears as an outlayer in the noise distribution.

The next step is to determine the minimum SNR threshold to perform clear peak detection. The methodology consist in visualizing the search space corresponding to different SNRs and decide either if the peak comes clearly out of the noise or not as shown in figure [5.27]. Empirically one can fix the threshold at 14 dB in order to be really sure to get the correlation peak. Nevertheless a 12 dB threshold can be used if one take some precautions, but one takes the risk of a wrong detection due to the presence of secondary peaks as shown in figure [5.27].

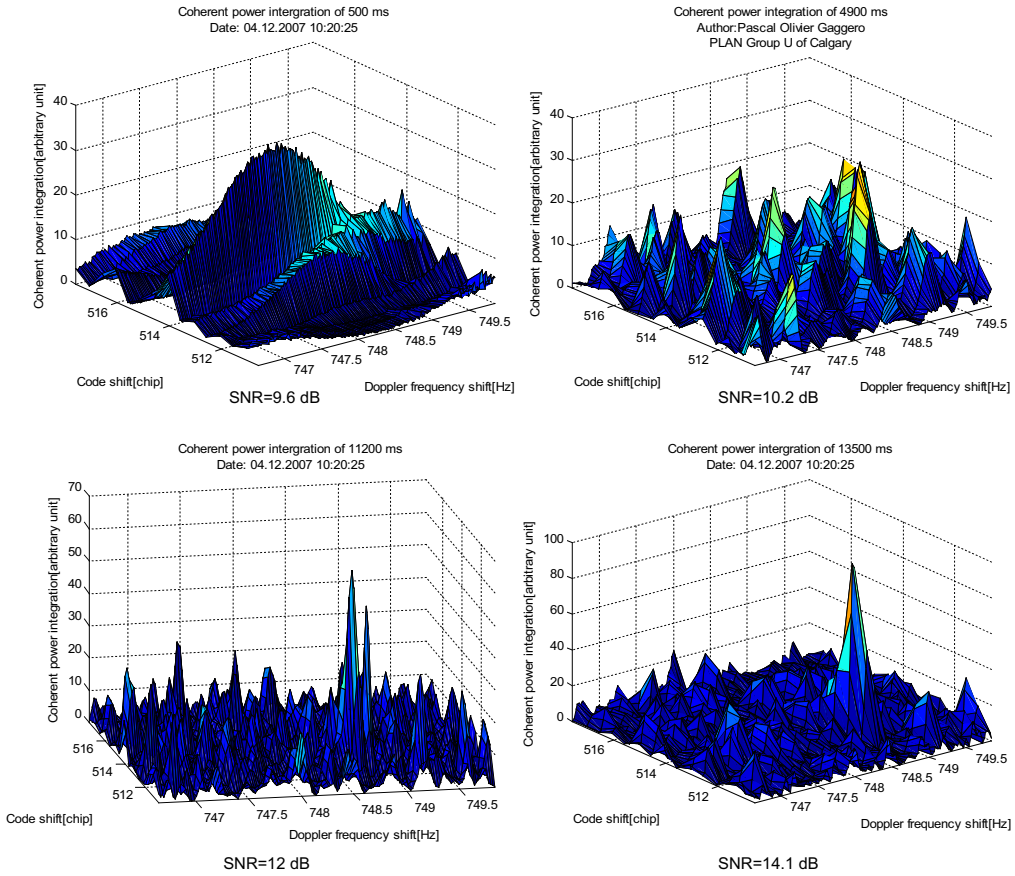

Figure 5.27: SV54(prn18) clk:Rub, Measured SNR versus visual observation.

Table [5.4] resumes the main results obtained doing the indoor acquisition on other satellites as well (see appendix [D.2.1]). The C/No is measured with a custom estimator based on Maximum Likelihood principle, thus this estimator will be denoted as Maximum Likelihood Estimator (MLE). Using this estimator the C/No in the corridor is between 2.5 and 3.5 dB-Hz. Nevertheless prn 15 is measured as 11.9 dB-Hz. This can be due to multipath or constructive interferences. All the GPS signals presented here have to go thought several walls made in concrete, wood and glass, so using the elevation and azimuth it is possible to visualize in the reality from where should the direct signal coming from. There is no evident relationship between the code fix time, C/No and direct signal path. This indicates that multipath and constructive/destructive interference play an important role. The prn 6 has not been successfully acquired after 30 second coherent integration, this is probably due to the fact that this satellite was low at the horizon (14.3 degrees) and azimuth (168 degrees). The consequence is that the signal has been probably attenuated by campus buildings that surround the CCIT and atmosphere. The measured C/No obtained via the reference receiver is 37 dB. If one assume an attenuation of 42 dB one get C/No in the corridor of -5 dB. One will demonstrate in the section

[5.3] that it not possible to acquire such signals. Table [5.4] summarizes the acquisition results.

sv (prn)	24(24)	33 (3)	45 (21)	55 (15)	54 (18)
MLE C/No [dB-Hz]	2.5	-2.1	3.9	11.9	3.5
SNR after 30s [dB]	17.3	12.8	18.7	26.7	18.3
over 14 dB after [s]	5.3	> 30	6.3	1.8	13.5
code fix after [s]	0.7	10.9	17.2	13.7	9.1
measured code delay [chip]	887.7	391.8	127.3	402.4	512.6
elevation	31.7	32.3	71.1	43.9	78.8
azimuth	107	303.6	108.3	70.2	224.9
open-sky C/No	43.8	43	48.0	46.8	47.8
attenuation	41.3	45.2	44.1	34.9	44.3

Table 5.4: Result of indoor acquisition using the Oscilloquartz 8607.

5.2.2 Other oscillators

Similar analysis can be conducted using other oscillators. Results are reported in appendix [D.2.1], [D.2.2], [D.2.3], [D.2.4] and [D.2.5]. Their results are summarized in tables [5.5], [5.6], [5.7] and [5.8].

sv (prn)	36 (6)	54 (18)	45 (21)	24 (24)
MLE C/No [dB-Hz]	3.6	4.4	16.23	14.86
SNR after 30s [dB]	18.7	19.2	31	29.63
over 14 dB after [s]	5.7	8.4	1.3	0.6
code fix after [s]	5	2.3	1.1	0.1
measured code delay [chip]	962.1	798.9	799	1017
elevation	17	75.9	73.9	43.2
azimuth	168.8	224.6	105.6	105.3
open-sky C/No	38.6	47.8	47.7	43.9
attenuation	35	43.4	31.47	29

Table 5.5: Result of indoor acquisition using the Oscilloquartz 8683.

sv (prn)	36 (6)	54 (18)
MLE C/No [dB-Hz]	2.1	4.5
SNR after 30s [dB]	16.9	19.4
over 14 dB after [s]	17.6	3.3
code fix after [s]	3.3	0.3
measured code delay [chip]	473.8	971
elevation	25.3	67.1
azimuth	168.8	222.3
open-sky C/No	41.7	48.6
attenuation	39.6	44.1

Table 5.6: Result of indoor acquisition using the Oscilloquartz 8663.

sv (prn)	33 (3)	36 (6)	54 (18)	45 (21)
MLE C/No [dB-Hz]	0.8	5.9	-2.2	8.87
SNR after 30s [dB]	15.7	20.7	11.8	23.6
over 14 dB after [s]	7.5	4.2	> 24	0.5
code fix after [s]	3.1	1.5	8.1	0.1
measured code delay [chip]	982.6	779.1	615.9	967.6
elevation	28.7	19.5	73.2	76.5
azimuth	307.5	168.8	224	102.5
open-sky C/No	42.6	39.5	48	47.9
attenuation	41.8	33.6	50.2	39

Table 5.7: Result of indoor acquisition using the Oscilloquartz 8788.

sv (prn)	54 (18)	45 (21)	24 (24)
MLE C/No [dB-Hz]	2.9	8.1	12.83
SNR after 30s [dB]	17.8	22.9	27.61
over 14 dB after [s]	1.3	3.8	0.6
code fix after [s]	0.2	0.9	0.4
measured code delay [chip]	682	535	390.3
elevation	84.8	65.3	26.8
azimuth	222.2	113	110.2
open-sky C/No	47.4	48.1	42.2
attenuation	44.5	40	29.37

Table 5.8: Result of indoor acquisition using the Efratom Rubidium.

5.2.3 Indoor positioning

Based on the code delay founded in the previous sections, it is possible to calculate a position solution for the indoor remote antenna at data recording start time. The processing idea is explained in figure [5.28]. A Matlab script called poscalculation.m is also available in the Matlab advanced tool folder of the electronic release of the thesis.

The minimum number of satellite needed is 4 to get full x,y,z coordinates. One can note that 3 satellites is sufficient if the user height is given as input. Here position with 4 SVs are calculated. Nevertheless 4 satellites do not provide an accurate position since they define a poor geometry. As shown in figure [5.29] with 4 satellites one achieves accuracy in the range of hundred meters. Whereas adding a 5th satellite, gives a better accuracy at least in this case. The best position calculated using the oscillator Oscilloquartz 8607, 30 second of coherent integration time and a 5 SV geometry gives an accuracy of about 20 meters in the horizontal plane and 100 meters for the height. Considering the attenuation of 40-45 dB measured in the corridor the accuracy of the position is interesting and this should further investigated. Adding more satellites to the solution may also provide a better accuracy by providing a better geometry to the solution.

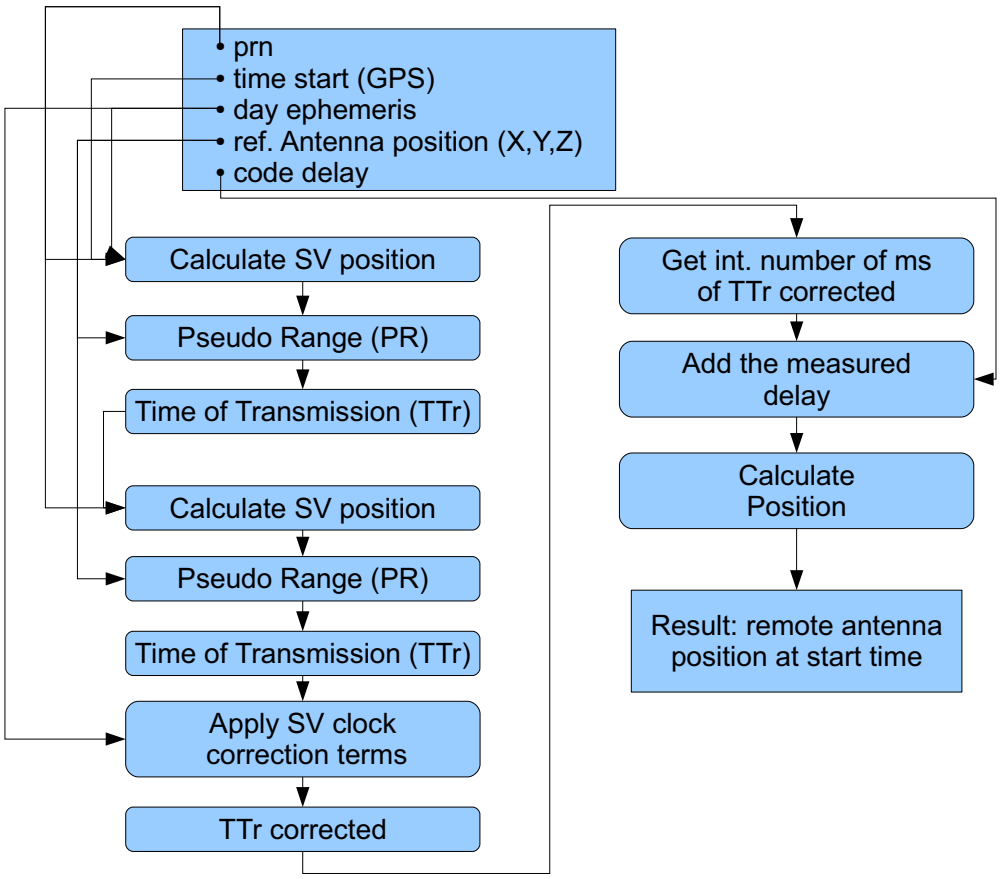

Figure 5.28: Calculation flow for calculating a position based on the code delay measurement.

Figure 5.29: Position calculated using the code delay found in the previous sections.

5.3 SNR and XO model

Considering several curves of the ratio of the theoretical and measured peak magnitude as function of the coherent integration time a common trend can be observed. This trend can be roughly modeled as a parabola. This allows to capture the general evolution of the SNR. By using this observation formula [2.11] can be extended in order to roughly take into account the fact that the coherent power accumulation growth is not ideal. In this way the following formula is obtained:

$$SNR = C/N_0 - a + 10 \cdot log_{10}(T_c) + 10 \cdot log_{10}(poly(n, T_c)) \tag{5.4}$$

where

$$poly(n, T_c) \tag{5.5}$$

is the polynomial model of degree n (here $n = 2$).

Plotting relation on the left side of figure [5.31] (5.4) using the parabola found in figure [5.30], one can observe the flattening of the SNR evolution at after about 30 second of coherent integration time. On the right side of figure [5.31] a measured SNR evolution is reported, it is interesting to note the saturation of the SNR predicted using a parabolic trend. The noisy shape of the measured SNR evolution is essentially due to the fact that before passing the 14 dB no peak is acquired. However further investigation can be conducted to establish a theoretical model of the SNR behavior.

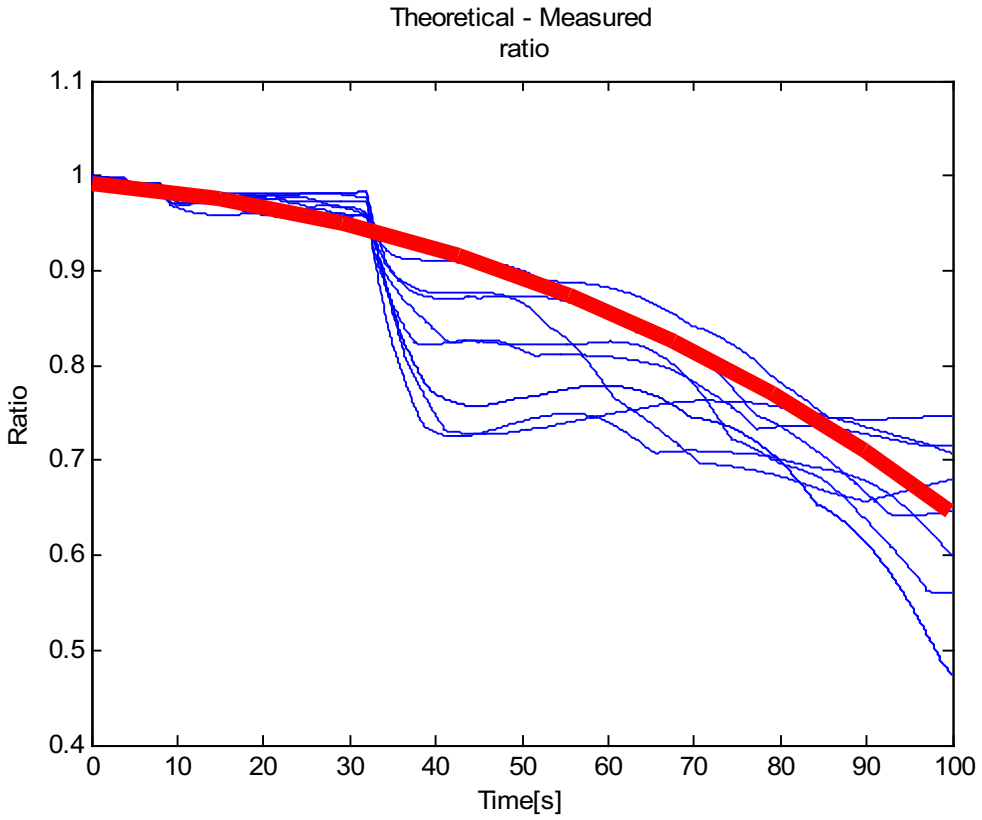

Figure 5.30: Parabolic curve modeling of the ratio of the theoretical and measured peak magnitude as function of the coherent integration time.

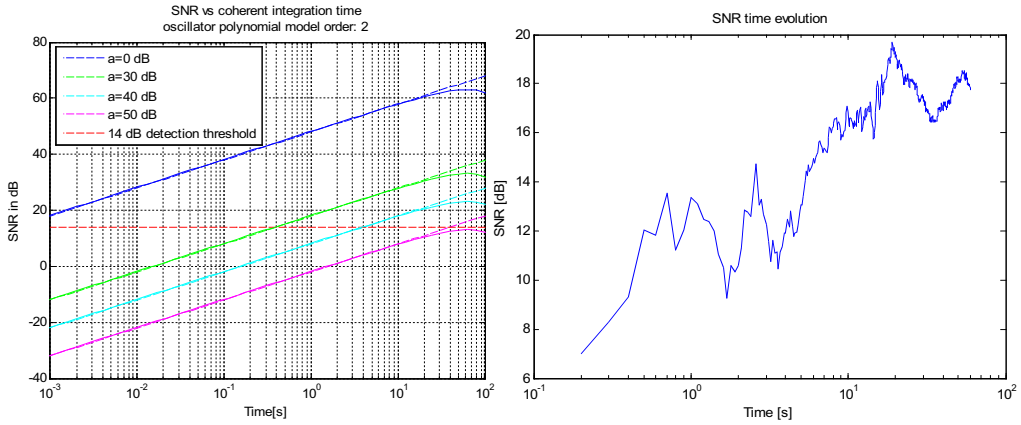

Figure 5.31: Left: trend modeling with a parabola, Right: Measured SNR evolution

5.4 Allan deviation

In this section the methodology described in section [4.4.6] is used to measure the Allan deviation observed in the GPS signal frequency.

Figure [5.32] displays the measurement realized with various oscillators on SV30 (prn30). The colors represent oscillators of comparable quality. The legend of figures [5.32], [5.33] and [5.34] follow the following rules:

- Red represents the oscillators with Allan deviation smaller than $5 \cdot 10^{-11}$ over an averaging time interval $0.2s < \tau < 10s$. In the data sheet there are two different value of Allan deviation : the typical and guaranteed one. The difference is the following:
  - Guaranteed means it is sure that the oscillator will meet the given specifications.
  - Typical means that in average the oscillator is characterized by this value.

  In the set of red marked oscillators tested there are the Oscilloquartz 8626 with an Allan deviation guaranteed lower than $5 \cdot 10^{-10}$ and a given typical value of $5 \cdot 10^{-11}$. The 8712 with a guaranteed value lower than $5 \cdot 10^{-11}$. So what is expected is that the 8712 is better than the 8626 in term of Allan deviation from the considered averaging times. It is important to note that the Fordahl manufactured TCXO 0727 has values specified in the datasheet. According to their engineers for this oscillator category it not common in the industry to measure the Allan deviation and to give it in the data sheet. Nevertheless Fordahl engineers provide us some estimations based on the phase noise measurement to determine the Allan deviation plot. This approach is called “phase noise to sigma tau conversion” and is restricted to certain averaging time (i.e. certain tau). They found that it should

be lower than $5 \cdot 10^{-10}$ on the previously considered averaging time interval. The red dashed horizontal line represents the $5 \cdot 10^{-11}$ threshold.

- Blue is for oscillators whose Allan deviation is guaranteed to be lower than $1 \cdot 10^{-11}$.

- Green is for oscillators whose Allan deviation is guaranteed to be lower than $1 \cdot 10^{-12}$. The 8607 is a very expensive and precise frequency reference which has been measured by the manufacturer at $7.47 \cdot 10^{-14}$ for $\tau = 1$s.

- Violet corresponds to measurements of the satellite clocks'Allan deviation done by other laboratories also using GPS taken from the articles [15] and [8].

The error bar computed in figure [5.33] are based one of the calculation technique describe in [20]. The errors bar is here to take into account for the fact that for large averaging time there is less samples than for smaller ones. So the averaging will be less efficient. For example if the $\tau = 1$s is calculated using 60 samples, there is only 6 samples for $\tau = 10$s. A coarse estimation of the error due to this effect can be obtained with this formula:

$$\pm E_b(\tau) = \frac{\sigma(\tau)}{\sqrt{N_\tau}} \tag{5.6}$$

where N_τ is the considered number of samples for this particular Allan deviation $\sigma(\tau)$. A better error estimation can be done using much advanced technique detailed in [20], but not applied in this work.
The data have been processed for all oscillators and for 2 different satellites namely SV 36 and 30 operating respectively with cesium and rubidium atomic clock. Comparing figures [5.32] and [5.34] the following comments can be done:

- The Oscilloquartz OCXO 8626 and the Fordahl TCXO 0727 appear to be of comparable quality in term of Allan deviation. Nevertheless under severe and quick temperature changes the OCXO will probably be better. Comparing these results with the satellite atomic clock measured by [15] and [8], one can expect that the two local measured oscillators are at least one order of magnitude worst than the SV clocks. So the expectation here is to measure the Allan deviation of the front-end oscillator. The measurements meet the characteristics reported in the data sheet.

- The Oscilloquartz OCXO 8712 performance is close to the one produced by the oscillator from the "blue" group. Even if on both considered data sets it appears to be slightly over the average of the blue group oscillator performances.

- According to what [15] and [8] measured, the 8712 and the blue group oscillators meet performances very similar to the on-board satellite clocks. So the measured Allan deviation can be influence by both clocks.

- Interesting are the results of the green oscillators that are at least one order of magnitude better in term of Allan variance for τ smaller than 10s compared to the satellite clock. So one should normally be able to neglect the short terms errors of the local oscillator and only observe satellite clock short term frequency errors (i.e. this could potentially be a method to remotely measure the satellite on-board clocks Allan deviation). The results shown in figure[5.32] shows that the green oscillator measured do not meet the local oscillator data sheet expected value, which should be much better than what is obtained. So one of the conclusions is that one is actually measuring the satellite clock. This is confirmed by the fact that these two curves are superposed also when considering the error bars drawn in figure [5.33]. Considering some oscillators on figure [5.34] it is worth to observe that the green and blue oscillators follow about the same trend also in agreement with what [15] and [8] measured.

- The conclusion is that the Cesium atomic clock measured in figure [5.32] is better in term of Allan deviation than the Rubidium clock of figure [5.34] for the time interval 1s$< \tau <$ 10s. An additional study of the Allan deviation for τ smaller than 1s (see figure [5.35]) shows that in fact rubidium oscillators outperform cesium clocks for τ smaller than 100ms in this data set.

To conclude this discussion about the measurement of the Allan deviation it is important to highlight the fact that other devices impact the estimation of the Allan deviation. Elements like frequency multipliers and PLLs add noise to the signal, so using a very good oscillator with poor frequency multiplier or PLLs may deteriorate the performance of the considered system. Here there was no evidence that those elements play a significant role in the presented results.

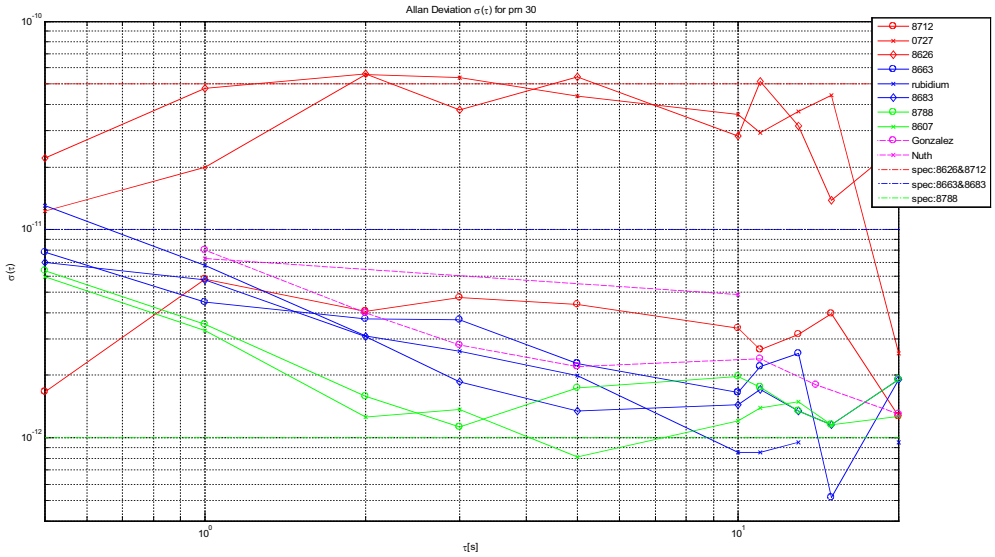

Figure 5.32: Allan deviation plot for various oscillators, for SV30, CS

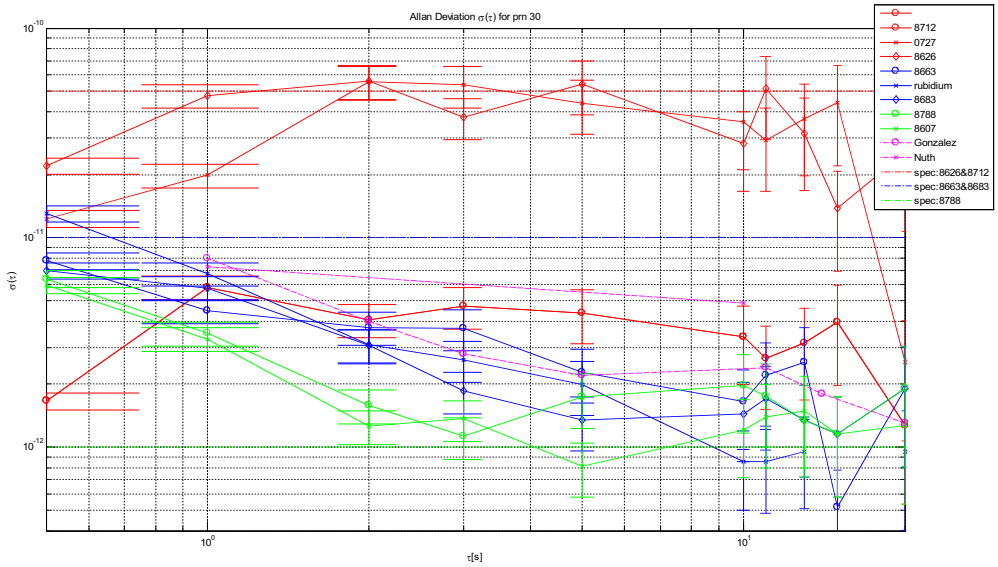

Figure 5.33: Allan deviation plot for various oscillators, with errors bars, for SV30, CS

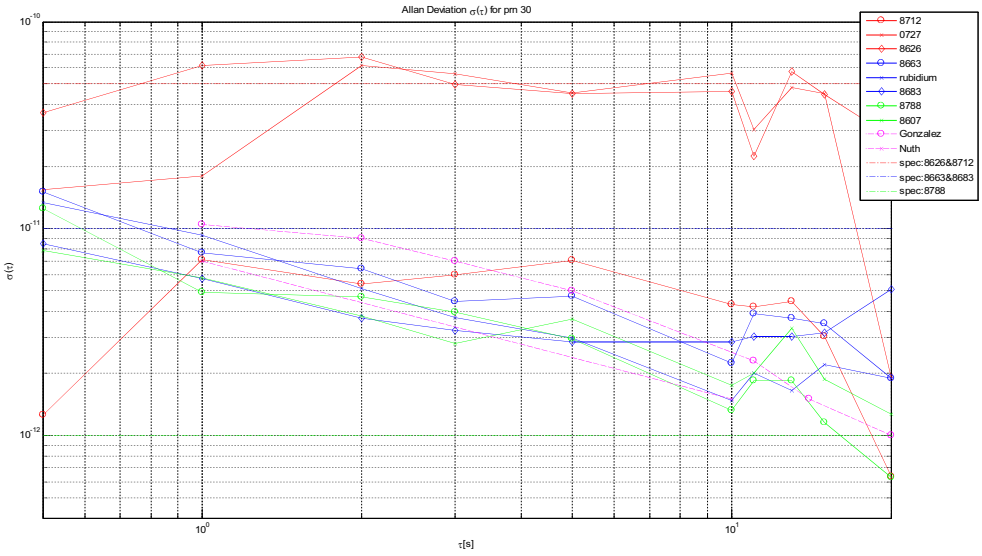

Figure 5.34: Allan deviation plot for various oscillators for SV36, Rb

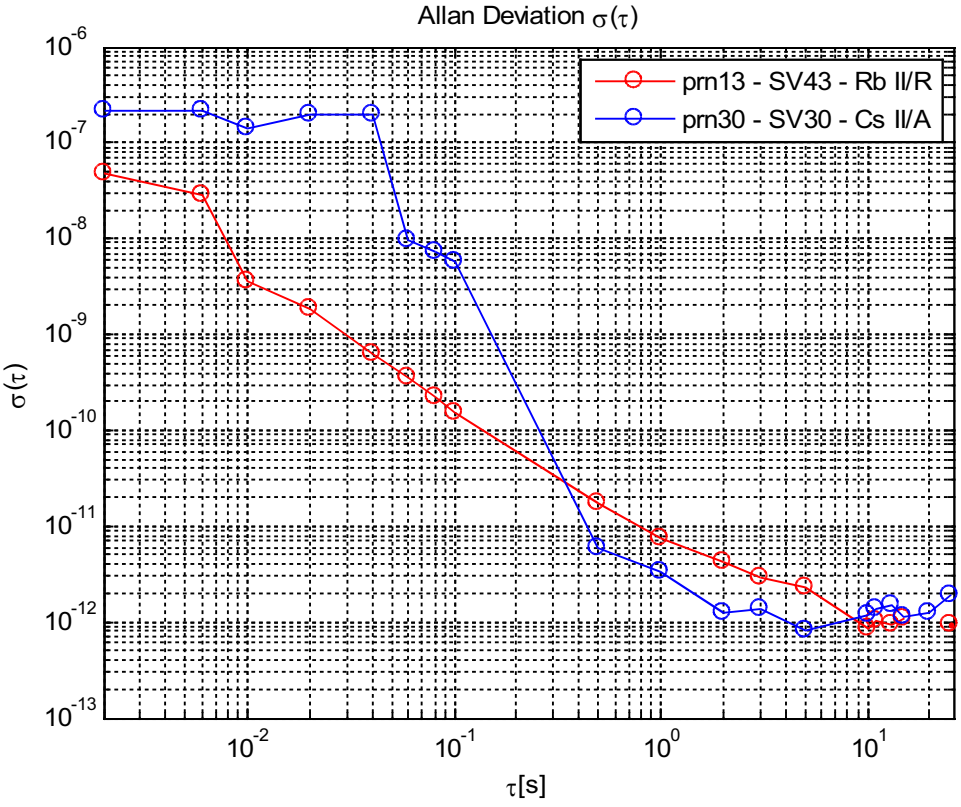

Figure 5.35: Allan deviation plot for various 2 different SVs using the Oscilloquartz 8607 as front-end time reference.

Chapter 6

Conclusions

6.1 Conclusions

In this thesis a set of quartz crystal oscillators has been test, in order to understood the impact of the local oscillator on the GPS L1 signal. Interesting phenomena have been discovered such as early bumps, peak magnitude drop and double peak. Further data analysis and experiments have to be conducted to provide a better understanding of the potential causes of the observed artifacts.
Power accumulation over 1 minute of coherent integration time has been demonstrated, potentially allowing to acquire extremely low power signal. However indoor tests show a saturation of the SNR curve evolution after 30 seconds of coherent integration time, this should be also further investigated.
A potential methodology for remotely measuring the satellite clock Allan deviation has been investigated. The results are well in agreement with the known SV on-board clock characteristics.
The acquisition of indoor signal attenuated by 40 to 45 dB has be successfully demonstrated using coherent integrations of 30 seconds. The extracted code delay has been used to find the position solution. In the best case an position with an accuracy of 20 m in the horizontal plan and of 100m for the height has be obtained, using a 5 satellite geometry.

6.2 Lessons learned

- In order to be able to calibrate correctly the nominal frequency of the oscillator, one has to dispose of an atomic frequency reference, for example a rubidium oscillator.

- Each oscillator has to integrate a voltage control input to allow the user to perform the calibration phase on the basis of an atomic standard.

- For the data analysis Dual Core computers are recommended.
- Having access to several fast computers accelerates the data analysis.
- A Graphical User Interface (GUI) allows a more intuitive use of the software than command line based programs. GUI also allows the developer to add useful features that can not be programmed otherwise.
- Due to the amount of data that has to be store, moved and processed, the way to handle the data problem is critical. For example one has to dispose of a portable hard drive to physically move data from a computer to an other. Moreover each computer has to dispose of at least 500 Gbytes of memory space on the hard drives.

6.3 Future works

The goal of this section is to give some ideas to be applied for future works .

6.3.1 Software

- Further GUI development.
- Optimization of the main routines such as correlations to increase the calculation speed.
- Explore the possibility to use the computer graphic card to parallelize the computation of the correlations.

6.3.2 Hardware

- Extend test to the MEMS based oscillators such as the ones manufacture by Sitime [1].
- Build PCBs[2] for vibration motors .

6.3.3 Experiments

- Testing the oscillator behavior under vibrating conditions. The idea is to use vibration motors similar to the one used in cell phone for the vibrating alarm. Those motors[3] are flat enough to be sticked on the oscillator hull and induce vibration. A vibration table can also considered to be used for future investigations.
- The effect of temperature variations on the oscillator, for example using hot air generated by a hair dryer, can also be explored.

[1] All ready purchased but not tested.
[2] Already designed and printed.
[3] Already purchased.

- The effect of accelerations can also be tested using a motion table already own by the PLAN group.
- Acquisition of open-sky attenuated signals. The attenuation can be realized with RF attenuators.
- Testing satellite GPS signals simulated by the GPS simulator driven with the oscillator Oscilloquartz 8607 in order to verify that the measured Allan deviation is related to the frequency reference used to generate the GPS signal.
- Investigation of the relation between position accuracy, used oscillator and integration time.

6.3.4 Data analysis

- Further investigations of the encountered phenomena such as early bumps, peak magnitude drops and double peak. The hypothesis of rapid frequency jump has to be further investigated and possibly verified with different signal processing techniques for example Time-Frequency analysis. The double peak phenomenon is not clear yet, its potential causes have still to be determined.
- Modelization of the stochastic process that causes the power drop observed in the accumulation process. A parametric model could be adopted and a series of parameters defining the characteristics of the process should be defined. The analysis of those parameters and their relationships with the Allan deviation, the integration time and other factors, could potentially ends up in more accurate characterization of the accumulation process and of the errors involved.
- Verify the repeatability of the performed tests by recording and analyzing new data sets.
- Extension of the analysis to the new clocks used for Galileo, Glonass and GPS.
- Possible definition of a methodology able to isolate the receiver and satellite clock error. For example using 2 receivers simultaneously. One of the receiver could be driven by the Oscilloquartz 8607 whose collected data could be considered as local oscillator errors free and be used to compensate the satellite clock errors on the second set of data recorded by and second receiver driven with a less good oscillator. This could potentially offers the possibility to isolate the effects due to the satellite and atmospheric effects from the ones due to the local oscillator.

Bibliography

[1] M. Abramowitz and I. A. Stegun. *Handbook of Mathematical Functions with Formulas Graphs and Mathematical Table*. Dover Publications, June 1965. [cited at p. 131]

[2] David W. Allan. Time and frequency time-domain characterization estimation and prediction of precise clocks and oscillators. *IEEE transaction on ultrasonic ferroelectrics and frequency control*, 1987. [cited at p. 40]

[3] Brendon Bentley. *An Investigation into the Phase Noise of the Quartz Crystal Oscillators*. PhD thesis, Stellenbosch University, 2007. [cited at p. 34, 186]

[4] John Robert A. Watson et al. Testing oscillator stability as a limiting factor in extreme high-sensitivity gps applications. In *Proceedings of ENC-GNSS Manchester*, 2006. [cited at p. 71]

[5] John Robert A. Watson et al. Impact of oscillator errors on imu-aided gps tracking loop performance. In *Proceedings of ENC-GNSS Geneva*, 2007. [cited at p. 71]

[6] Gregory T. French. *Understanding the GPS*. Georesearch, 1996. [cited at p. 20]

[7] Grace Xingxin Gao. Gnss over china. *Inside GNSS*, July/August 2007. [cited at p. 24]

[8] F. Gonzales. Short term gnss clock characterization using one-way carrier phase. *Frequency Control Symposium, 2007 Joint with the 21st European Frequency and Time Forum. IEEE International*, May 29 2007-June 1 2007. [cited at p. 110, 111]

[9] Elliott D. Kaplan. *Understanding GPS principles and applications 2nd Edition*. Artech house, 2006. [cited at p. 123]

[10] Charles Kittel. *Introduction to Solid State Physics*. Wiley, 2004. [cited at p. 31]

[11] Prof. Gérarad Lachapelle. *Advanced GNSS Theory and Application - ENGO625*. University of Calgary, 2007. [cited at p. 10, 14, 15, 22]

[12] Lute Maleki. Advance atomic clock. *IEEE Frequency Control Symposium*, 2000. [cited at p. 51, 186]

[13] Neil W. Ashcroft N. David Mermin. *Solid State Physics*. Brooks Cole, 1976. [cited at p. 31]

[14] microcrytal. Ov-1564-c2. *data sheet*, 2007. [cited at p. 48, 186]

[15] V. Nuth. An evaluation of various space clocks for gps iif. *33rd Annual Precise Time and Time Interval (P P I) Meeting*. [cited at p. 110, 111]

[16] THE WHITE HOUSE Office of the Press Secretary. Statement by the president regarding the united states decision to stop degrading global positioning system accuracy. *press release*, may 1, 2000. [cited at p. 11]

[17] Hewlet Packard. Fundamentals of quartz crystal oscillator. *Application note 200-2*, may 1997. [cited at p. 34, 186]

[18] John F. Raquet. Gnss receiver design. [cited at p. 16, 185]

[19] Tom Creel Arthur J. Dorsey Philip J. Mendicki Jon Little Richard G. Mach Brent A. Renfro. The legacy accuracy improvement initiative. *GPS World*, March 1, 2006. [cited at p. 13, 14, 185]

[20] W.J. Riley. A test suite for the calculation of the time domain frequency stability. *1995 IEEE International Frequency Control Symposium*, 1995. [cited at p. 110]

[21] Yves Schwab Dominik Schneuwly. crystal quartz oscillators. In *telecom-sync*, 1995. [cited at p. 34, 186]

[22] Yves Schwab. Oscilloquartz presentation. 2007. [cited at p. 45, 186]

[23] Col Allan Ballenger Commander GPS Wing Space and Missile Systems Center. Smc transformation epicenter. In *Presentation to CSA Panel*, November 30 2006. [cited at p. 13, 185]

[24] swiss army. *Conduite tactique XXI NSA N° 292-9594 51.20 f.* swiss army, 2004. [cited at p. 29, 185]

[25] Vectron. Ocxo's oven controlled crystal oscillators. *application note*. [cited at p. 43, 186]

[26] John R. Vig. Quartz crystal resonators and oscillators. In *ieee tutorial*, 2007. [cited at p. 28, 29, 34, 43, 185, 186]

[27] Larry D. Vittorini. Optimizing indoor gps performance. *GPS World*, 2003. [cited at p. 81]

[28] J. R. Vig F. L. Walls. Fundamental limits on the frequency instabilities of quartz crystal oscillators. *Proc. 1994 IEEE Int'l Frequency Control Symposium pp. 506-523*, 1994. [cited at p. 39]

[29] J. R. Vig F. L. Walls. Fundamental limits on the frequency stabilities of crystal oscillators. *IEEE transaction on ultrasonic, ferroelectrics, and frequency control*, 1995. [cited at p. 47]

[30] John Robert A. Watson. *High-Sensitivity GPS L1 Signal Analysis for Indoor Channel Modelling*. PhD thesis, University of Calgary, 2005. [cited at p. 71]

Appendices

Appendix A

Mathematical developments

A.1 Probability density function of the acquisition output in absence of signal

In this appendix, the probability density function (pdf) of the random variable obtained at the output of the acquisition block is analyzed. In particular the case of noise only, i.e. when the useful signal component is not present, is considered. The random variable at the output of the acquisition block is not Gaussian. Moreover the pdf of the decision variable obtained in absence of useful signal can be used to fix the decision threshold enabling the detection process [9, ch 5.8 p. 221-223].

A.1.1 Receiver architecture

The acquisition block depicted in fig. [A.1] is based on the same working principle used for the software receiver implemented in the oscillatorAnalyzer software. The structure in fig. [A.1] is however simple enough to allow a theoretical analysis of the acquisition block, avoiding all the programming details implemented in the oscillatorAnalyzer software.
In this case the input signal is the Gaussian process

$$\eta[n] \sim \mathcal{N}\left(0, \sigma^2\right)$$

with

$$E\left[\eta[n]\right] = 0$$

and

$$Var\left[\eta[n]\right] = \sigma^2$$

This noise will be propagated trough the system, leading to the final decision variable $Z = S(\tau, F_D)$. $S(\tau, F_D)$ is, in general, a function of the code delay τ and the normalized

Doppler frequency F_D tested by the acquisition block. More in detail we have:

$$F_D = (f_I + f_d)T_s$$

where f_I[1] is the intermediate frequency, f_d[2] the Doppler shift and T_s the sampling period.

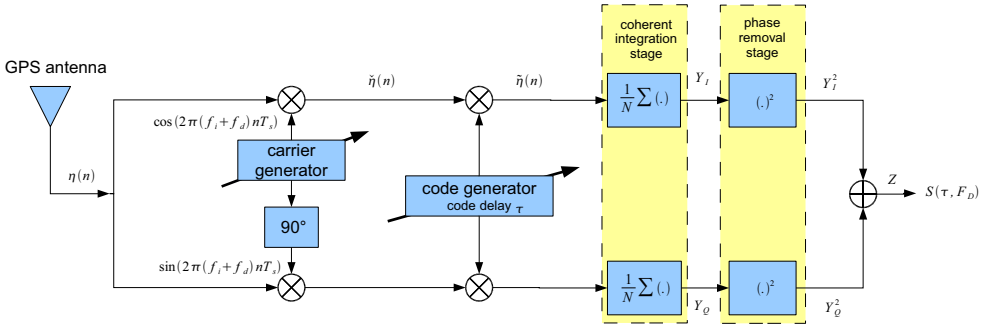

Figure A.1: Receiver architecture feed with a Gaussian noise.

The purpose of this appendix is to demonstrate that $Z = S(\tau, F_D)$ is exponentially distributed:

$$Z \sim \text{Exp}\left(0, \frac{1}{2\sigma_y^2}\right) \tag{A.1}$$

that is

$$f_Z(z) = \frac{1}{2\sigma_y^2} \exp\left(-\frac{z}{2\sigma_y^2}\right) \tag{A.2}$$

where σ_y^2 is the variance of the random variables Y_I and Y_Q (see fig. [A.1]).

A.1.2 Useful properties

In the following the independence of two random variables will be denoted by $X \perp\!\!\!\perp Y$.

Variance formulas

The variance is defined as follows:

$$Var[X] = E[X^2] - E^2[X] \tag{A.3}$$

Let's consider the sum of the two random variables X and Y, then

$$Var[X+Y] = Var[X] + Var[Y] + 2Cov(X,Y) \underbrace{=}_{X \perp\!\!\!\perp Y} Var[X] + Var[Y] \tag{A.4}$$

[1] In generally chosen to be 4 time the sampling frequency

[2] This term could be negative, but in order to work correctly the receiver has to respect the following condition: $f_I - |f_d|_{max} > 0$

Let's consider $\{X_i\}_{i=1}^{N}$, a set of independent and identically distributed (iid) random variables, with variance $Var[X_i]$ then:

$$Var\left[\sum_{N} X_i\right] = NVar[X_i] \tag{A.5}$$

Let's consider a real number α and a random variable X then:

$$Var[\alpha X] = \alpha^2 Var[X] \tag{A.6}$$

The proof of the last equation can be easily obtained by using the definition of the variance (A.3):

$$Var[\alpha X] = E[\alpha^2 X^2] + E^2[\alpha X] = \alpha^2 E[X^2] + \alpha^2 E^2[X] = \alpha Var[X] \tag{A.7}$$

Expectation formula

Let be X and Y two random variables, then

$$E[X + Y] = E[X] + E[Y] \tag{A.8}$$

If X, Y are independent it is possible to prove:

$$E[X \cdot Y] = E[X] \cdot E[Y] \tag{A.9}$$

A.1.3 Variance propagation

In this section the variance of input process $\eta[n]$ is propagated through the system depicted in fig. [A.1]. At first the noise process is multiplied, in the in-phase (I) and quadrature (Q) branches, by two orthogonal sinusoids at the frequency F_D (see figure[A.1]). This operation implies a variance change. So one is interested in knowing $Var[\check{\eta}[n]]$ in function of $Var[\eta[n]] = \sigma^2$. $\check{\eta}[n]$ denotes the random process obtained in the I branch by multiplying $\eta[n]$ by $\cos(2\pi F_D n)$.
It is possible to write, from the variance definition (A.3),:

$$\begin{aligned} Var[\check{\eta}[n]] &= Var[\eta[n] \cdot cos(.)] && \text{(A.10)} \\ &= E[\eta^2[n] \cdot \cos^2(2\pi F_D n)] - \underbrace{E^2[\eta[n] \cdot \cos(2\pi F_D n)]}_{\underbrace{E^2[\eta[n]]}_{=0}\, E^2[\cos(2\pi F_D n)]=0} && \text{(A.11)} \\ &= E[\eta[n]^2 \cos^2(2\pi F_D n)] = \sigma^2 \frac{1}{2} + \sigma^2 \frac{1}{2} \cos(4\pi F_D n) && \text{(A.12)} \end{aligned}$$

The high frequency term in eq. (A.12), $\sigma^2 \frac{1}{2} \cos(4\pi F_D n)$, can be neglected since it will be filtered by the coherent integration stage that acts as a low-pass filter. In this way it is possible to assume:

$$Var[\check{\eta}[n]] = \sigma^2 \frac{1}{2} \tag{A.13}$$

The effect of the code multiplication can be evaluated in a similar way. In particular, the code $c[n]$ can take only 2 values, -1 and +1, thus

$$Var[\tilde{\eta}[n]] = Var[\eta[n]\cos(2\pi F_D n)\, c[n]] = Var[\check{\eta}[n]c[n]] \quad (A.14)$$

$$= E[\tilde{\eta}^2[n]] \underbrace{E[c^2[n]]}_{=1\forall n} - \underbrace{\underbrace{E^2[\eta[n]]}_{=0} E^2[cos(.)c[n]]}_{=0} \quad (A.15)$$

$$= E[\check{\eta}^2[n]] = Var[\check{\eta}^2[n]] = \frac{1}{2}\sigma^2 \quad (A.16)$$

It is now necessary to evaluate the effect of the integration stage. Using equation (A.6), (A.4), (A.5), (A.16), it is possible to write:

$$Var\left[\frac{1}{N}\sum_{n=0}^{N-1}(\tilde{\eta}[n])\right] = \frac{1}{N^2}\sum_{n=0}^{N-1}(Var[\tilde{\eta}[n]]) \quad (A.17)$$

$$= \frac{1}{N^2} N Var[\tilde{\eta}[n]] = \frac{\sigma^2}{2N} \underbrace{=}_{def} Var[Y_I[n]] \quad (A.18)$$

At this point of the calculation process, two independent random variables, Y_I and Y_Q, have been obtained. With $Var[Y_I[n]] = Var[Y_Q[n]] = \frac{\sigma^2}{2N}$ [3]. Their expectations are $E[Y_i] = E[Y_Q] = 0$. Moreover, the operations that have led to Y_I and Y_Q are all linear. This implies that Y_I and Y_Q are normally distributed. Thus their pdfs are given by:

$$f_{Y_I}(y_I) = \frac{1}{\sqrt{2\pi\sigma_Y^2}} \exp\left\{-\frac{(y_I - E[Y_I])^2}{2\sigma_y^2}\right\} = \frac{1}{\sqrt{2\pi\sigma_Y^2}} \exp\left\{-\frac{y_I^2}{2\sigma_y^2}\right\} \quad (A.19)$$

$$f_{Y_Q}(y_Q) = \frac{1}{\sqrt{2\pi\sigma_Q^2}} \exp\left\{-\frac{(y_Q - E[Y_Q])^2}{2\sigma_Y^2}\right\} = \frac{1}{\sqrt{2\pi\sigma_Q^2}} \exp\left\{-\frac{y_Q^2}{2\sigma_Y^2}\right\} \quad (A.20)$$

The final decision variable is given by $Z = Y_I^2 + Y_Q^2$. In order to determine the pdf of Z, the following marginalization property can be used:

$$f_{Y_I}(y_I) = \int_{y_Q} f(y_I, y_Q) dy_Q \quad (A.21)$$

For the demonstration of (A.21), it is possible to use the fact that Y_I and Y_Q are independent so, from the definition of independence, the joint pdf is:[4]

$$f(y_I, y_Q) = f_{Y_I}(y_I) f_{Y_Q}(y_Q) \quad (A.22)$$

By using (A.22), one gets:

$$f_{Y_I}(y_I) = \int_{y_Q} f(y_I, y_Q) dy_Q = \int_{y_Q} f_{Y_I}(y_I) f_{Y_Q}(y_Q) dy_Q = f_{y_I}(y_I) \int_{y_Q} f_{y_Q}(y_Q) dy_Q \quad (A.23)$$

[3] The Q branch can be calculate exactly the some way as the I branch

[4] by def. of pdf we also have: $\int_{y_I}\int_{y_Q} f(y_I, y_Q) d_{y_i} d_{y_q} = 1$

For the normalization properties of pdfs, $\int_{y_Q} f_{y_Q}(y_Q)dy_Q = 1$. Thus

$$f_{Y_I}(y_I) = f_{Y_I}(y_I) \underbrace{\int_{y_Q} f_{y_Q}(y_Q)dy_Q}_{=1} = f_{Y_I}(y_I) \tag{A.24}$$

This demonstrates eq. (A.21).

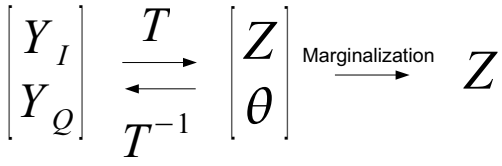

Figure A.2: Mathematical computation flowchart: at first a variable change is applied, the final distribution of Z is then obtained by marginalizing the joint pdfs.

As describe on figure[A.2], the idea is to define a transformation T (T^{-1} denotes its inverse) in order to operate a change of variable and to use the marginalization theorem to obtain the final distribution of Z. Let's at first define T:

$$T : \begin{cases} Z = Y_I^2 + Y_Q^2 \\ \theta = \arctan\left(\frac{Y_Q}{Y_I}\right) \end{cases} \tag{A.25}$$

The inverse transformation is given by:

$$Y_I = \sqrt{Z}\cos(\theta) \tag{A.26}$$

$$Y_Q = \sqrt{Z}\sin(\theta) \tag{A.27}$$

T could be seen as a transformation in the polar coordinate system see figure[A.3].

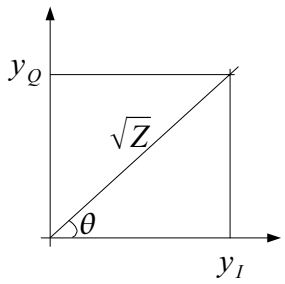

Figure A.3: T could be seen as a transformation in the polar coordinate system.

By applying this transformation to the joint pdf $f(Y_I, Y_Q)$ we have:

$$f(y_I, y_Q) \xrightarrow{T} f(T^{-1}(Z, \theta))|J(T)| \tag{A.28}$$

where $J(T)$ is the Jacobian and, by definition, is given by:

$$J(T) = \begin{pmatrix} \frac{dY_I}{dZ} & \frac{dY_I}{d\theta} \\ \frac{dy_Q}{dZ} & \frac{dy_Q}{dQ} \end{pmatrix} = \begin{pmatrix} \frac{1}{2\sqrt{Z}}\cos(\theta) & -\sqrt{Z}\sin(\theta) \\ \frac{1}{2\sqrt{Z}}\sin(\theta) & \sqrt{Z}\cos(\theta) \end{pmatrix} \tag{A.29}$$

$|J(T)|$ is the determinant of the Jacobian:

$$|J(T)| = \frac{1}{2}\cos^2(\theta) + \frac{1}{2}\sin^2(\theta) = \frac{1}{2} \tag{A.30}$$

By using eq. (A.22), (A.20) and (A.19), one gets:

$$f(y_I, y_Q) = \frac{1}{2\pi\sigma_y^2}\exp\left\{-\frac{1}{2\sigma_y^2}(y_I^2 + y_Q^2)\right\} \tag{A.31}$$

and, by applying relations eq. (A.28) to eq.(A.31) finally

$$f(z, \theta) = \frac{1}{2\pi\sigma_y^2}\exp\left\{-\frac{1}{2\sigma_y^2}z\right\}\frac{1}{2} \tag{A.32}$$

is obtained.
From the definition of the transformation T, one can see that $Z > 0$ because it is a squared module. Moreover $-\pi < \theta < \pi$ by definition of the arctangent function. So by applying those constrains and the marginalization theorem one gets (A.21):

$$f(Z) = \int_{-\pi}^{\pi} f(z, \theta) \tag{A.33}$$

$$= \int_{-\pi}^{\pi} \frac{1}{2\pi\sigma_y^2}\exp\left\{-\frac{1}{2\sigma_y^2}z\right\}\frac{1}{2}d\theta \tag{A.34}$$

$$= \frac{1}{2\sigma_y^2}\exp\left\{-\frac{1}{2\sigma_y^2}z\right\} \text{ (if z>0)} \tag{A.35}$$

So Z results exponentially distributed.

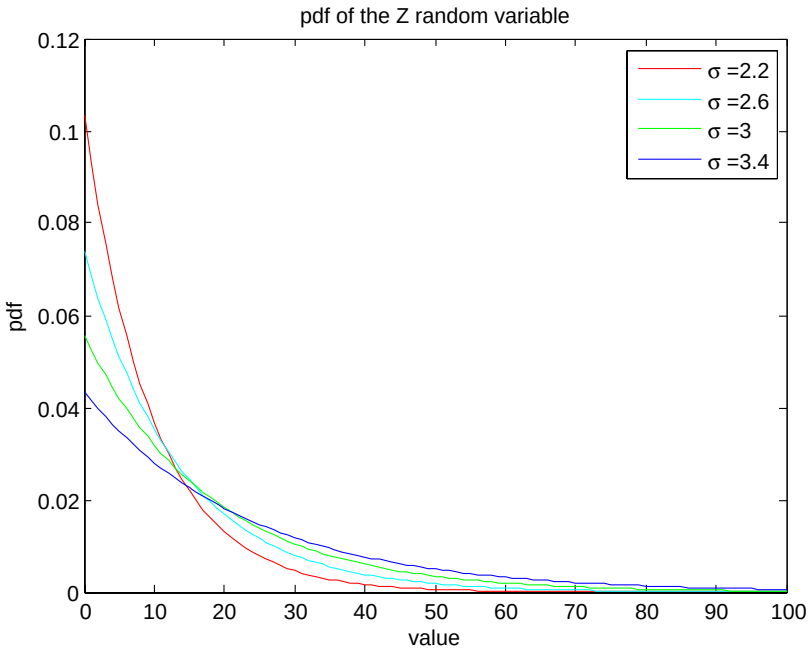

Figure A.4: Graph of the pdf function for different sigma value.

Alternative demonstration:

Instead of using a variable change and the marginalization theorem, it is possible to a different approach. By defining $R_I = Y_I^2$, it is possible to write $f_{R_I}(r_I) = \frac{d}{dr_I} F_{R_I}(r_I) = \frac{d}{dr_I} P(R_I < r_i) = \frac{d}{dr_I} P(Y_I^2 < r_i)$[5]. So now one has to compute $P(Y_I^2 < r_i)$:

$$P(R_I < r_i) = P(Y_I^2 < r_i) = P(-\sqrt{r_I} < Y_I < \sqrt{r_I}) \tag{A.36}$$

We can justify equation (A.36) by looking at the representation in figure [A.5]:

[5]small f represents the pdf; capital F is the integral of small f and represents the cumulative density function (cdf).

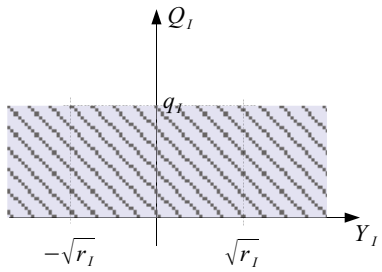

Figure A.5: The blue hatching area is where the condition $R_I < r_I$ is true, then if one restricts this to the parabola $R_I = Y_I^2$ the two points $\sqrt{-r_I}$ and $\sqrt{r_I}$ are obtained.

Then one can continue by re-writing the last equation in the following form:

$$P(-\sqrt{r_I} < Y_I < \sqrt{r_I}) = P(Y_I < \sqrt{r_I}) - P(Y_I < -\sqrt{r_I}) \tag{A.37}$$

This last equation is visualized in fig. [A.6].

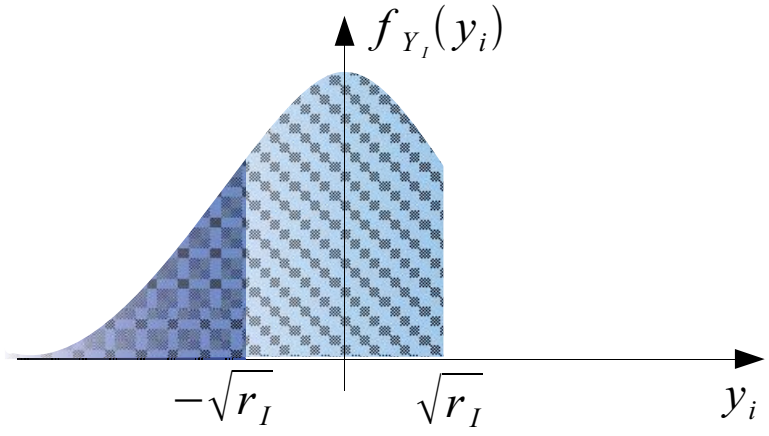

Figure A.6: By definition of pdf, one knows that the area under the curve is the probability. So the light blue area is simply area difference between the two hatched surfaces.

Since Y_I is normally distributed it is possible to write:

$$
\begin{aligned}
f_{R_I}(r_I) &= \frac{d}{dr_I}\left\{P\left(-\sqrt{r_I} < Y_I < \sqrt{r_I}\right)\right\} && \text{(A.38)}\\
&= \frac{d}{dr_I}\{P(Y_I < \sqrt{r_I}) - P(Y_I < -\sqrt{r_I})\} && \text{(A.39)}\\
&= \frac{d}{dr_I}\{P(Y_I < \sqrt{r_I})\} - \frac{d}{dr_I}\{P(Y_I < -\sqrt{r_I})\} && \text{(A.40)}\\
&= f_{Y_I}(\sqrt{r_I})\frac{1}{2\sqrt{r_I}} - f_{Y_I}(-\sqrt{r_I})\left(-\frac{1}{2\sqrt{r_I}}\right) && \text{(A.41)}\\
&= \frac{1}{2\sqrt{r_I}}\left\{f_{Y_I}(\sqrt{r_I}) + f_{Y_I}(-\sqrt{r_I})\right\} && \text{(A.42)}\\
&= \frac{1}{2\sqrt{r_I}}\left[\frac{1}{\sqrt{2\pi\sigma^2}}\exp\left\{-\frac{1}{2}\frac{\sqrt{r_I}^2}{\sigma^2}\right\} + \frac{1}{\sqrt{2\pi\sigma^2}}\exp\left\{-\frac{1}{2}\frac{(-\sqrt{r_I})^2}{\sigma^2}\right\}\right] && \text{(A.43)}\\
&= \frac{1}{\sqrt{r_I}}\frac{1}{\sqrt{2\pi\sigma^2}}\exp\left\{-\frac{1}{2}\frac{r_I}{\sigma^2}\right\} && \text{(A.44)}\\
&= \frac{r_I^{-\frac{1}{2}}}{\sqrt{2\pi\sigma^2}}exp\left\{-\frac{r_I}{2\sigma^2}\right\} && \text{(A.45)}
\end{aligned}
$$

Eq. (A.46) is a χ_1^2 distribution.The general form of the Chi-square pdf is:

$$
f(x;k) = \begin{cases} \dfrac{1}{2^{k/2}\Gamma(k/2)}\, x^{k/2-1}e^{-x/2} & \text{for } x > 0,\\ 0 & \text{for } x \le 0, \end{cases} \qquad \text{(A.46)}
$$

where $\Gamma(\cdot)$ is the Euler Gamma function [1, p.255].
In this case $x = \frac{1}{\sigma^2}$, $k = 1$, the gamma function of $\frac{1}{2}$ equal $\Gamma(\frac{1}{2}) = \sqrt{\pi}$ so we get:

$$
f_{R_I}(r_I) = \frac{1}{\sqrt{r_I}}\frac{1}{\sqrt{2\pi\sigma^2}}\exp\left\{-\frac{1}{2}\frac{r_I}{\sigma^2}\right\} \qquad \text{(A.47)}
$$

By using the same methodology, one can derive $f_{R_Q}(r_Q) = \frac{1}{\sqrt{r_Q}}\frac{1}{\sqrt{2\pi\sigma^2}}\exp\left\{-\frac{1}{2}\frac{r_Q}{\sigma^2}\right\}$.
The pdf of the sum of 2 independent random variables is the convolution of the 2 pdfs:

$$
f_Z(z) = f_{R_I}(z) * f_{R_Q}(z) \qquad \text{(A.48)}
$$

Instead of calculating directly the convolution it is possible to use the following property

$$
f_Z(z) = f_{R_I}(z) * f_{R_Q}(z) = \mathcal{F}^{-1}\left\{\mathcal{F} f_{R_I}(z)\mathcal{F} f_{R_Q}(z)\right\} \qquad \text{(A.49)}
$$

where $\mathcal{F}$ and $\mathcal{F}^{-1}$ denote the Fourier and the Inverse Fourier Transforms.
From the table of Fourier Transforms we have:

$$
\mathcal{F}\{f(x;k)\} = \chi(t;k) = (1 - 2it)^{-k/2} \qquad \text{(A.50)}
$$

Eq. (A.46) has been defined for $\sigma = 1$, so one need some calculations to get the formulas for the generic σ. One can use the property of the Fourier transform:

$$\frac{1}{|\alpha|} f\left(\frac{x}{\alpha}\right) \longleftrightarrow F(\alpha t) \tag{A.51}$$

Thus eq. (A.46) can be rewritten as follows:

$$\frac{1}{\sqrt{2\pi\sigma^2 r_I}} \exp\left\{-\frac{1}{2}\frac{r_I}{\sigma^2}\right\} = \frac{1}{\sqrt{2\pi\sigma^4 \frac{r_I}{\sigma^2}}} \exp\left\{-\frac{1}{2}\frac{r_I}{\sigma^2}\right\} = \frac{1}{\sigma^2}\frac{1}{\sqrt{2\pi\frac{r_I}{\sigma^2}}} \exp\left\{-\frac{1}{2}\frac{r_I}{\sigma^2}\right\} \tag{A.52}$$

By defining $\alpha = \frac{1}{\sigma^2}$ and applying formula (A.51):

$$\frac{1}{\sigma^2}\frac{1}{\sqrt{2\pi\frac{r_I}{\sigma^2}}} \exp\left\{-\frac{1}{2}\frac{r_I}{\sigma^2}\right\} \longleftrightarrow (1 - 2i\sigma^2 t)^{-1/2} \tag{A.53}$$

The next step is to apply eq. (A.49): $\left((1 - 2i\sigma^2 t)^{-1/2}\right)^2 = (1 - 2i\sigma^2 t)^{-1}$ and finally

$$\mathcal{F} f_{R_I}(z) \mathcal{F} f_{R_Q}(z) = (1 - 2i\sigma^2 t)^{-1} \tag{A.54}$$

$$\updownarrow \tag{A.55}$$

$$f_Z(z) = \frac{1}{2\sigma^2} \exp\left\{-\frac{z}{2\sigma^2}\right\} \text{ (x>0)} \tag{A.56}$$

Appendix B

PCB layout and electronic scheme

In this appendix some details about the PCB design for the different oscillators is reported. In particularly:

- Figure[B.1] reports the electronic scheme of the 8626 dedicated PCB.
- Figure[B.2] shows 8626 dedicated PCB layout.
- Figure[B.3] reports the 8712 PCB electronic scheme.
- Figure[B.4] reports the 8683 PCB electronic scheme.
- Figure[B.5] reports the 8663 and 8788 PCB electronic scheme.
- Table[B.1] is the part list for the following oscillator PCB board: ACXOVS-AV5, 8626, 8712, 8663 and 8683.
- Figure[B.6] reports the electronic common to all Fordahl TCXO (i.e. 0724, 0727 and 0734). This also includes the PCB board layout.
- Table[B.1] is the part list for the previously cited TCXO oscillators.

B.1 8626

The PCB design for the Oscilloquartz 8626 and for the micro crystal OCXOVS-AV5 are exactly the same. It is interesting to note here that the output is not loaded with a 50Ω resistor but with a 1kΩ resistor in parallel with a 5 pF capacitor.

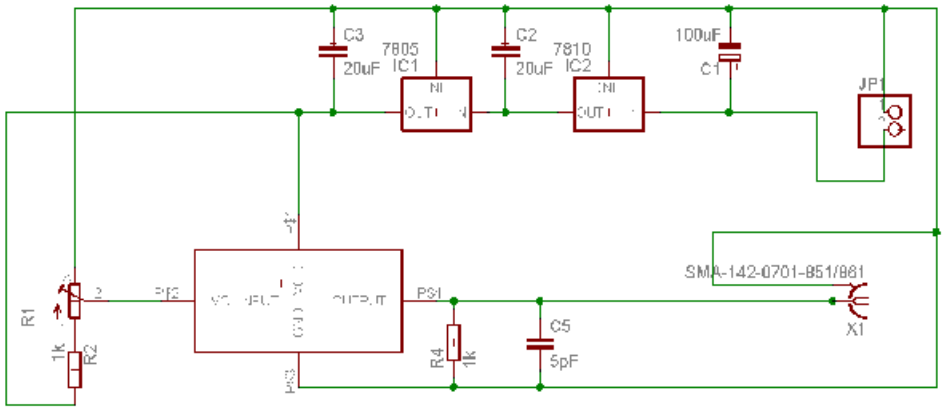

Figure B.1: Electronic scheme for the Oscilloquartz 8626 and the micro crystal OCXOVS-AV5.

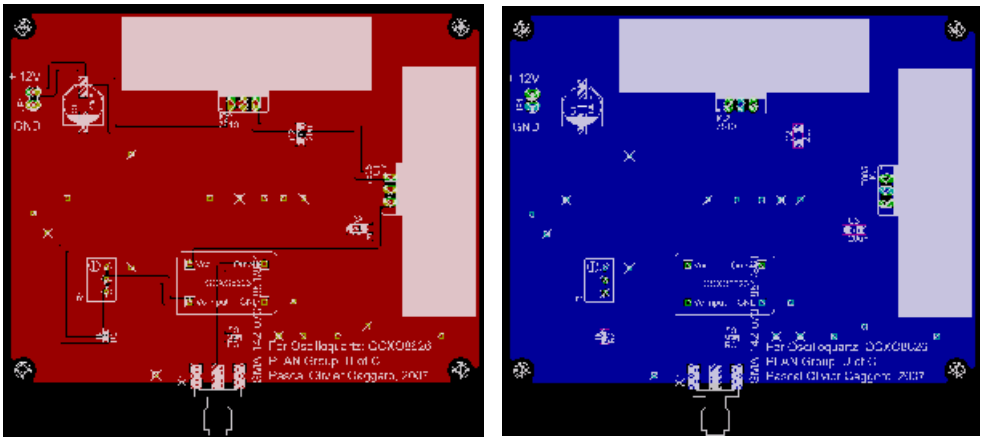

Figure B.2: PCB implementation for the Oscilloquartz 8626 and the micro crystal OCXOVS-AV5.

B.2 8712

The following figures show the electronic schematics of the 8712 support component only because the PCB design follows the same principle as the previous one.

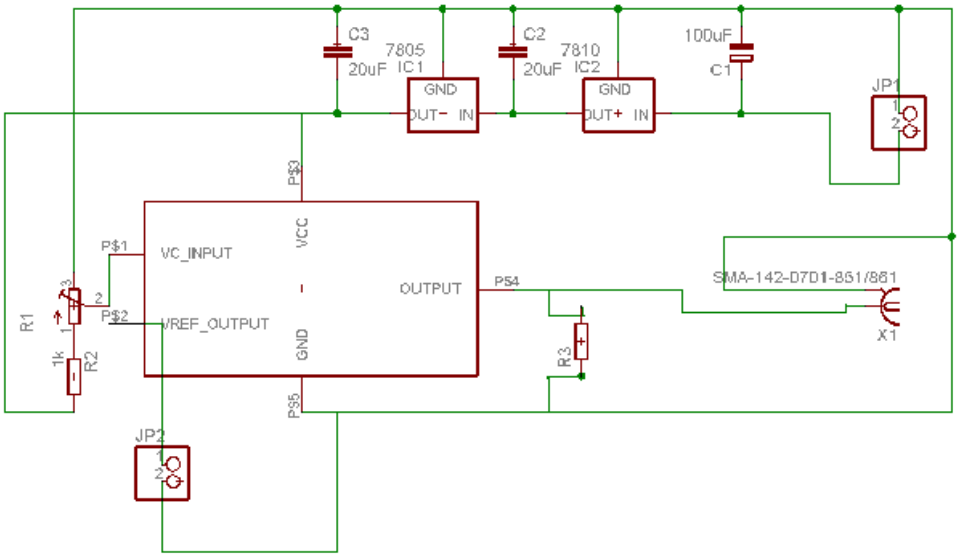

Figure B.3: Electronic scheme for the Oscilloquartz 8712.

B.3 8683

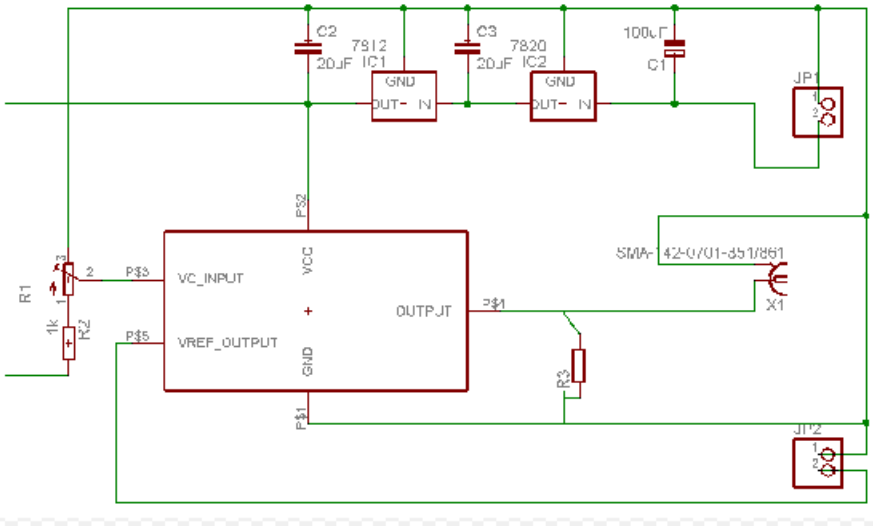

Figure B.4: Electronic scheme for the Oscilloquartz 8683.

B.4 8663 and 8788

The oscilloquartz 8663 and 8788 share the same PCB design.

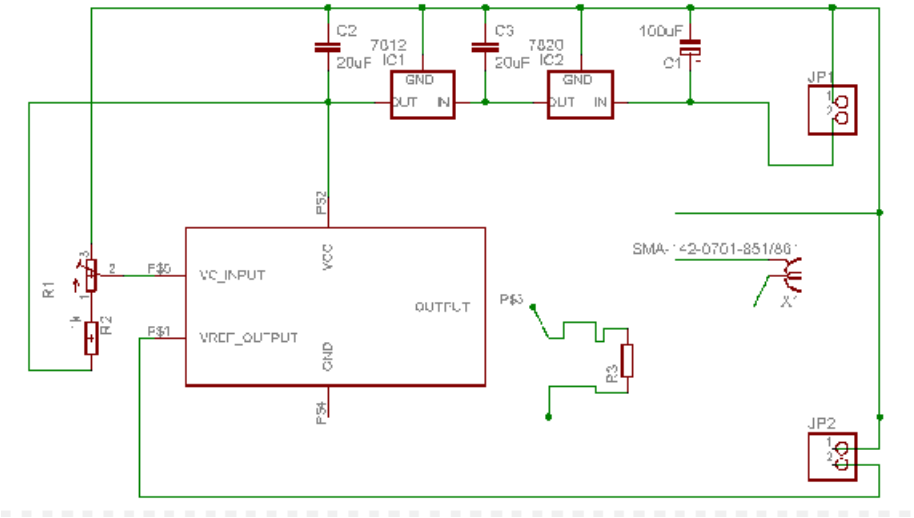

Figure B.5: Electronic scheme for the Oscilloquartz 8663 and 8788.

name	type	value	reference number	board
C1	electrolytic capacitor	100μF	ECE-V1EA101P	all
C2, C3	ceramic capacitor	22μF	ECJ-3YB1C226M	8712, OCXOVS-AV5
C2, C3	ceramic capacitor	22μF	C4532X5R1E226M	8663, 8788, 8683, 8636
C5	ceramic capacitor	5pF	ECJ-1VC1H050C	8626, OCXOVS-AV5
R2	resistor	1kΩ	ERJ-3EKF1001V	all
R3	resistor	50Ω	ERJ-3EKF49R9V	all
R4	resistor	1kΩ	RG1608P-102-B-T5	8626, OCXOVS-AV5
R1	trim resistor	20kΩ	3299W-1-203LF	all
IC1	linear voltage regulator	12V	UA7812CKC	8788, 8663, 8683
IC2	linear voltage regulator	20V	L7820CV	8788, 8663, 8683
IC1	linear voltage regulator	5V	UA7805CKCS	8626, 8712, OCXOVS-AV5
IC2	linear voltage regulator	10V	L7810CV	8626, 8712, OCXOVS-AV5
X1	RF connector	-	142-0701-851	all
-	heat sink	-	7-345-2PP-BA	all

Table B.1: Part list for Oscilloquartz circuit board.

B.5 Fordahl TCXO

The Fordahl TCXO 0724,0727 and 0734 share the same support circuitry design. It is interesting to note here that the IC's used for the power supply circuit aren't cooled by heat sinks, but they directly diffuse the heat into the PCB ground plate. The filter at the output of the oscillator is used to convert the HC-MOS compatible(square-wave) signal into a sinus wave. The filter design as been provided by Fordahl SA which implements this circuit in the sinus output version of the oscillators[1].

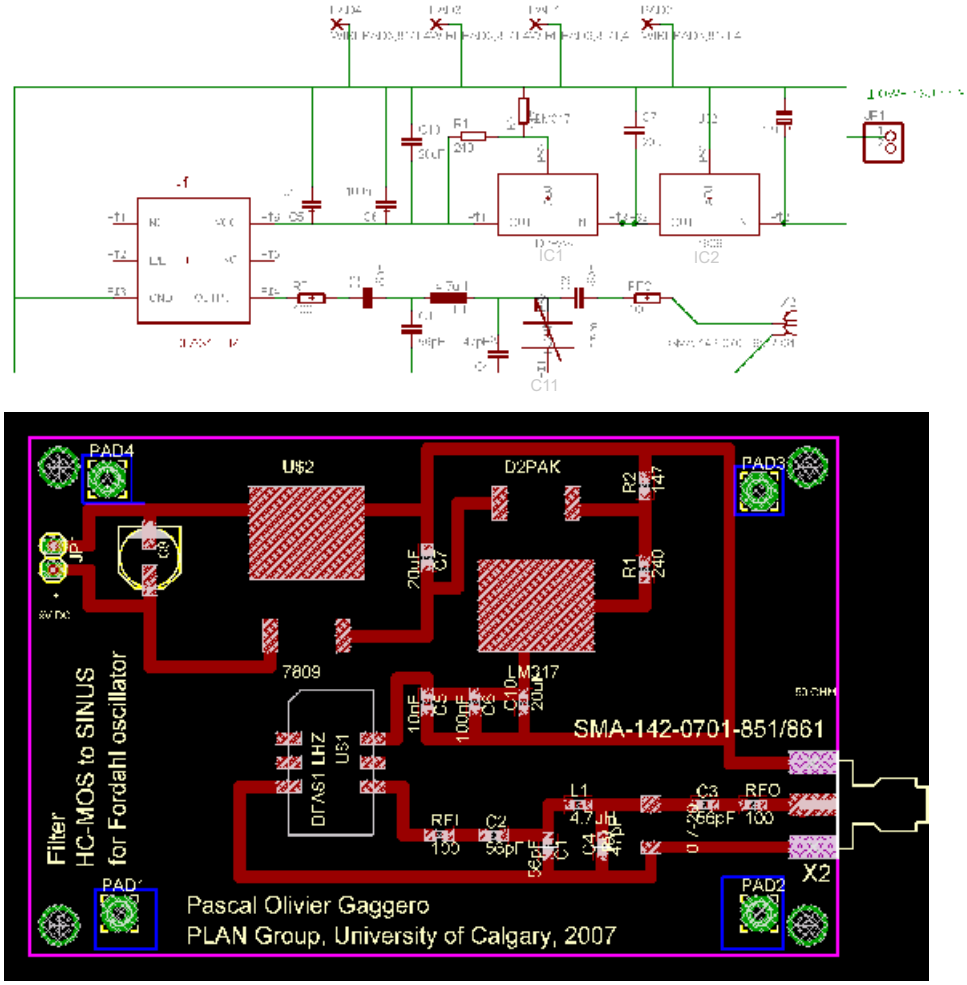

Figure B.6: Electronic scheme for the Fordahl TCXO.

[1]Not available anymore.

name	type	value	reference number	board
C1,C2,C3	ceramic capacitor	56pF	GRM1885C1H560JA01D	all
C4	ceramic capacitor	47pF	GRM1885C1H470JA01D	all
C5	ceramic capacitor	10nF	GRM188R71E103KA01D	all
C6	ceramic capacitor	100nF	GRM188R71E104KA01D	all
C7, C10	ceramic capacitor	22μF	ECJ-3YB1C226M	all
C9	electrolytic capacitor	100μF	ECE-V1EA101P	all
C11	trim capacitor	0.7-20pF	2807S1R020NHD4BAA	all
L1	inductance	4.7μH	LQM18FN4R7M00D	all
RFI,RFO	ceramic resistor	100 Ω	ERA-3YEB101V	all
R1	ceramic resistor	240 Ω	MCR03EZPFX2400	all
R2	ceramic resistor	147 Ω	ERJ-3EKF1470V	all
IC1	linear voltage regulator	adjustable(3.3V)	LM317BD2TR4G	all
IC2	linear voltage regulator	9V	L7809CD2T-TR	all
X1	RF connector	-	142-0701-851	all

Table B.2: Part list for Fordahl circuit board.

Appendix C

Methodology

C.1 Methodology

The goal of this section is to document as precisely as possible the entire data collection methodology with the intent of allowing researchers to reproduce the measurements and results.

C.1.1 Oscillator preparation

First of all one must allow the oscillators a sufficient warm-up period, to allow their operating characteristics to approach those specified by the manufacturer. Noting that this operation could last up to 2 weeks for the Oscilloquartz BVA 8607[1]. The oscillators have also been locked into a separate room to ensure none will perturbate the experiment. In this investigation the warm-up started on the 26th of November 2007 at 2 p.m. . During the entire warm-up time, the power supply was regularly checked to make sure the oscillator bench has not been unpluged, or otherwise disturbed[2].
When the warm-up period was completed, the oscillators were relocated to the lab via a trolley carrying both the oscillators and their un-interruptible power supply. One has then to calibrate the oscillators with a counter[3] fed with a rubidium frequency reference[4] as depicted in figure [C.1].

[1] An approximative warm-up time is given in table[4.1].
[2] Unpluging the UPS trig a sound alarm.
[3] Universal counter: Agilent 53131A
[4] Efratom division: FRK CCN 1A1D1A

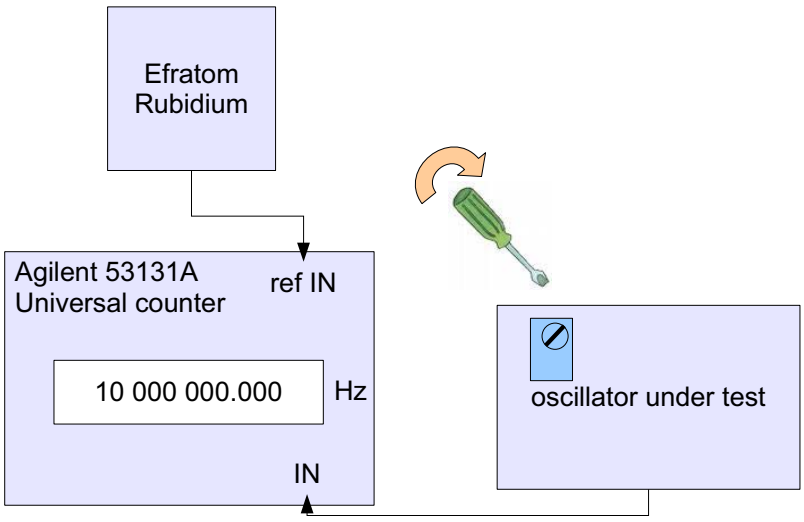

Figure C.1: Experimental setup used for the oscillator calibration.

One can observe the output signal of each of the oscillators by using an oscilloscope. The results are presented in figure[C.2]. One should also observe that the oscillators of the first column in figure [C.2] output a distorted signal, that is according to the Oscilloquartz engineers, due to Harmonics[5]. Oscillators with distorted signals have harmonics guaranteed lower than 25dBc[6], whereas for the other oscillator it is lower than 30dBc. In the 3rd column, one can observe the filtered[7] signal emitted by the oscillators with a square wave output. It is interesting to note that no signal distortion can be observed.

[5] See corresponding data sheet.
[6] dBc is a unit reported to the carrier value i.e. 25dB lower than the carrier(0dB per def.)
[7] The filter transform the square wave signal into a sinusoid.

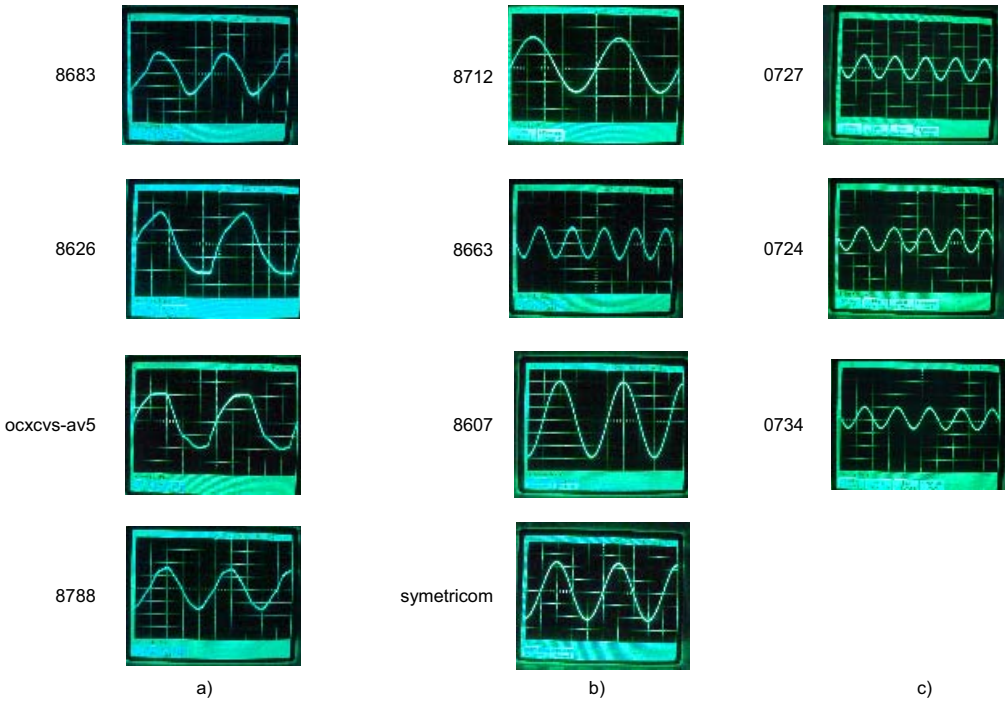

Figure C.2: View of the oscillator output signals; a) osc. with harmonics < -25dBc, b)< -30dBc, c) output of the square to sinus filter.

C.1.2 recording data

Here the data collection method is explained step by step, with the intent of insuring the repeatability of the experiment and to make the reader understand how the data have been recorded.

Step 1: getting the hardware ready

The Following steps should be followed:

1. Bring the oscillators into the lab and calibrate them following the methodology explained in section[C.1.1].

2. Configure a Novatel OEM4 GPS receiver enclosed in a DL4 box.

   - Connect the 12V power supply.
   - Connect receiver serial port "com1" $\leftrightarrow$ PC serial port[8].
   - Turn the receiver ON.

[8]data logger PC

3. Configure the Front-End[9].

   - Plug the JTAG cable into the ”JTAG” ↔ PC parallel port.
   - Plug the NI cable into the ”NI-DAQ” ↔ PC NI-DAQ acquisition card.
   - Connect front-end receiver serial port ”com1” ↔ PC serial port.
   - Plug the PPS cable into the ”PPS” input ↔ OEM4 I/O port.
   - Connect the dedicated 9V power supply.

Step 2: receiver configuration

On the data logger PC the steps described in figures [C.3] and [C.4] has to be executed.

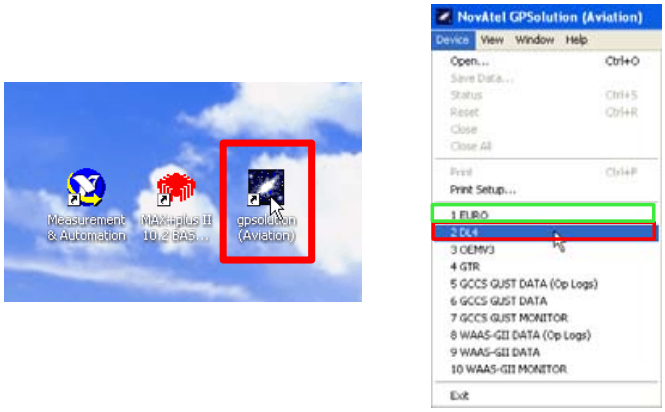

Figure C.3: Open the software called aviation solution and select DL4 device.

[9] the euro3M card is in the front-end with the FPGA

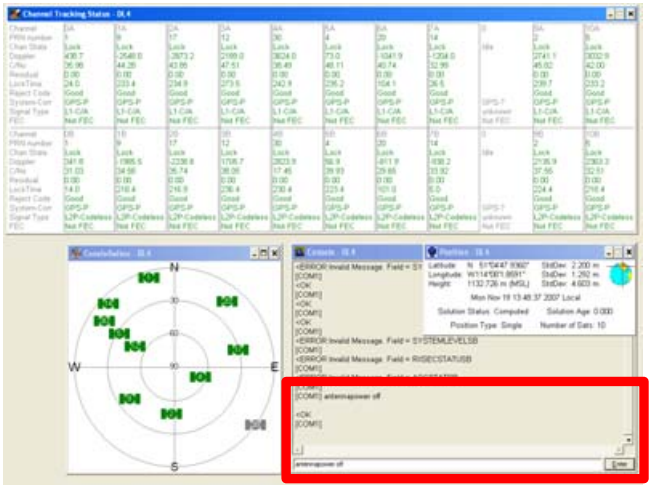

Figure C.4: In the command window enter the “antennapower off” command.

Repeat the same operations for the Euro3M, as indicated in the green box inside figure[C.3]. Once both receivers have received the “antennapower off” command, one can connect the GPS antenna to both receivers, using a splitter[10], to one of the available roof antenna[11].Then one allows the receivers to determine their position, and complete downloading of the GPS almanac (i.e. let them work for 20 minutes with open-sky conditions before proceeding).

Step 3: FPGA configuration

One needs to program the FPGA as indicated in figure [C.5], to suit the collection of the desired data format for the given experiment (i.e. in this case the configuration is to record 3 bits quantized I and Q data on L1 + the PPS pulses, further packaged into 32 bit words for transmission to the PC).

[10]Mini-circuits: splitter ZAPD-2.
[11]In this case E2.

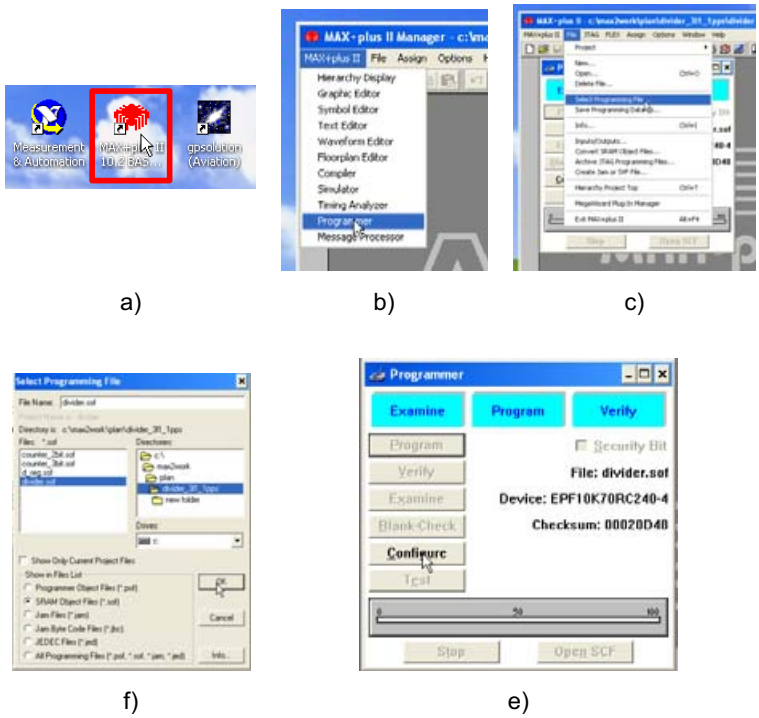

Figure C.5: Steps to program the FPGA.

Step 4: external oscillator

For the open-sky data collection:

1. Verify the external oscillator frequency with the method described in section[C.1.1] and adjust it if necessary to have the smallest offset possible to the nominal frequency.

2. Connect the oscillator output into the front-end “CLK” input.

3. In the aviation solution PC software:

   - Select the EURO3M as indicated in the green box in figure [C.3].
   - In the command window enter:
     - externalclock [ocxo, tcxo, rubidium] [5 , 10]mhz[12]
     - clockadjust disable[13]

4. Determine ready status of the receiver, in the aviation software receiver status window verify that the following conditions are met:

[12]Per example: externalclock ocxo 10mhz.
[13]This prevents the EURO3M steering the input frequency.

- antenna not powered
- almanac valid
- position solution valid
- clock steering disabled
- external oscillator PLL locked

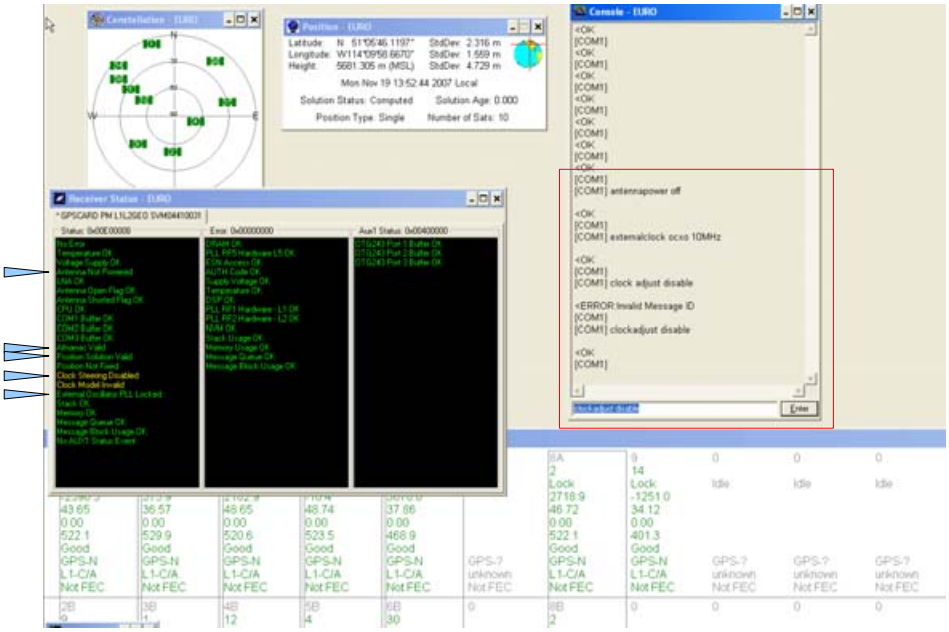

Figure C.6: Instructions to give to the EURO3M, in the case of an open sky data collection.

In the case of a remote indoor antenna follow this procedure:

1. Verify the external oscillator frequency with the method described in section[C.1.1] and adjust it if necessary.
2. Connect the oscillator output into the front-end “CLK” input.
3. Connect the front-end to the remote indoor antenna.
4. In the aviation solution:
   - Select EURO3M.
   - In the command window enter:
     - antennapower on[14]

[14]This time the antenna needs power, contrary to the roof antennas which are powered separately.

- externalclock [ocxo, tcxo, rubidium] [5 , 10]mhz[15]
- clockadjust disable[16]

5. Determine ready status of the receiver, in the aviation software receiver status window verify that the following conditions are met:
   - antenna powered
   - almanac valid
   - position solution, should be yellow/invalid because the receiver will not track the satellites in this configuration.
   - clock steering disabled
   - external oscillator PLL locked

Step 5: data recording

Before starting recording data one can take a screen capture of the channel tracking status from the EURO3M or from the DL4, so one will have a reference to use concerning the satellite signal strength at this moment. Then one has to exit the aviation solution software.
In the NavLabInterface distribution locate Utilities\slog.exe. Launch this software in command line mode: with "cd" command go to the directory where slog.exe is situated and then enter "slog oem4_30oct07_MethB.slg". It's also possible to simply drag and drop the oem4_30oct07_MethB.slg file on the slog.exe icon, as this script drives the DL4 receiver via slog. It also contains the pps sequence, so one must wait for the pps sequence start before recording data:

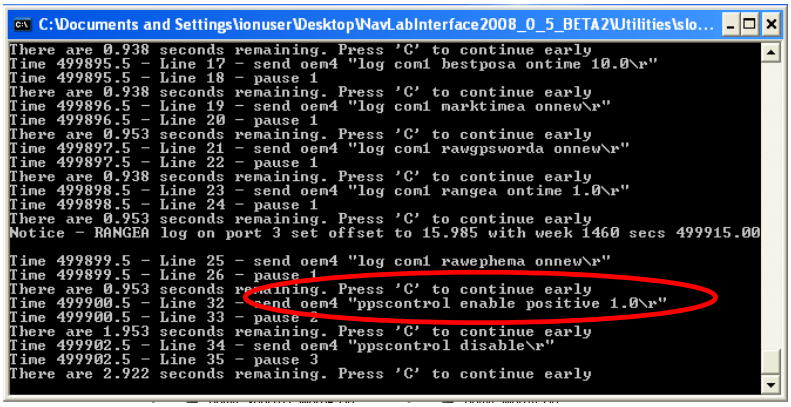

Figure C.7: One must wait for the pps sequence to start before recording data.

[15]Fer example: externalclock ocxo 10mhz.
[16]This avoids the EURO3M steering the frequency input.

To record the data one selects the destination hard drive by executing the correct data logging executable see figure [C.8]. The produced file size will depend on the I and Q data recording time, with a rule of thumb of 1.1 GB per minute of data. One can note that files bigger than 3GB will cause problems in the data processing software, preprocessor due to implementation limitations. For this reason one should choose to take data sets approximately 2.5 minutes in length. Figure [C.8] report the data recording software output. Where 360 "half buffers acquired" corresponds to about 2.5 minute of recorded data.

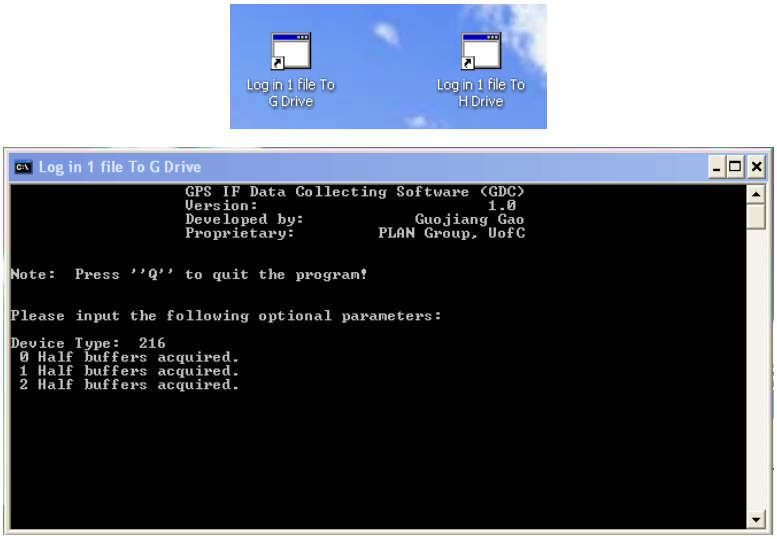

Figure C.8: Data recorder software output window, 360 "half buffers acquired" corresponds to about 2.5 minutes.

Appendix D

Experiment appendix

For more comment concerning the figure presented in this section see chapter [5].

D.1 Long integration time on different SV:

This section shows the equivalent data than the one presented in [5.1] but for SV36(prn6) insteed of SV30(prn30).

D.1.1 Fordahl 0727

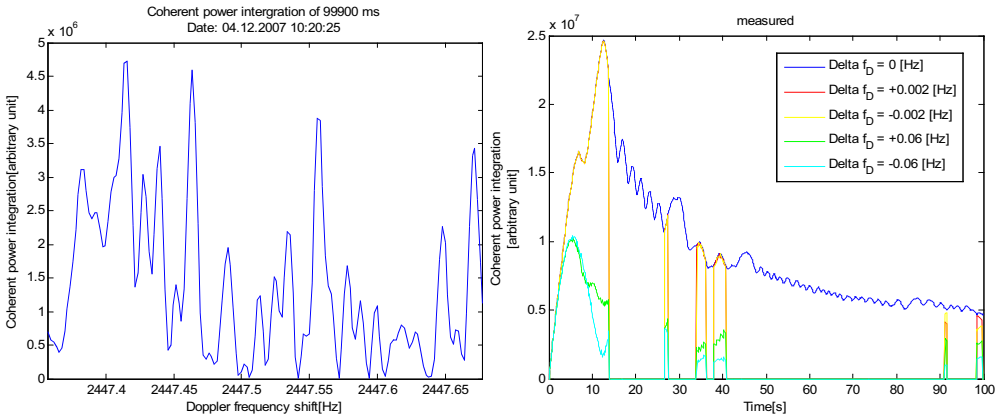

Figure D.1: SV36(prn6) clk:Rub, Left: Search space view after 99.9 second of coherent integration time; Right: Evolution of the peak magnitude;

D.1.2 Oscilloquartz 8626

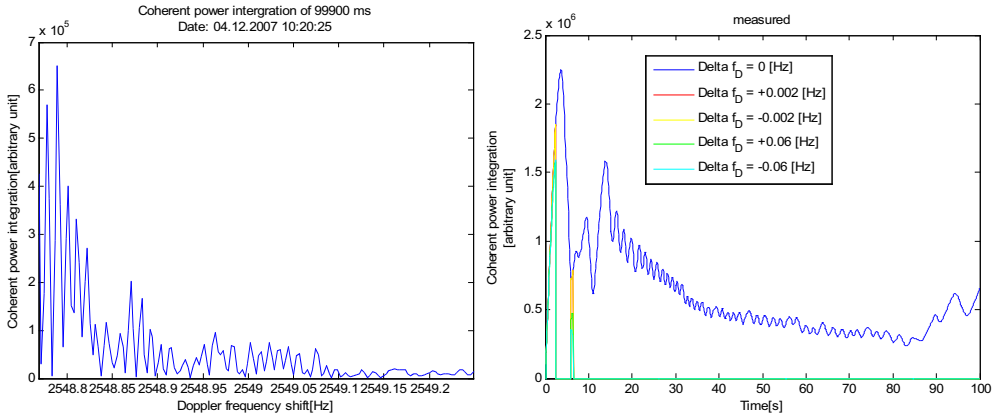

Figure D.2: SV36(prn6) clk:Rub, Left: Search space view after 99.9 second of coherent integration time; Right: Evolution of the peak magnitude;

D.1.3 Oscilloquartz 8712

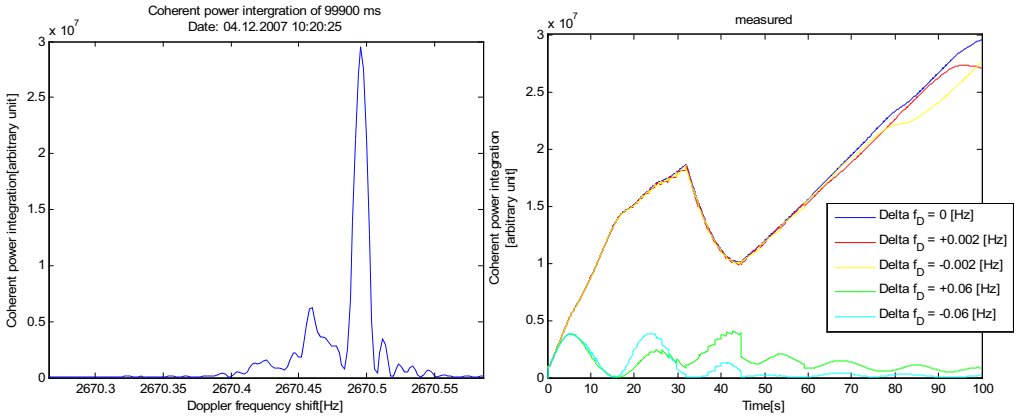

Figure D.3: SV36(prn6) clk:Rub, Left: Search space view after 99.9 second of coherent integration time; Right: Evolution of the peak magnitude;

D.1.4 Oscilloquartz 8683

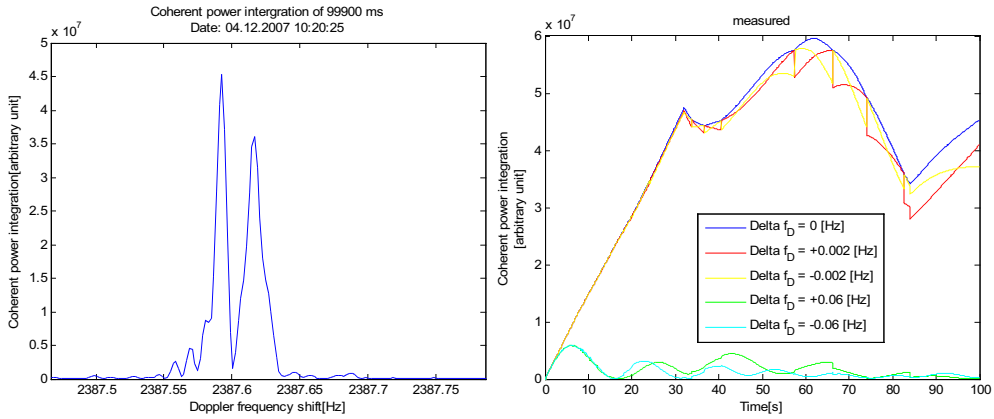

Figure D.4: SV36(prn6) clk:Rub, Left: Search space view after 99.9 second of coherent integration time; Right: Evolution of the peak magnitude;

D.1.5 Oscilloquartz 8663

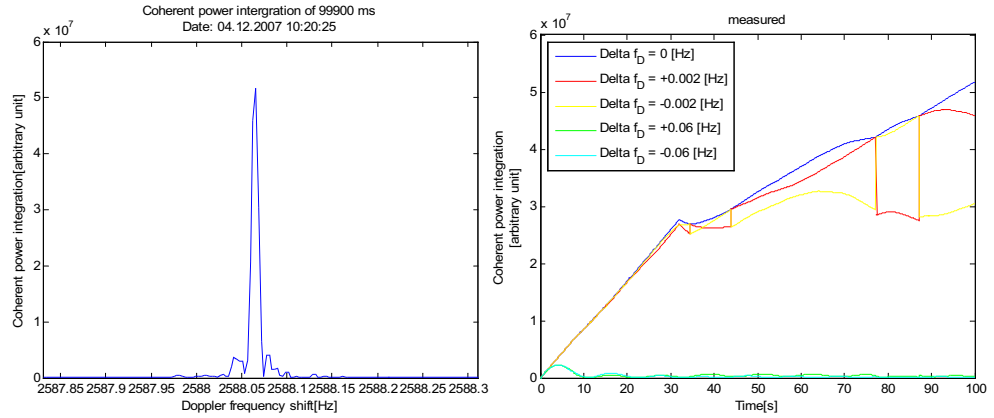

Figure D.5: SV36(prn6) clk:Rub, Left: Search space view after 99.9 second of coherent integration time; Right: Evolution of the peak magnitude;

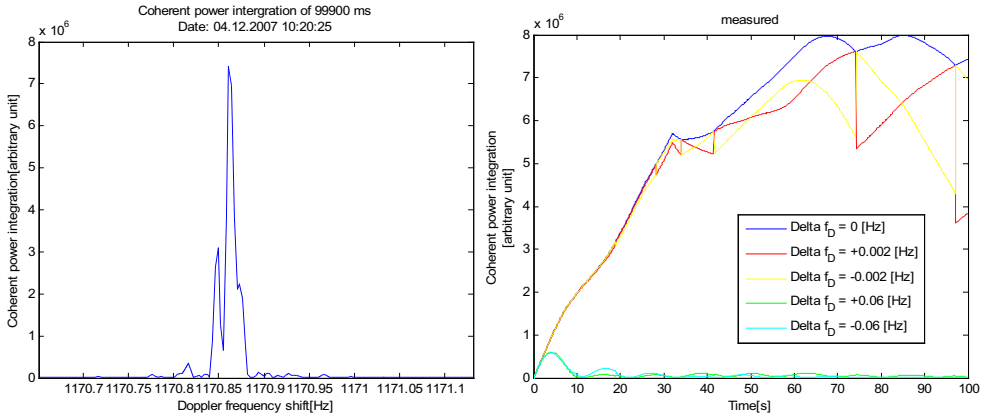

Figure D.6: SV43(prn13) clk:Rub, Left: Search space view after 99.9 second of coherent integration time; Right: Evolution of the peak magnitude;

D.1.6 Oscilloquartz 8788

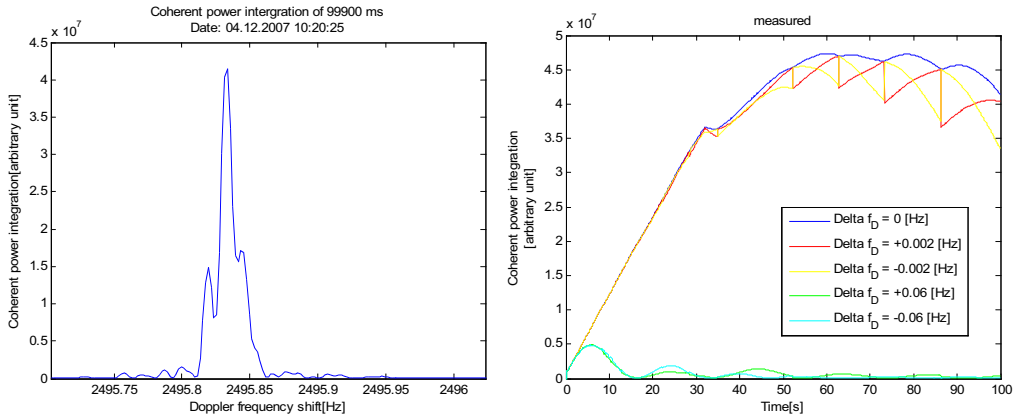

Figure D.7: SV36(prn6) clk:Rub, Left: Search space view after 99.9 second of coherent integration time; Right: Evolution of the peak magnitude;

D.1.7 Oscilloquartz 8607

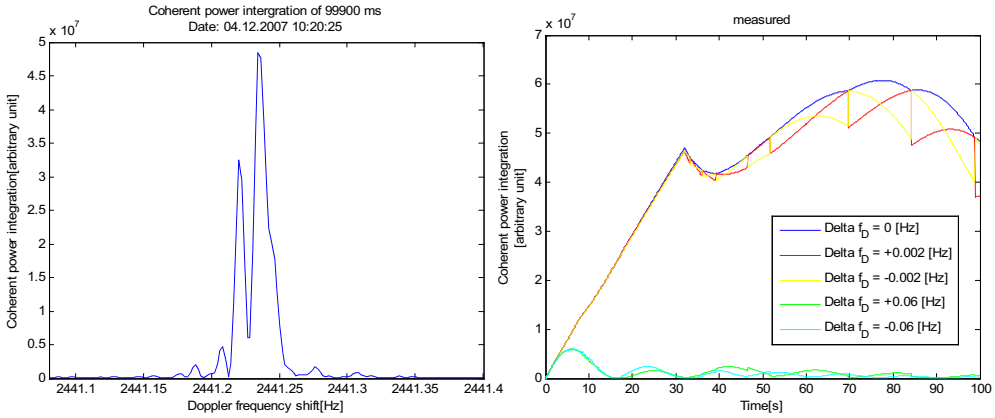

Figure D.8: SV24(prn24) clk:Cs, Left: Search space view after 99.9 second of coherent integration time; Right: Evolution of the peak magnitude;

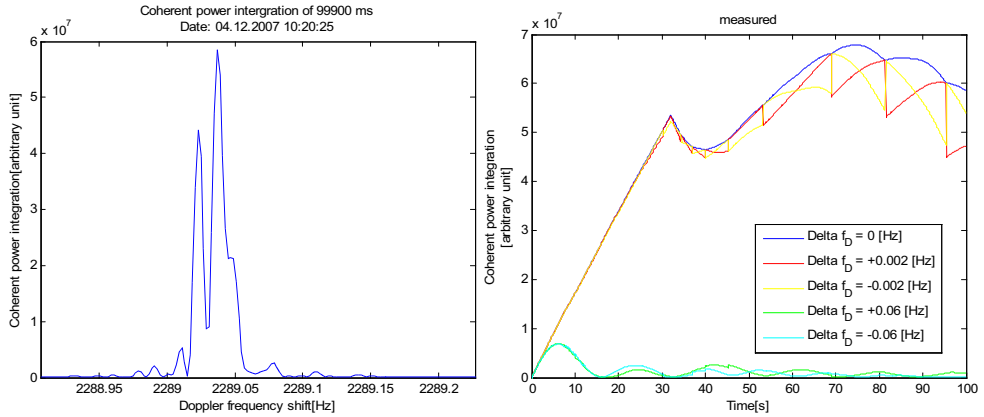

Figure D.9: SV36(prn6) clk:Rub, Left: Search space view after 99.9 second of coherent integration time; Right: Evolution of the peak magnitude;

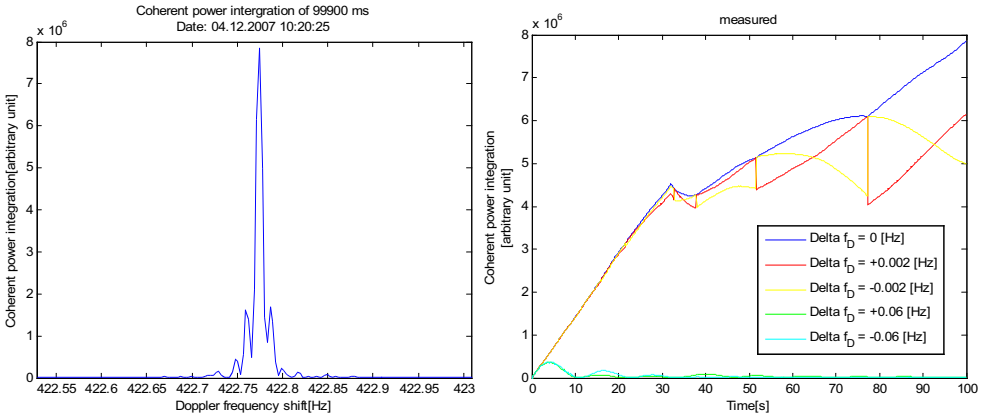

Figure D.10: SV43(prn13) clk:Rb, Left: Search space view after 99.9 second of coherent integration time; Right: Evolution of the peak magnitude;

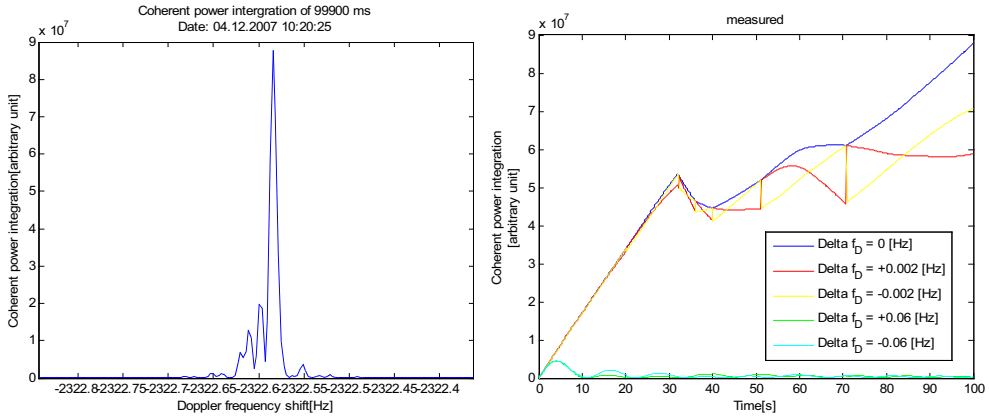

Figure D.11: SV61(prn2) clk:Rb, Left: Search space view after 99.9 second of coherent integration time; Right: Evolution of the peak magnitude;;

D.1.8 Efratom Rubidium

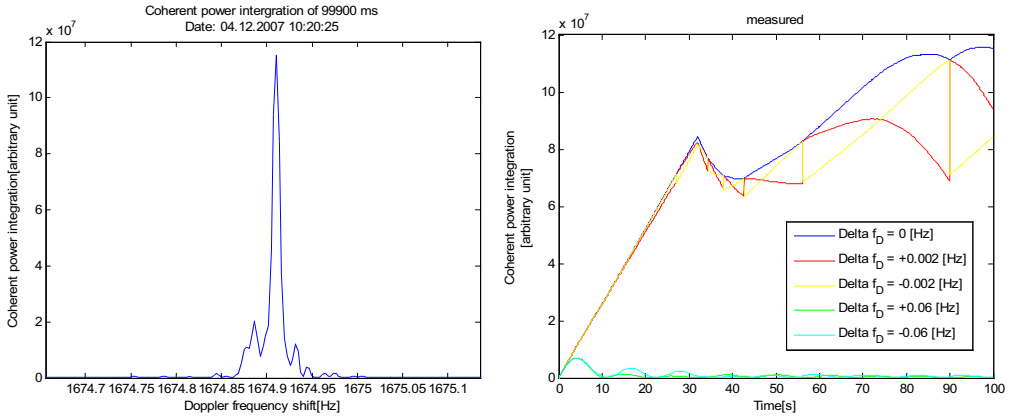

Figure D.12: SV36(prn6) clk:Rub, Left: Search space view after 99.9 second of coherent integration time; Right: Evolution of the peak magnitude;

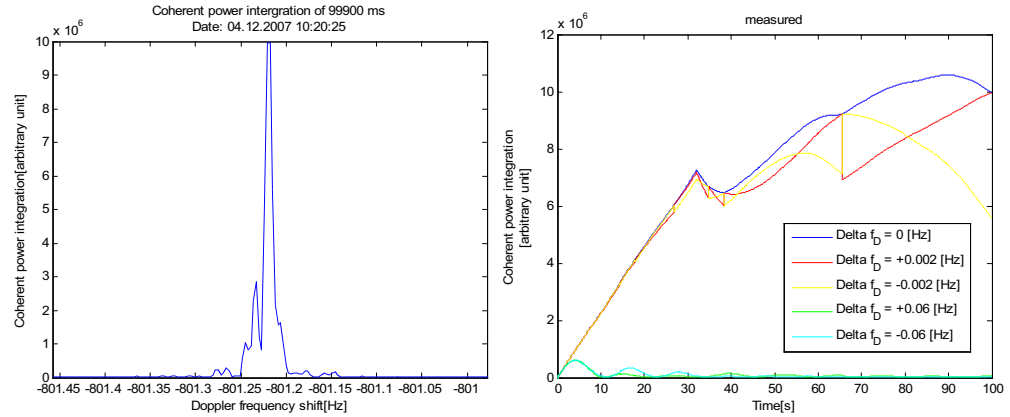

Figure D.13: SV43(prn13) clk:Rub, Left: Search space view after 99.9 second of coherent integration time; Right: Evolution of the peak magnitude;

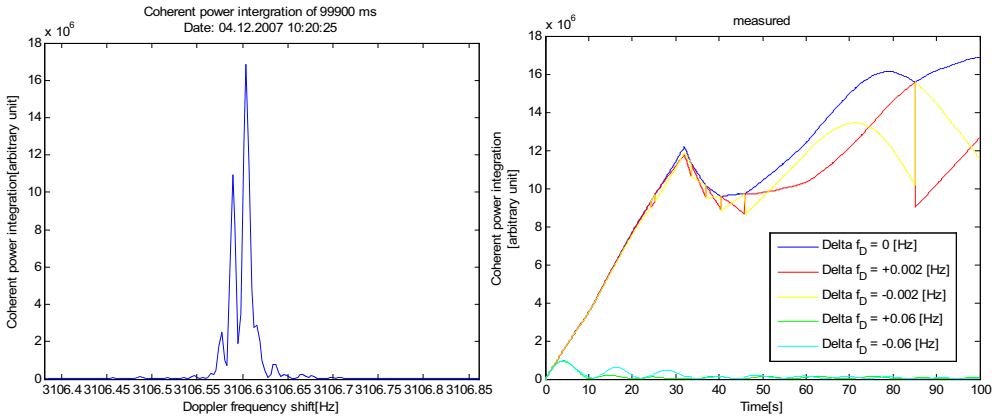

Figure D.14: SV45(prn21) clk:Rub, Left: Search space view after 99.9 second of coherent integration time; Right: Evolution of the peak magnitude;

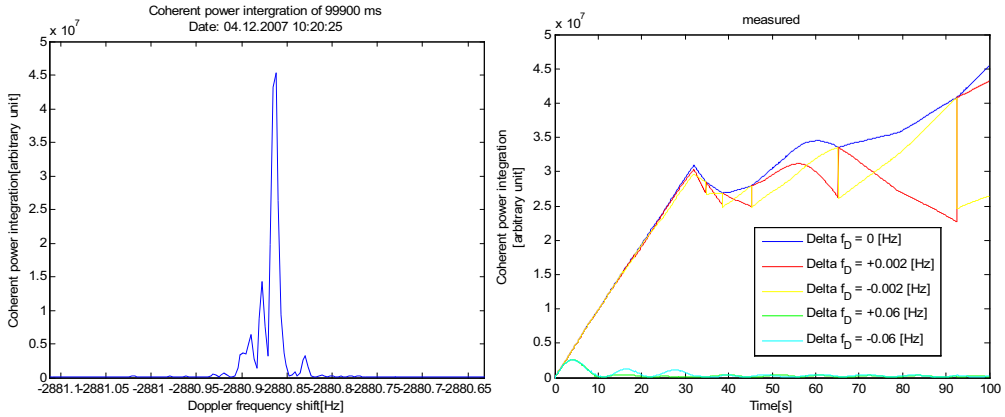

Figure D.15: SV61(prn2) clk:Rub, Left: Search space view after 99.9 second of coherent integration time; Right: Evolution of the peak magnitude;

D.2 Indoor acquisition

D.2.1 Oscilloquartz 8607

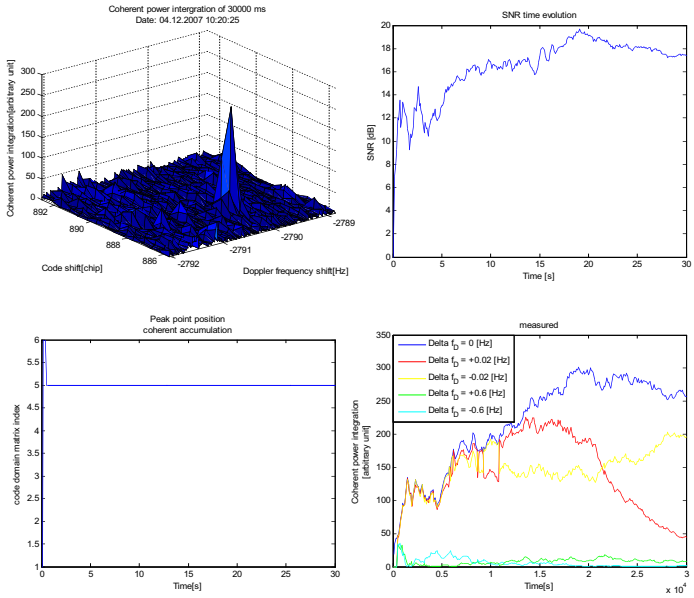

Figure D.16: SV24(prn24) clk:Cs, Indoor GPS signal acquisition.

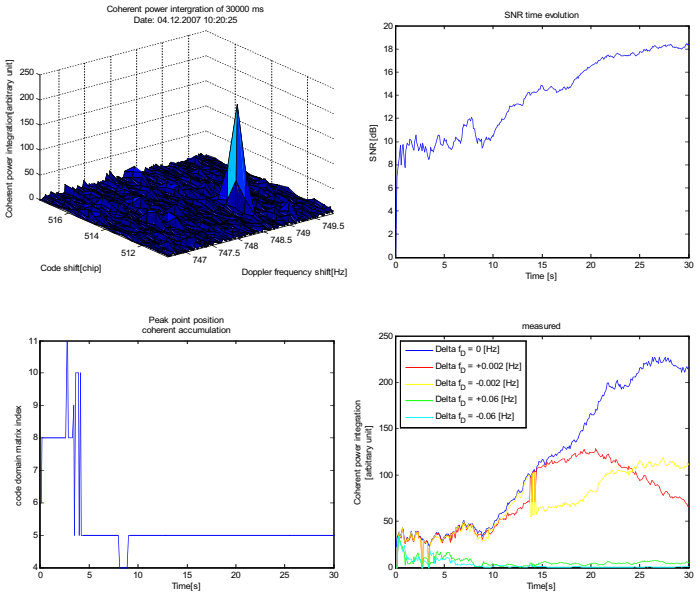

Figure D.17: SV54(prn18) clk:Rb, Indoor GPS signal acquisition.

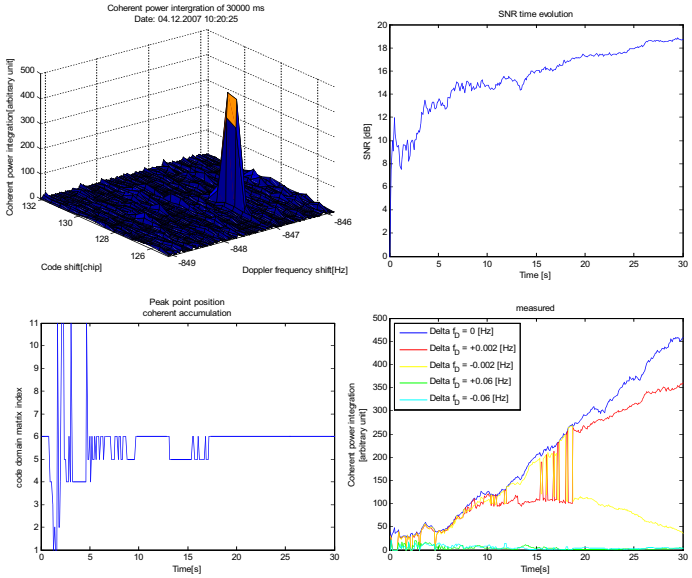

Figure D.18: SV45(prn21) clk:Rb, Indoor GPS signal acquisition.

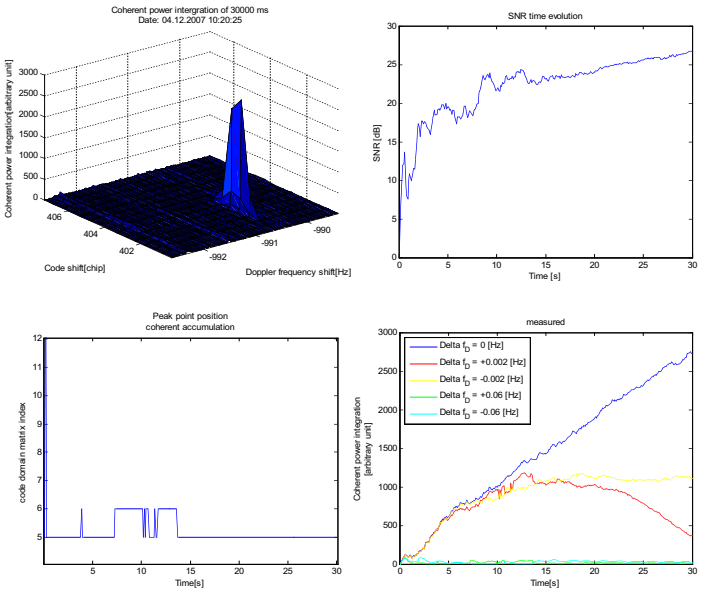

Figure D.19: SV55(prn15) clk:Rb, Indoor GPS signal acquisition.

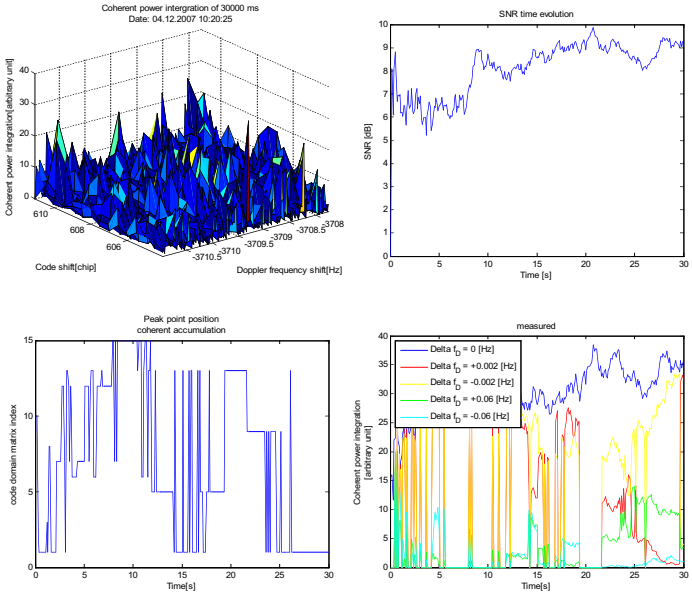

Figure D.20: SV36(prn6) clk:Rb, Here it as not been possible to acquire the signal

D.2.2 Oscilloquartz 8683

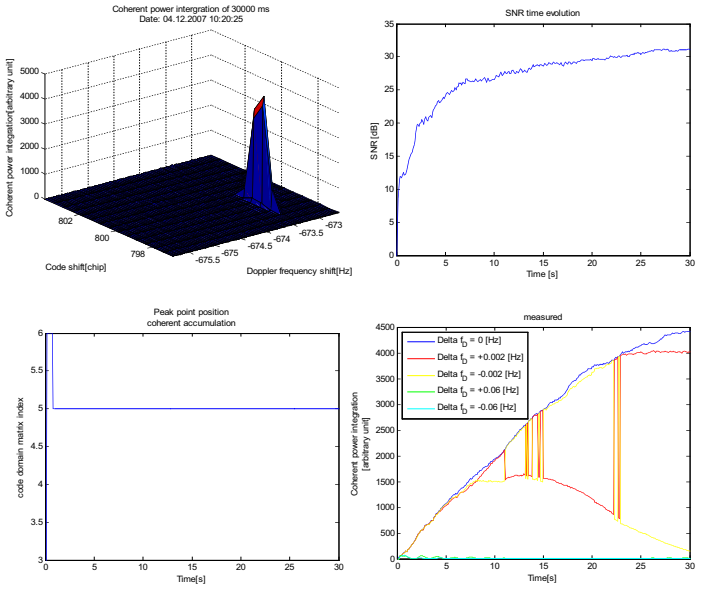

Figure D.21: SV45(prn21) clk:Rb, Indoor GPS signal acquisition.

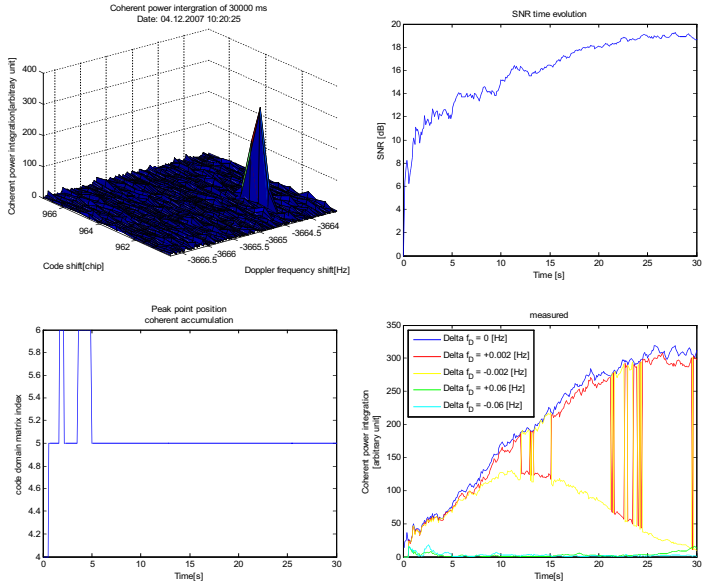

Figure D.22: SV36(prn6) clk:Rb, Indoor GPS signal acquisition.

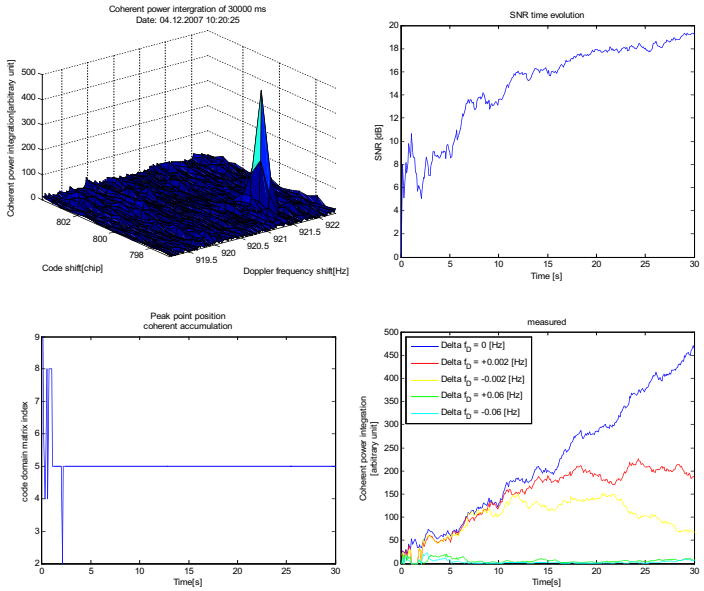

Figure D.23: SV54(prn18) clk:Rb, Indoor GPS signal acquisition.

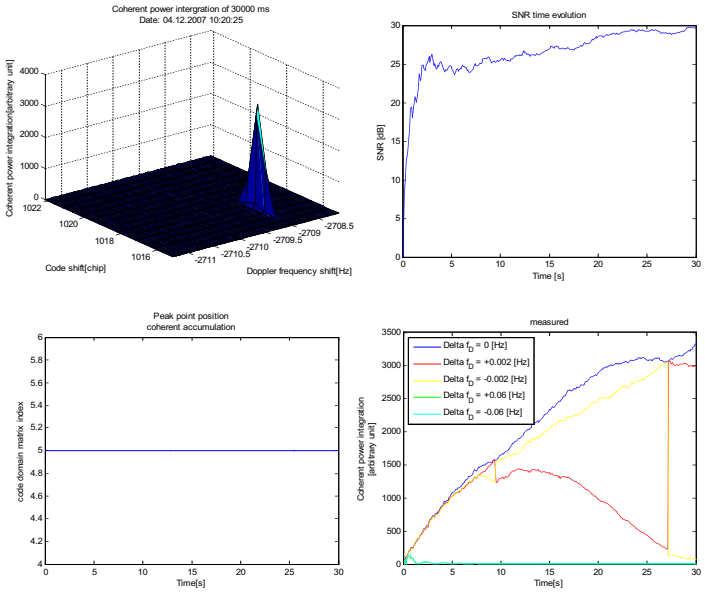

Figure D.24: SV24(prn24) clk:Cs, Indoor GPS signal acquisition.

D.2.3 Oscilloquartz 8663

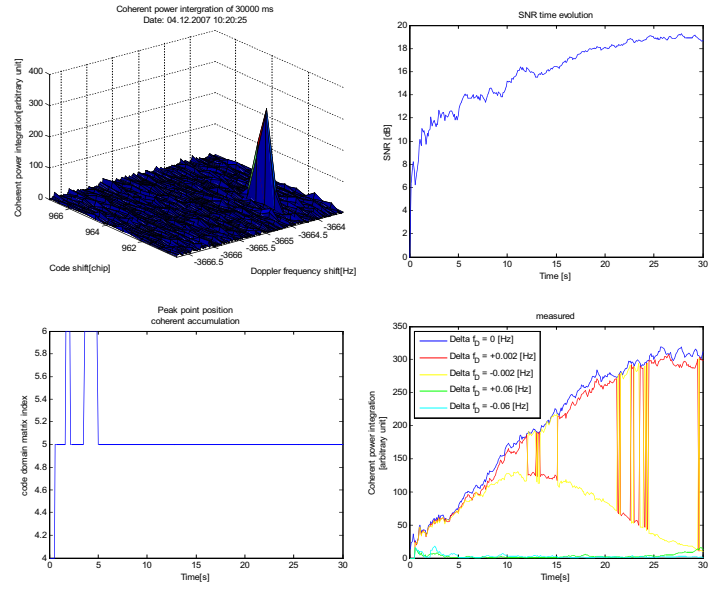

Figure D.25: SV36(prn6) clk:Rb, Indoor GPS signal acquisition.

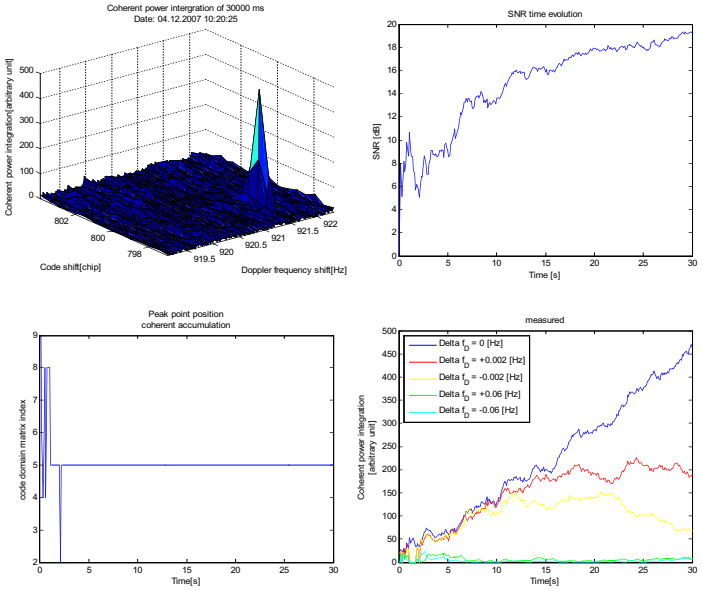

Figure D.26: SV54(prn18) clk:Rb, Indoor GPS signal acquisition.

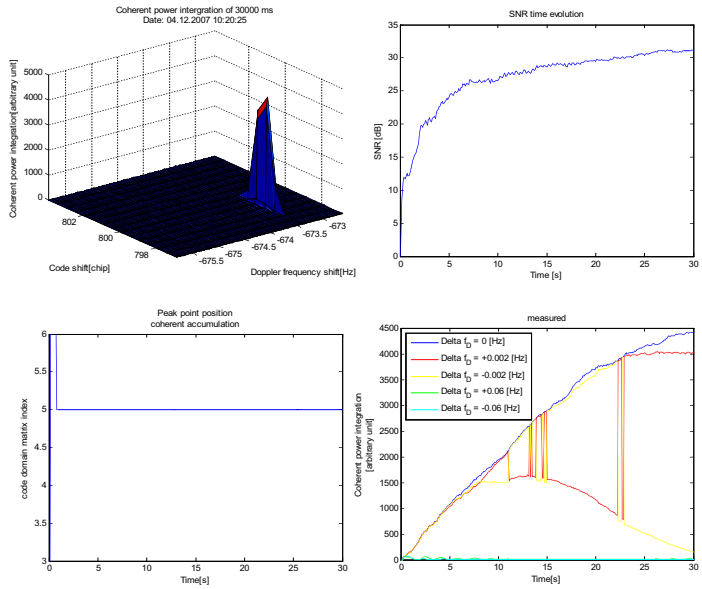

Figure D.27: SV45(prn21) clk:Rb, Indoor GPS signal acquisition.

D.2.4 Oscilloquartz 8788

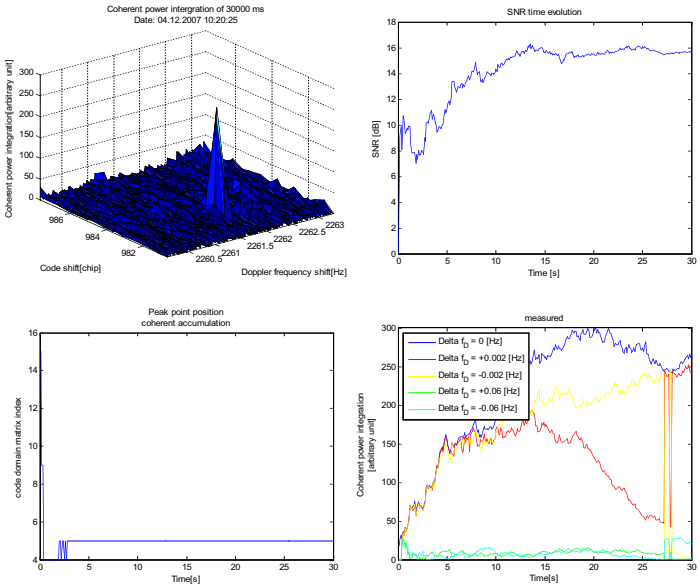

Figure D.28: SV33(prn3) clk:Cs, Indoor GPS signal acquisition.

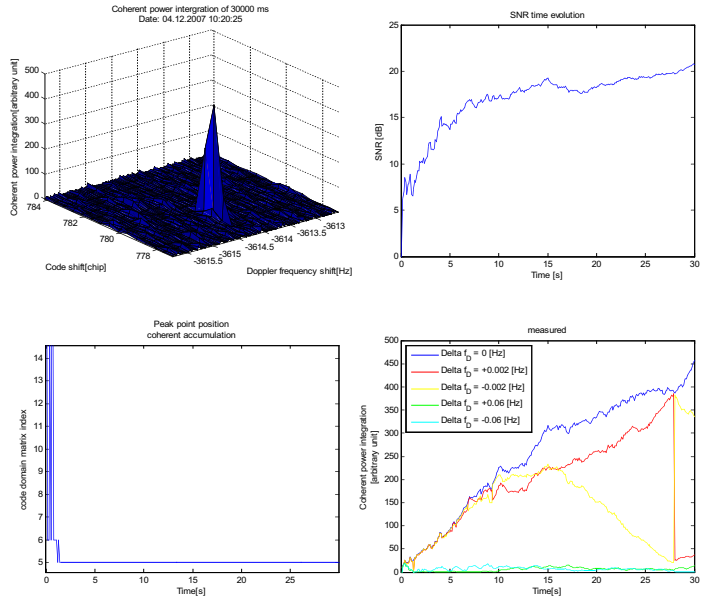

Figure D.29: SV36(prn6) clk:Rb, Indoor GPS signal acquisition.

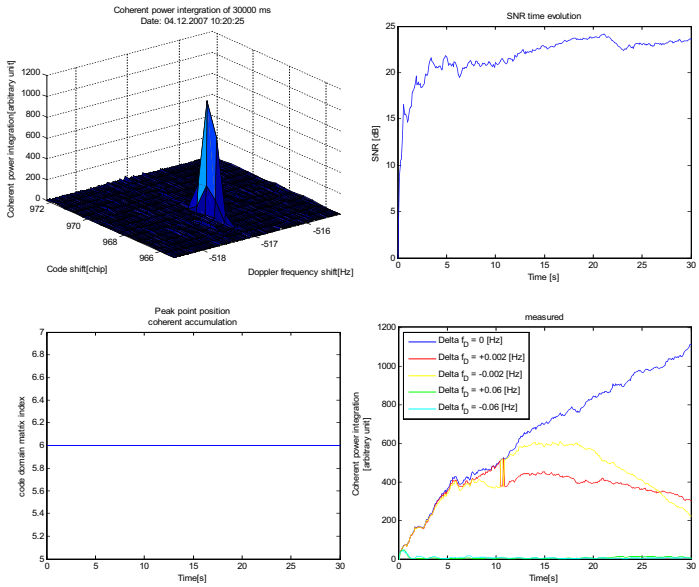

Figure D.30: SV45(prn21) clk:Rb, Indoor GPS signal acquisition.

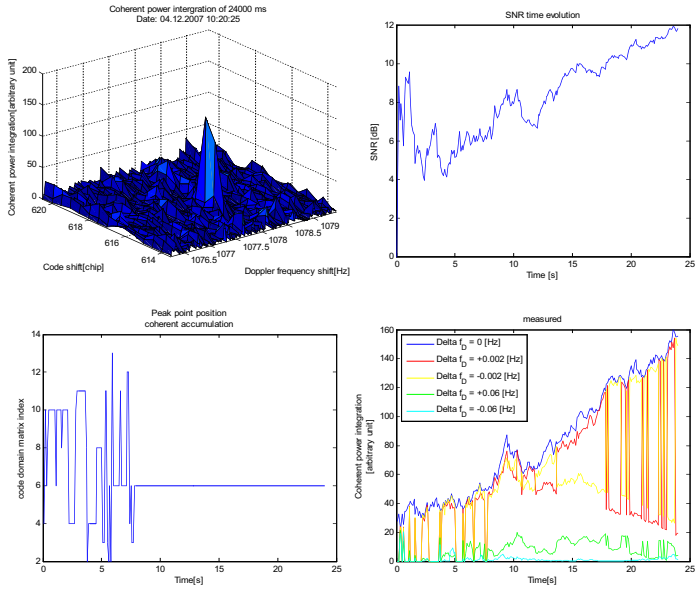

Figure D.31: SV54(prn18) clk:Rb, Indoor GPS signal acquisition.

D.2.5 Efratom Rubidium

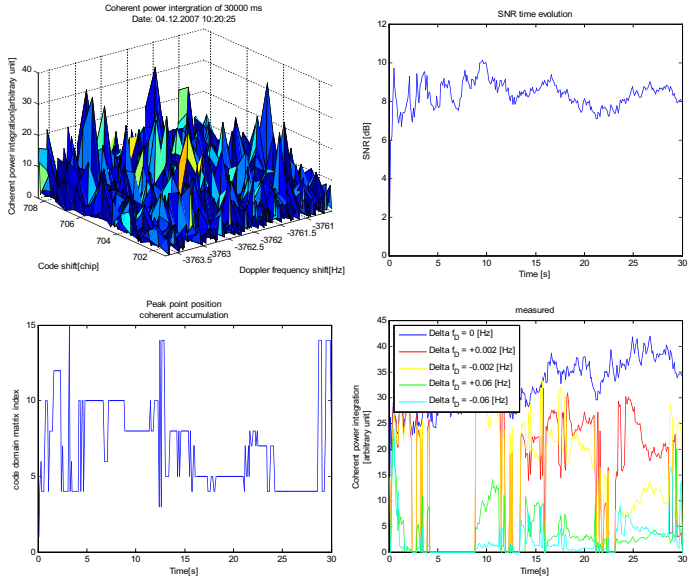

Figure D.32: SV36(prn6) clk:Rb, Indoor GPS signal acquisition.

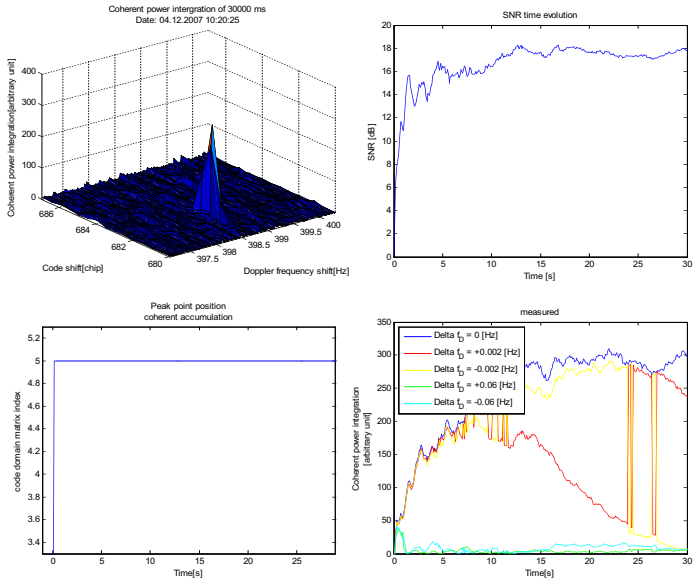

Figure D.33: SV54(prn18) clk:Rb, Indoor GPS signal acquisition.

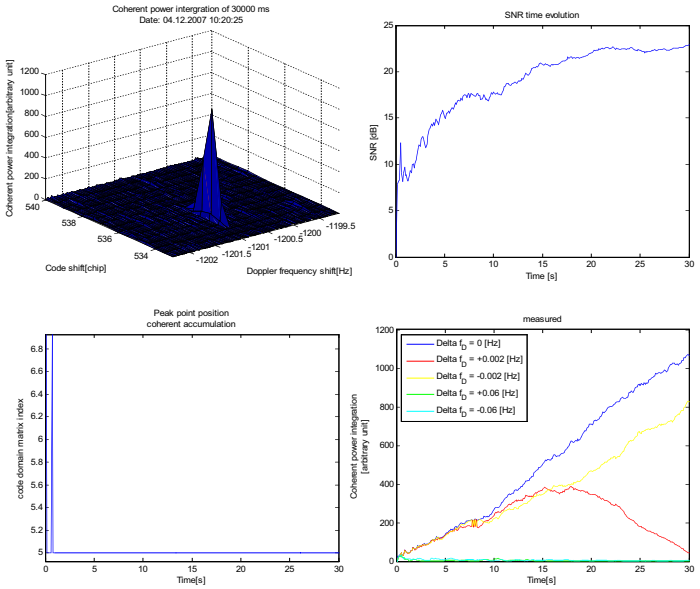

Figure D.34: SV45(prn21) clk:Rb, Indoor GPS signal acquisition.

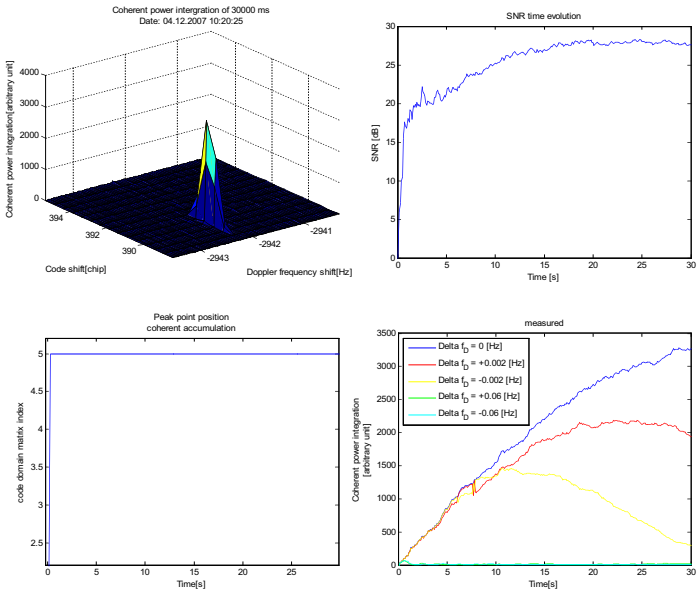

Figure D.35: SV24(prn24) clk:Cs, Indoor GPS signal acquisition.

Appendix E

NavLabInterface user's manual

This manual is based on the NavLabInterface2008(v 0.6) "authorized release". Check releaseInfo.txt in the root folder for more information about releases. The "authorized release" includes a single data set and some already precessed data for demonstration purposes. The program need the .NET 3.0 library to be installed on the computer, more over the software needs to be executed in administrator mode.

E.1 Getting started

This section will bring the reader through the steps to get his first signal acquisition. Begin with the 3 step reported in figure [E.1], [E.2] and [E.3].

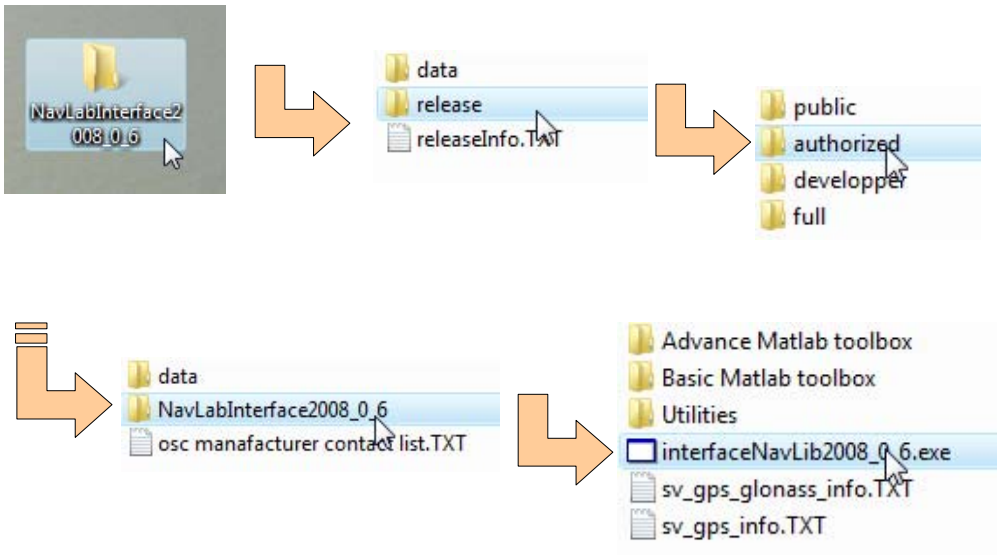

Figure E.1: Execute NavLabInterface2008.exe.

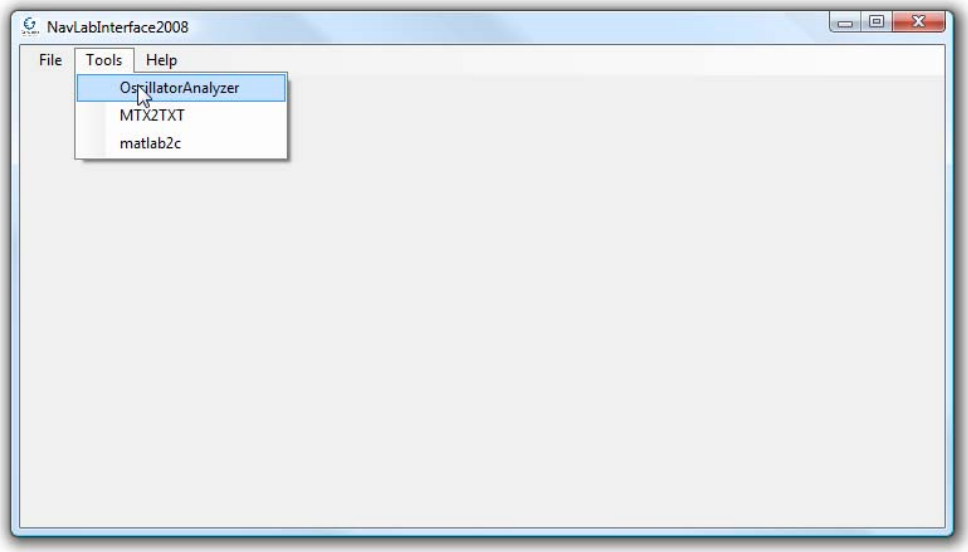

Figure E.2: Select the OscillatorAnalyzer.

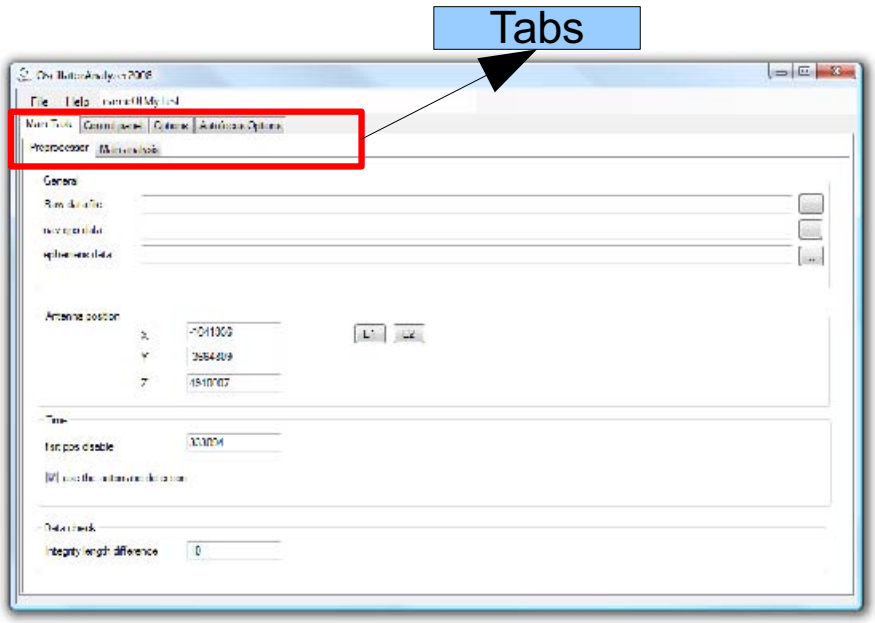

Figure E.3: One uses a tabs base navigation interface

As indicated in figure [E.4]:

- Go in the tab "Options".
- Select a work folder. All program outputs will be saved in this folder.

- Enter an experience folder name where to save the current processed data within the work folder

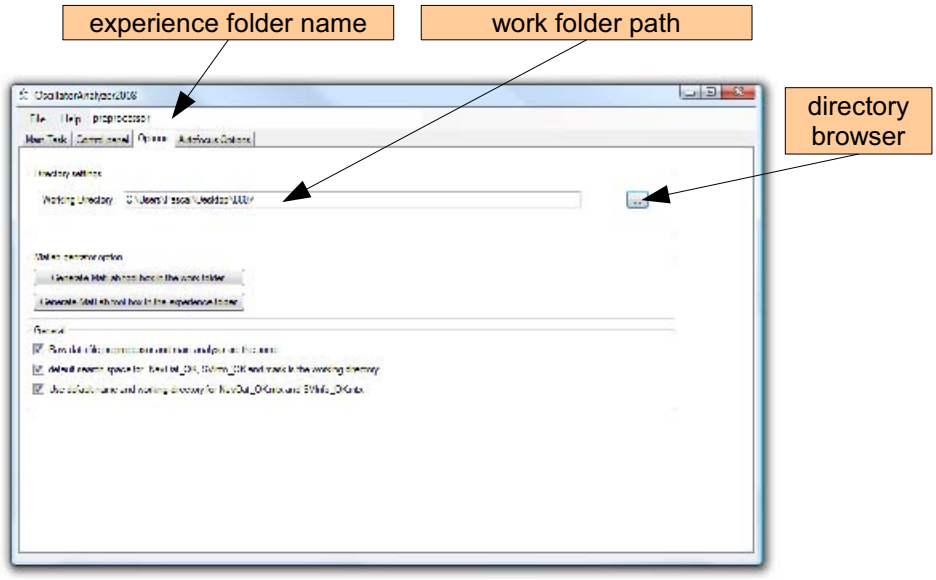

Figure E.4: Here one will enter a Work folder name corresponding to the tested oscillator and a experience folder named preprocessor, referring to the next processing step.

- Go in the tab “Main task” and select “Preprocessor” (see figure [E.5]).
- Select the appropriate file using the file selection button[1]
- Enter the antenna coordinates[2], here one directly click on the E2 button to select pre-recorded coordinate.
- Enter the approximate GPS time of data collection in second, here 424215.
- The last option called “integrity length difference” is used when if all the different recorded satellite data aren’t corrupted for more information see [4.4.4]
- Go to “Control Panel” (see figure [E.6]).
- Check the preprocessor box and click the “execute button“, the processing time can vary from a computer to an other typically this precessing step will take between 5 and 10 minutes. The progress bar and the program output in the log window will information the user about the current processing status (see figure [E.7]).

[1] the button with the 3 points
[2] X, Y, Z format

- At the end of the process the output file should looks like displayed in figure [E.8].

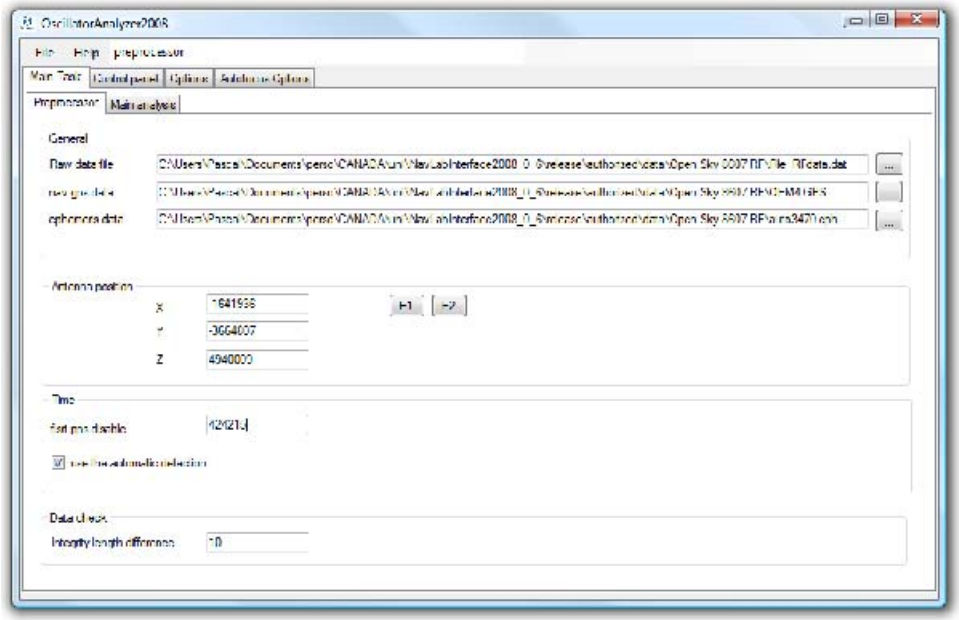

Figure E.5: Enter the parameters as display above..

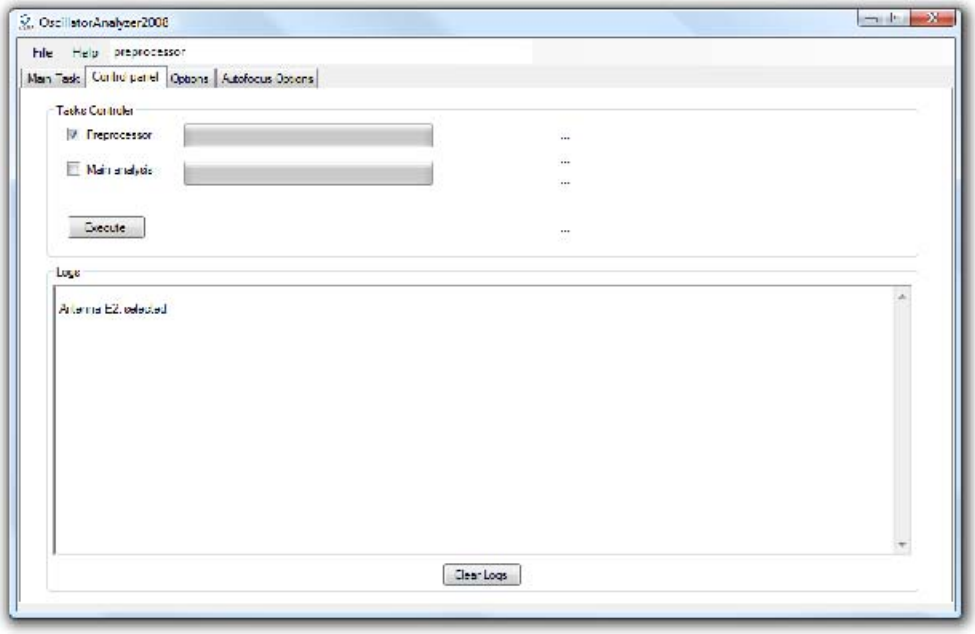

Figure E.6: Launch the calculation. One can note the "log" window where the program gives information about undertaken actions. Here he notify, the user selected antenna E2.

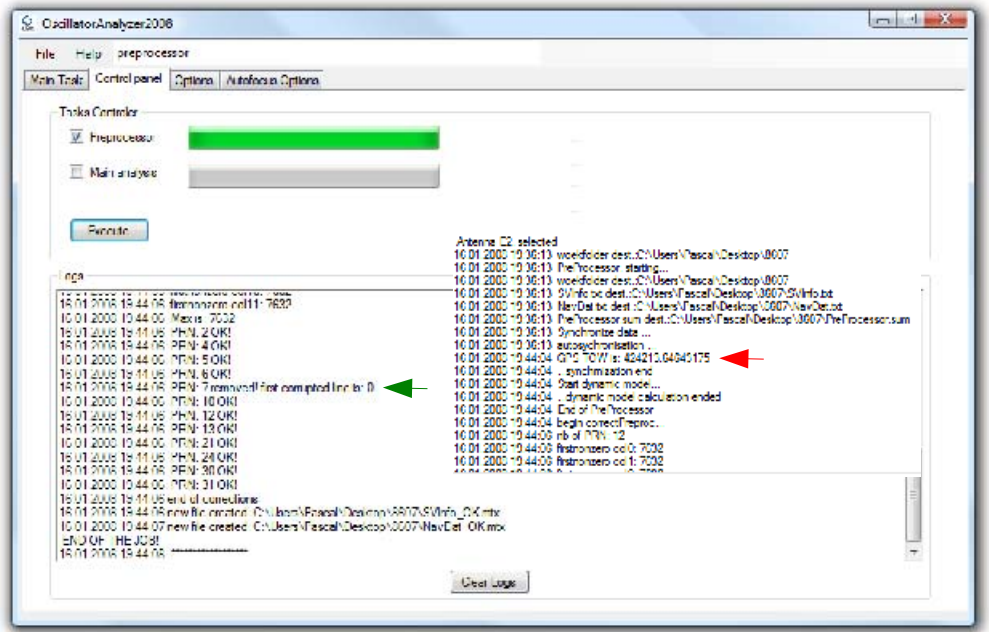

Figure E.7: If the preprocessor has been executed successfully, one gets this result. The time at which the RF data begin is given here(red arrow). The green arrow highlight the message informing the user a prn has be removed because the data where corrupted from line n here, line 0.

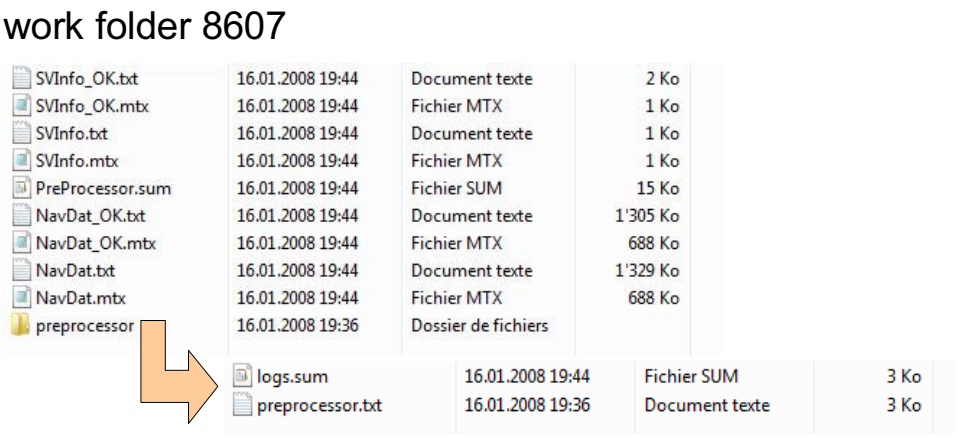

Figure E.8: Resulting outputs in the work folder.

Now we are ready to acquire the signal:

- Change the experiment folder name into "test1".
- Then go to "main task" and "main analysis" (see figure [E.9]).
- Select the satellite by choosing the channel, where channels correspond with the lines of SVInfo_OK.txt file. For example the satellite one the second line is selected by choosing channel 1.
- Then enter the correlation options, by clicking on the button "strong signal 2".
- Launch the calculation process by selecting main "analysis" on the "control panel", make sure you uncheck the "preprocessor" box, otherwise it will first execute the preprocessor and then the main analysis (see figure [E.9]).

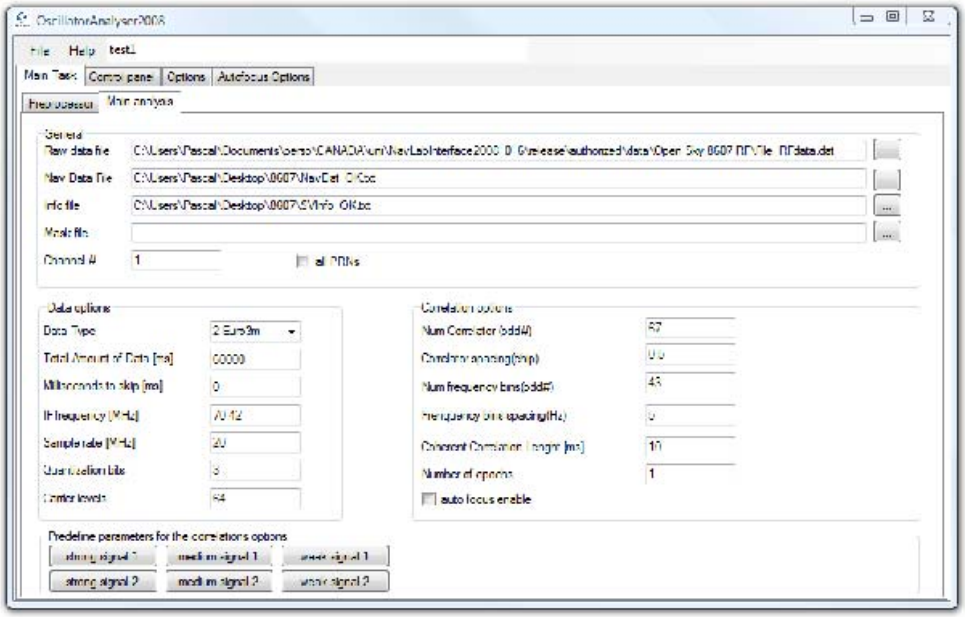

Figure E.9: Parameter for the acquisition of “test1”.

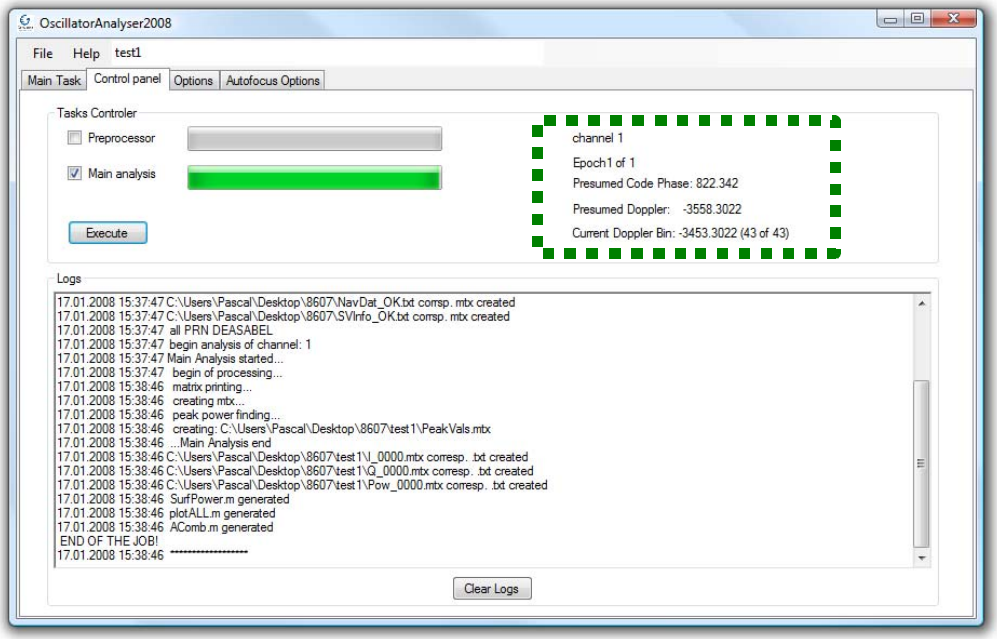

Figure E.10: At the end it should appears like that. Please note the user information given to the user(green box).

To visualize the result execute the automatically generated Matlab file: test1plotAll.m . This will gives the result depicted on figure [E.11].

```
%version - 0.6RC4 - automatically generated matlab file
%Oscillator Analyser - Matlab - plotAll
%author: Pascal Olivier Gaggero
%pascal.gaggero@unine.ch
%University of Neuchatel(switzerland), Calgary(Canada)
%Copyright: PLAN Group, University of Calgary
%15 january 2008
%-------------------------------------------------------------
load Pow_0000.txt;
SurfPower(Pow_0000);
title({'Coherent power intergration of 10ms';'Date: 17.01.2008 15:38:46'});
```

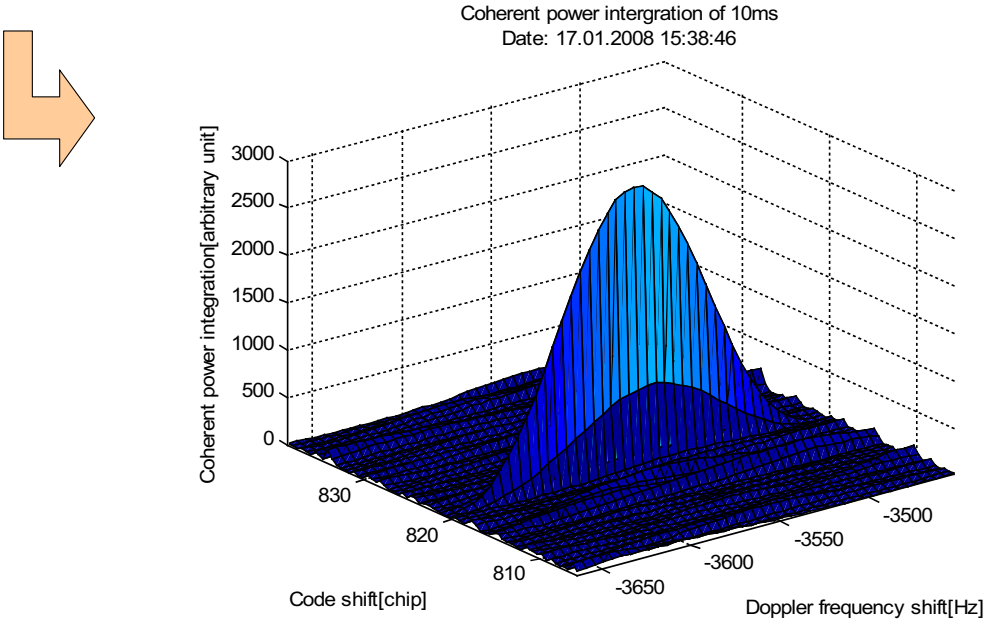

Figure E.11: Result of a simple acquisition.

E.2 Acquisition parameters

In the "main analysis" tab there is two options field: "data options" and "correlation options". The "data options" field correspond to the format in which the RF data have been recorded. The user can also skip a certain amount of data at the beginning of the file ("Millisecond to skip"). If the data have been recorded using the custom Euro3M-FPGA front-end the other parameter do needs to be modified.
The "data options" will essentially define how the program will process the data:

- **"Num Correlator":** indicates the program the number of different correlator to consider in the code domain (this must be an odd number).
- **"Correlator Spacing"**: code delay between the various correlators.
- **"Num Frequency Bin"**: is the size of the Doppler frequency domain (must be odd too).

- **"Frequency bins spacing"**: elementary step between the different bins in the frequency domain.
- **"Coherent Correlation Length"**: is the coherent integration time used to calculate each epoch.
- **"Number of epochs"**: is the number of different epochs to be calculated, maximum 9999.
- **"auto focus enable"**: tells the software to perform a automatic focus on the peak using the options of the "Autofocus Options" tab.

E.3 Troubleshooting

- **Double peak**: If one observes a double peak problem, it mean that the program don't correctly compensate for the data bits, this is essentially a synchronization problem. Potential sources are:
  - Wrong approximate start time in the preprocessor.
  - Wrong ephemeris file, typically of the wrong day.
  - Corrupted RF data file.

  The easiest way to verify if the data don't exihibit double peak problem is to calculate 20 epoch of 10 ms each. If the peak appears normally in each epoch the data synchronization is correct, otherwise some of the figure will show a double peak.
- **See only noise**: If no peak is observed on the output figures this could be caused by various sources:
  - If the acquired signal is a weak signal the coherent integration as to be increased. Or several epoch has to be combined together to reach the required SNR for the detection. For this purpose use allComb.m. Typically weak signal conditions are observed for indoor data set, but also on low elevation satellites.
  - If the front-end local oscillator outputs a shifted frequency. For example if the nominal frequency of the oscillator is 10.2MHz instead of the required 10.0MHz. The peak will be shifted of $0.2MHz \cdot \frac{1575.42MHz}{10MHz} = 31MHz$. The consequence is that the search space will not be correctly centered, and it will requires manual search space adjustment(see [E.4.1]). Ideally the oscillator has to be calibrated to reach a precision of $\pm 0.02Hz$, this leads to a peak shift of $3Hz$. The conclusion is that the user has to set is search space parameter up taking into account the potential oscillator frequency precision errors.
  - The signal is to weak at all to be acquired.

E.4 Focusing on the peak

It is necessary to be able to focus the search space on the peak position in order to work with smaller frequency bins spacing when integrating over long coherent integration time period (see [4.1]). Conceptually one could simply decrease the frequency bins spacing and increasing proportionally the bins number to keep the same search space. The problem is that one will then increase considerably the processing time, which is a function of the search space size.
The general principle of focusing algorithm is:

1. Acquisition of the signal.
2. Searching for the peak position.
3. Centering the search space around the founded peak position.
4. Increase the resolution and the integration time in the correlation options.
5. Loop to the first point.

At each step one has to increase the coherent integration time of each epoch otherwise at a certain point one will observe the peak to closely and it becomes impossible to determine the peak position (see the same problem in an other context: **??**f:peakclose]). In order to save calculation time after some iteration steps one will fix the code delay i.e one only take 1 single correlator. This assumes the peak position is not much affected by oscillator frequency error.

E.4.1 Manually

After each focusing step the user has to find the signal peak position and modify manually the SV parameter saved in SVInfo_Ok.txt(see [4.17]). The predicted Doppler (zero order parameter) and predicted code delay has to be replaced by respectively the founded peak position in frequency domain and in the code domain. This method is quite time consuming in term of human work charge that is why the software implement an automatic focus feature. Nevertheless under weak signal condition the manual focusing methodology stay the only valid solution.

E.4.2 Automatically

The automatic focus is enable by checking the "auto focus enable" checkbox on the "main analysis" tab. The algorithm will successively apply the correlation option defined in the "autofocus options" tab[3]. The basic focus algorithm will use the first 9 step as depicted in figure [E.12]. This function only work if the coherent integration time of a single epoch is sufficient to acquire the signal and determine the peak position. Figure [E.12] shows the default autofocus parameters of the software.

[3]The user has to check "use this step" to use the step.

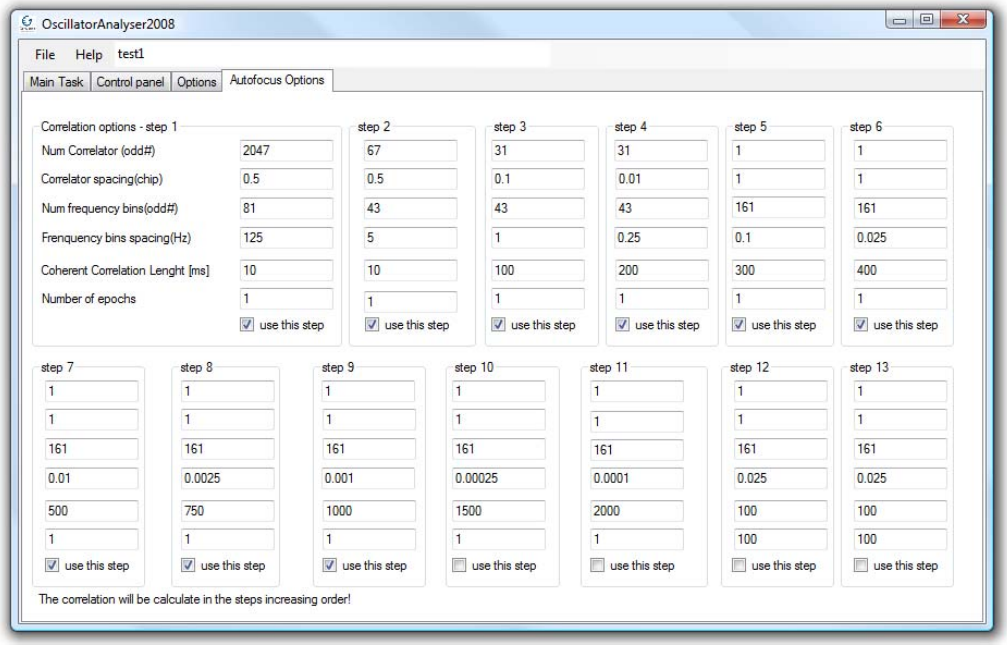

Figure E.12: Default autofocus parameters. One can note the increase coherent integration time when frequency bin spacing decreases. Interesting is also that only the 4 first steps have more than one correlator, the other step simply assume a known code delay.

E.5 Extra features

- **"all PRNs"**: tells the program to process all the prn defined in "SVInfo_Ok.txt" file using the current options.
- **"File ↪ save"**: saves the current GUI configuration in the current experiment folder in a text file .txt with the some name than the experiment folder.
- **"File ↪ load"**: allows the user to load previously saved parameter.
- **Matlab toolbox**: One can generates the Matlab toolbox inside the work and experiment folder by click on the corresponding button in the "Option" tab. The generated .m files will have the parameter corresponding to the current correlation option i.e. the parameters display on the "main analysis" tab.

E.6 Other available tools

There are two other tools package in the NavLabInterface2008 v0.6:

- **MTX2TXT**: Is used to transform .mtx files into .txt files. One can gives many file as entry.

- **matlab2c**: Is a function that transposes a Matlab .m script into a .txt file which contains copy past ready code for a c++ function generating the Matlab code. Nevertheless the "
  n" chart should be manually replaced in the c++ function by "

  n"

E.7 Matlab toolbox

E.8 AllComb.m

For this script the user have to gives several input arguments (see figure [E.13]), listed and explained here:

- **start:** Is the start epoch number. For example starting the coherent integration at after 40s assuming 100ms epoch will implies start=400.
- **num_comb:** Is the number of epoch to coherently integrate. For example again assuming 100 ms epoch, for 10 second integration time num_comb.
- **coh_int_time:** Is the epoch duration in millisecond i.e. 100ms epoch implies coh_int_time=100ms
- **epochDigits:** This is a back ward compatibility argument. So if the epoch file are of the form of I_xxx ↪ epochDigits=3 or I_xxxx ↪ epochDigits=4
- **showSideIndex:** Indicates to the script that the user what to plot the side index power accumulation on the coherent integration power accumulation evolution graph.
- **var1/2:** Are symmetrical side indexes i.e. if the frequency bin step is 0.1Hz and the var1=2 it will plot the accumulated power corresponding to a shift 0.2 Hz compared to the peak frequency position.
- **set_lenght:** Gives length of a set in unit of epochs. i.e. if set_lenght=10 and epoch of 100ms second are considered one get sets of 1 second.
- **inSeparateWindow:** If equal to 1 all the script output figure will be produced in separated windows. Otherwise a more compact result display is adopted.
- **accumulationEnable:** If equal to 1 shows the power accumulation results.
- **allDetailsEnable:** If equal to 1 it shows an extended set of plots.
- **statisticsEnable:** If equal to 1 the statistics results are shown.

- **pdfEnable:** If equal to 1 the pdf analysis is displayed.
- **hist_point:** Correspond to the number of point to used for each rode in the histogram for the pdf analysis.
- **NoiseValueEstimationMode:** If equal to 0 it estimate the noise parameters over the whole search space. If equal to 1 the script will used a fix noise mean value given in variable fixedNoiseValue and the noise variance given in the variable fixedNoiseVarValue. If equal to 2 the noise value is estimated over an area of the width defined by the variable estimatorAreaWidth. This area should not contain any peak or GPS signal.
- **fixedNoiseValue:** See NoiseValueEstimationMode.
- **fixedNoiseVarValue:** See NoiseValueEstimationMode.
- **estimatorAreaWidth:** See NoiseValueEstimationMode.
- **allanVarianceEnable:** If equal to 1 it enable the calculation of the Allan variance.
- **plotEachAllan:** If equal to 1 it plot each frequency error plot corresponding to individuals allanVarPoint
- **allanVarPoint:** Is a vector that gives the different averaging time to compute in unit of epoch.
- **dopplerFstep:** Is the frequency bin step used during the data processing.
- **L1frequency:** Define the GPS l1 frequency in MHz
- **OscillatorOutputFrequency:** Take nominal frequency output value.
- **allanYlLw, allanYHigh, allanXlLw, allanXHigh,:** Are display parameter for the plot windows size.
- **interpollation:** If equal to 1 enable the interpolation of the peak, this function has been implemented for testing purpose and should be further investigated to be really use full.
- **inter_sample_width:** gives the interval between sample for the fitting used in the interpolation function.
- **snrEnable:** If equal to 1 it turns on this feature.
- **CoverNoOpenSky:** Gives the C/No value for the SNR evolution plot.
- **snrDetectionLimit:** Plot an horizontal line on the SNR graph.

- **attenuation:** Is a vector of that contain 4 attenuation value in dB corresponding to the 4 different colors on the SNR plot.
- **logSpace:** Define the size of the SNR plot window.
- **oscMomdelDegree:** Gives the order of the model used for modeling the power behavior.
- **moviesEnable:** Record the time evolution of certain plot in a .avi movie file.
- **moviename:** Give the name under which the created .avi as to be saved.
- **compression:** Gives which compression codec as to be used.
- **fps:** Gives the image frame rate for the movie.

If the script has been generated by the OscillatorAnalyzer, it is ready to go with the right options.

```
%version - 0.6b06 - automatically generated matlab file
% multiple analyser - mm.*.m
%author: Pascal Olivier Gaggero
%pascal.gaggero@unine.ch
%University of Neuchatel(switzerland), Calgary(Canada)
%Copyright: PLAN Group, University of Calgary
%18 january 2008
%
%option of the script----------------------------------------

clear all;                              % clear all the variable
close all;                              % close all a mdim
clc;                                    % clear command window

%----data option
start=1;                                % start epoch
num_cumb=10;                            % from 1 to max ??
coh_int_time=120;                        % length of the coherent integration time [ms]
epochDigits=3;                          %backward compability option : xxx=3, : xxxx=4

showSideIndex=1;                        % 1=on 0=off
var1=1;                                 % side- index accumulation
var2=30;                                % side index accumulation

set_length=0;                           % set lenght for blue book estimator

%----display
inSeparateWindow=1;                     % display all the graph in separate windows
accumulationEnable=1;                   % display the power accumulation plots
allDetailsEnable=0;                     % display all the figures(only in separate window mode)

%----Statistical analysis
statisticsEnable=0;                     % 1=on 0=off
pdfEnable=0;                            % 1=on 0= of
hist_point=10;                          % point per bin in the pdf histogram
```

Figure E.13: Extract of the user options from AllComb.m .

E.9 plotAll.m

This script plot all individual epoch results in separate figures (i.e. 1 epoch per figure). To use it simply launch the scripts within the sample directory than the epoch files.

E.10 surfpower.m

Contains a custom plot function, and is not intended to be edited by the user.

List of Symbols and Abbreviations

Abbreviation	Description	Definition
UofC	University of Calgary	page 1
UniNE	University of Neuchâtel	page 1
GNSS	Global Navigation Satellite System	page 9
GPS	Global Positioning System	page 9
ION	Institute of Navigation	page 6
PCB	Printed Circuit Board	page 7
GUI	Graphic User Interface	page 7
NAVSTAR	Navigation System for Timing and Ranging	page 10
C/A	Coarse Acquisition	page 10
SV	Satellite Vehicle	page 11
CEP	Circular Error Probable	page 14
EM	Electro-magnetic	page 14
AGPS	Assisted GPS	page 15
CDMA	Code Division Multiple Access	page 16
PRN	Pseudo Random Noise	page 16
SS	Search Space	page 16
RF	Radio Frequency	page 18
pdf	probability density function	page 20
SNR	Signal to Noise Ratio	page 21
NIST	National Institute of Standards and Technology	page 30
RLC	Resistors, Inductors and Capacitors	page 32
UPS	Uninterruptible Power Supply	page 65
XO	Crystal Oscillator	page 35
VCXO	Voltage Controlled Crystal Oscillator	page 36
TCXO	Temperature Compensated Crystal Oscillator	page 36
OCXO	Oven Compensated Crystal Oscillator	page 37
DOCXO	Double Oven Compensated Crystal Oscillator	page 37
BVA	Boitier à Viellissement Amélioré	page 38
ppm	Part Per Million	page 38

Abbreviation	Description	Definition
IC	Integrated Circuits	page 48
CMOS	Complementary Metal-Oxide-Semiconductor	page 48
MEMS	Microelectromechanical Systems	page 48
PPS	Pulse Per Second	page 54
EMI	Electro Magnetic Interference	page 64
FPGA	Field-Programmable Gate Array	page 55
CCIT	Calgary Center for Innovative Technologies	page 60
$\sigma(\tau)$	Allan Deviation	page 40
χ	Electro-negativity	page 32
ψ	quantum state	page 49

List of Figures

List of Tables